The University of Nottingham

UNITED KINGDOM · CHINA · MALAYSIA

Combustion Aided by a Glow Plug in Diesel Engines under Cold Idling Conditions

Qile Li, B.Eng (Hons)

Thesis submitted to the University of Nottingham for the degree of Doctor of Philosophy, May 2016

Dedicated to my Father, Mother and Sister who have given me continuous support, love and belief in me at all times.

Abstract

Combustion Aided by a Glow Plug in Diesel Engines under Cold Idling Conditions

Qile Li, 2016

Glow plugs are widely used to promote the desired cold start and post-cold start combustion characteristics of light duty diesel engines. The importance of the glow plug becomes more apparent when the compression ratio is low. An experimental investigation of combustion initiation and development aided by the glow plug has been carried out on a single cylinder HPCR DI diesel engine with a low compression ratio of 15.5:1. High speed imaging of combustion initiated by the glow plug in a combustion bomb has been used to add understanding of initiation process. Complementary CFD studies have been carried out using ANSYS Fluent 14.0 to explore the interactions between the glow plug and the spray behavior.

Observation of successful combustion initiation show that two conditions must be met, compression heating and heat transfer from the glow plug must raise temperature of gas nearby to at least 413^{o}C and the vapour/air equivalence ratio no lower than 0.15-0.35. The initiation site was at spray edge close to the glow plug, the flame grew locally before expanding downstream in direction of spray penetration after the end of the main injection.

Experimental studies carried out on the engine indicated that the engine IMEP, heat release and combustion stability were continuously improved by using the glow plug at ambient temperatures higher than the temperature requiring the glow plug for initiation of combustion. A rapid development of premixed combustion was achieved associated with improved engine work output, heat release rate and cycle-by-cycle

stability. The premixed combustion was enhanced by strengthening spray vaporization through the glow plug. In this study, the combustion behavior was enhanced by the glow plug up to ambient temperature of 20°C. Initiation delay was shortened by a rapid development of combustion aided by the glow plug. An initiation delay model was developed to account for both physical part (transport delay) and chemical part (chemical delay). The transport delay (ms) is equivalent to the time for spray to transport to the vicinity of the glow plug, dictated by parameters including S, distance between the glow plug tip and the injector tip (mm); P_{Rail}, rail pressure (bar); d_0, injector nozzle hole diameter (μm) and P, in-cylinder pressure (bar). The chemical delay (ms) accounts for the time required for local mixture to go through cool flame reactions, the chemical delay is dictated by parameters including glow plug tip surface temperature (K), distance between the glow plug tip surface and spray edge (mm) and in-cylinder pressure (bar):

$$\tau = \frac{6.9S^2}{(P_{Rail}-P)^{0.5}d_0} + 2.4P^{-1.02}\exp\left(\frac{2100}{T_{GP}/(0.38x+1)}\right)$$

Table of Contents

Acknowledgements

I would like to express my deepest gratitude towards Professor Paul Shayler, Head of the Engines Research Group at the University of Nottingham for sharing a wealth of knowledge and ideas and doing so in a manner that was, for me, always inspiring and rewarding. I would also like to convey to him my profound thanks for securing a Research Assistantship throughout the studies.

Secondly, my appreciation goes to Dr Michael McGhee for his persistent guidance and assistance offering a tremendous amount of his time during the early part of this investigation. I would like to thank Dr Antonino La Rocca for his assistance on upgrading the combustion bomb rig.

My gratitude extends to Ford Motor Company for their supports on the test facilities; to technicians in particular Mr John Lane and Mr Nigel Sykes for their technical supports on the rig maintenance; to Dr David Hann and the CAMERA centre for their collaboration and the use of the high speed camera; to other members of the Engines Research Group past and present, who offered me a warm welcome and have been sharing the pleasures throughout the timeline of this research project.

I am of course deeply indebted to my beloved Father, Gang Li, my Mother, Shanling Cai, and my Sister, Qiyi Li, who have provided me with every opportunity and encouragement which I could not and would never wish for more.

Nomenclature

A	Multiplying factor (-)
a	Crank radius (m)
B	Bore (m)
B_m	Spalding mass transfer number (-)
C_a	Coefficient of contraction (-)
C_D	Drag coefficient (-)
c_l	Liquid specific heat capacity (J/kg-K)
c_g	Gas specific heat capacity (J/kg-K)
D	Diameter of glow plug tip (m)
D_{fa}	Binary diffusion coefficient (m^2/s)
d	Droplet diameter (m)
d_0	Nozzle hole diameter (μm)
E_a	Activation Energy (J/mol)
h	Convective heat transfer coefficient (W/m^2-K)
k_l	Liquid thermal conductivity (W/m-K)
k_g	Gas thermal conductivity (W/m-K)
L	Stroke (m)
l	Con-rod length (m)
l_c	Characteristic length (m)
$\dot{m}_d$	Droplet vaporization rate (kg/s)
m_l	Liquid fuel mass (kg)
$m_{trapped}$	Trapped mass (kg)
N	Engine speed (rev/min)

n	Adjustable constant (-)
Oh	Ohnesorge number (-)
P	Pressure (bar)
P_{Rail}	Rail pressure (bar)
$\dot{Q}_d^c$	Convective heat transfer rate (W)
$\dot{Q}_d^r$	Radiative heat transfer rate (W)
R	Universal gas constant (J/mol-K)
Re	Reynolds number (-)
S	Spray tip penetration/Glow plug tip to injector tip distance (mm)
Sc	Schmidt number (-)
Sh_0	Modified Sherwood number (-)
$\overline{S_p}$	Mean piston speed (m/s)
T	Temperature (K)
U	Internal energy (J)
u	Jet velocity (m/s)
u_d	Droplet velocity (m/s)
V	Volume (m^3)
V_s	Swept volume (m^3)
V_c	Clearance volume (m^3)
V_{inj}	Injection velocity (m/s)
v_l	Liquid kinetic viscosity (m^2/s)
We_g	Gas Weber number (-)
We_l	Liquid Weber number (-)
x	Distance between glow plug tip surface and spray edge (mm)

Y_s	Vapour mass fraction at droplet surface (-)
$Y\infty$	Vapour mass fraction away from droplet surface (-)

Greek Symbols

ρ_l	Liquid density (kg/m^3)
ρ_f	Fuel vapor density (kg/m^3)
ρ_a	Air density (kg/m^3)
ρ_g	Gas density (kg/m^3)
ρ_{energy}	Energy density (J/cm^3)
τ	Initiation delay (ms)
$\tau_{transport}$	Transport delay (ms)
$\tau_{chemical}$	Chemical delay (ms)
σ	Stephan-Boltzman constant (-)
σ_l	Liquid surface tension (kg/s^2)
μ_g	Gas dynamic viscosity (kg/m-s)
μ_l	Liquid dynamic viscosity (kg/m-s)
θ	Spray cone angle/ Crank angle (degrees)
$\emptyset$	Equivalence ratio (-)

Abbreviation

ATDC	Degrees After Top Dead Centre
ASOI	After Start of Combustion
^{o}CA	Degrees Crank Angle
BDC	Bottom Dead Centre
CAD	Computer Aided Engineering

CAN	Control Area Network
CFD	Computational Fluid Dynamics
CI	Compression Ignition
CO	Carbon Monoxide
CO_2	Carbon Dioxide
CoV_{IMEPg}	Coefficient of Variation in Gross Indicated Mean Effective Pressure (%)
$CR_{effective}$	Effective Compression Ratio
DI	Direct Injection
ECU	Engine Control Unit
EGR	Exhaust Gas Recirculation
EOI	End of Injection
FIE	Fuel Injection Equipment
GP	Glow Plug
HC	Hydrocarbon
FMEP	Frictional Mean Effective Pressure
HPCR	High Pressure Common Rail
HSDI	High Speed Direct Injection
IMEPg	Gross Indicated Mean Effective Pressure
IMEPn	Net Indicated Mean Effective Pressure
ITC	Infinite Thermal Conductivity
NEDC	New European Driving Cycle
NO_x	Nitrogen Oxide
NVH	Noise Vibration Harshness
PM	Particulate Matter

SMD	Sauter Mean Diameter
StD_{IMEPg}	Standard Deviation in Gross Indicated Mean Effective Pressure (bar)
TDC	Top Dead Centre

Chapter 1 Introduction

1.1. Introduction

Turbocharged direct injection engines with high pressure common rail injection are currently the most fuel efficient type of engines used in main stream automotive applications. In Europe, the high speed direct injection (HSDI) diesel engine now takes a similar proportion of the market to the gasoline engine [1, 2]. However, there remain areas of performance in need of further improvement, particularly at reduced ambient temperatures during engine post-cold start performance. The trend over recent years towards the use of lower compression ratios has exacerbated the problem[3]. Recent studies [3, 4] indicated either increasing number of pilot injections or using glow plug with high tip temperature would effectively mitigate the poor idle stability of a low compression diesel engine under cold conditions. The drawback of increasing number of pilot injections is making idle speed control through main combustion more difficult, as the fuel delivered to the main injection is reduced. Fuel economy would become worse if increasing fuelling level of the main injection to improve idle speed control whilst to maintain satisfactory idle stability.

To make the best use of the glow plug under cold idling condition, it is important to understand the role of the glow plug and parameters influencing its performance. This thesis presents experimental and computational investigations to further examine the role and its influence on combustion. It has been reported in several publications [5-9] that the glow plug initiate the combustion in the vicinity of the glow plug, but it was unclear if the glow plug plays a major role in promoting the local vaporization of liquid droplets which mix to produce a locally combustible mixture, or it plays a more restricted role in providing a high temperature

zone to facilitate a self-sustaining reaction of premixed mixture. It has been reported by Perrin et al. [10] that combustion initiation was achieved if well prepared mixture was available near a heat source, but it was not sure the minimum temperature the heat source should give and the minimum equivalence ratio of the mixture. It has been shown in [3, 4, 11, 12] that both glow plug temperature and glow plug to spray edge proximity were important parameters influencing combustion initiation and development under cold conditions, but the mechanisms leading to these outcomes were not well explained. To answer these questions, a single cylinder HPCR DI diesel engine with a low compression ratio of 15.5:1 and a combustion bomb with optical access were used to perform experimental studies, in addition, computational studies were presented in this thesis to obtain an understanding of the influence of the glow plug on spray vaporization.

1.2. Background

1.2.1. Diesel Engine Cold Start and Idle Performance

Diesel engine cold idle performance is paid greater attention in the current investigation. However, understanding the influences during cold start will no doubt deepen the knowledge of cold idling. Diesel engine start process, as has been described in [13, 14], can be summarized into three major phases: from key on to the first fire; the phase of firing-assisted cranking and the last, from the second phase through the start-up to idle. Throughout all three phases, avoiding misfire and to have a large work output is essential to reduce start time and successfully achieve idling state. When the firing is initiated, IMEP turns the engine against friction but the assistance from the start motor is still required, this period that follows is the firing-assisted cranking defined by engine speeds that are markedly higher than those during normal cranking but the engine will stall if the starter motor is disengaged. Continued cranking will raise the engine operating temperature and subsequently reduce oil viscosity, which is important as friction at bearing surfaces is reduced[4]. A successful engine start is finally achieved when the friction is reduced to a level that engine work output can overcome and the speed increases to idle, i.e., $IMEP \geq FMEP$.

Start performance of diesel engine deteriorates when the starting temperature falls. This is associated with long start time and reduced cranking speed. [15]. The main cause is the increase of engine oil viscosity at low temperatures which significantly increases engine friction, the secondary cause is reduced starter motor output, which is a consequence of poor battery performance. At temperature below -10^{o}C, the increase in frictional losses was initially greater than the available work produced by combustion resulting in extended start times[4]. Shayler et al. [16] investigated the influence of oil temperature on engine FMEP by performing engine tear down tests. They observed a

disproportionate increase in engine FMEP with reducing oil temperature below 0°C. The use of low viscosity oils as demonstrated by Caracciolo and McMillan[17], was an effective way to reduce the temperature at which successful starting was possible to a point where starting was limited by battery performance. Reducing FMEP due to crankshaft main bearing which contribute significant portion to total engine FMEP improves cold start performance, as investigated by Shayler et al. [18], bearing friction was reduced by increasing the thermal contact resistance at the back surface of the bearing shells, increasing contact resistance by reducing the contact area to 20% of the original gave a reduction in friction of just over 20%. More recently, engine FMEP reduction was able to be reduced by using a modified oil system allowing separately control of oil flow feeding to the crank train, as demonstrated by Shayler et al. [19], 8% of total engine FMEP reduction was achieved by reducing pressure of oil fed to the crankshaft from 2.1 bar absolute to 1.5 bar absolute at fully warm conditions, the reduction of friction was expected to be larger when engine was operating under colder conditions [19].

In addition to poor cold start performance attributed to higher engine FMEP, cold in-cylinder temperatures can hinder engine IMEP necessary to reach idle away from cranking speeds[4]. Engine cold start performance is not significantly deteriorated when the compression ratio is low. Work conducted by MacMillan [3] investigated the effect of cold starting on two compression ratios, 18.4:1 and 15.4:1. The compression ratio was reduced by increasing the size of the piston bowl. Start performance did not deteriorate when the compression ratio was reduced, because lower peak heat release rate caused by lower in-cylinder temperature reduced heat losses to cold walls and the blowby mass was lower attributed to lower in-cylinder pressure. At cold starting temperatures when the engine speed was 300 rpm, the lower compression ratio was capable of higher producing higher value of IMEP. Longer combustion durations around TDC

also allows more mixing and subsequently larger cumulative heat release[4]. Similar investigation regarding the influence of reducing compression ratio on cold start performance has been studied by Pacaud et al. [5] using a common rail 4 cylinder DI diesel engine with optical access. The start delay was 1.1s at ambient temperature of 20°C with high compression ratio (17.1:1) and extended to 17.5s when compression ratio was reduced to 13.7:1. Reducing start temperature down to -25°C using the same calibration, the start delay for high compression ratio (17.1:1) extended to 5.7s, the starting was unable to be achieved for low compression ratio (13.7:1) when the starting temperature was below 0°C even with the glow plug switched on. They assumed it was because inadequate fuel vapour was generated.

The idle phase commences immediately after start-up where maintaining a fixed speed is required with minimal deviation. Whilst engine start becomes difficult with colder temperatures, work conducted by MacMillan [3] indicated that engine cold start performance is generally not deteriorated by reducing compression ratio provided that an proper injection strategy is employed. The cold idle performance, however, is significantly worse. MacMillan [9] concluded that at high compression ratio under idling conditions, a single-pilot-plus-main strategy was sufficient to achieve large positive work output at all tempertaures studied between -20°C to 10°C. However, the cycle-by-cycle stability was largely deteriorated at lower temperatures, it was impossible to have CoV_{IMEPg} smaller than 10% at -20°C. Cold idling quality became worse when the compression ratio is low, MacMillan et al. [3, 20, 21] found that although the deterioration of cycle-by-cycle stability can be mitigated thourgh the approporiate injection strategy and modest glow plug temperatures at high compression ratio, this was insufficient when the compression ratio was low.

Minimizing the likelyhood of engine misfire and ensuring rapid development of premixed combustion is important to ahieve satisfactory cycle-by-cycle stability under cold idling conditions. Payri et al. [22] found improved cycle-by-cycle stability is associated with pre-combustion state which, depending on rapid development of early phase of combustion induced by multiple pilot injections. Factors influencing early development of combustion have been investigated by McGhee [4] using a quiescent optical vessel, it was concluded that the number of pilot injections and the glow plug temperature have highest influence. The work conducted by both MacMillan et al. [3, 20, 21] and McGhee et al. [4, 11, 23] indicate improvement in cold idle performance at low compression ratio is achieved by increasing glow plug temperature and increasing number of pilot injections, which significantly increases the rate of fuel preparation. The early heat release is improved and resulted in significantly less variation in the heat release rate profiles.

1.2.2. Hot Ignition Source

Starting aids have been extensively used at cold temperatures to improve cold start and idle performance. Starting aids can be generally divided into two major categories. The first type refers to hot ignition source, which supplies energy to local fuel air mixture in its proximity such as the glow plug. The second consists of three approaches: cetane improver, which is a chemical, has the effect of increasing diesel fuel’s cetane number; intake heater, which heats intake charge and engine parts heater which increase temperature of engine components to assist engine cold start. The glow plug is the most widely used component to assist engine start [24-26] and improve post-start idle performance for light duty diesel engines [27, 28]. The glow plug is required especially when the temperature is reduced and compression ratio is low, as has been suggested in the literature already referenced to [11, 23, 29, 30].

A glow plug is pencil-shaped piece of metal with a heating element at the tip. The heating element, when electrified, heats due to electrical resistance and begins to emit light in the visible spectrum. Hence is termed 'glow plug'. Voltage is supplied to glow plug when the glow plug is used. Glow plug temperature is able to reach more than 1000ºC in a few seconds. High operating temperature, short heating-up time, low voltage input and long life service are the main demands that mordern glow plug must fullfil [31]. Glow plugs are installed in the cylinder head. The glow rod heats charge in combustion chamber by extending through cylinder head in the DI engine, as illustrated in Figure 1-1.

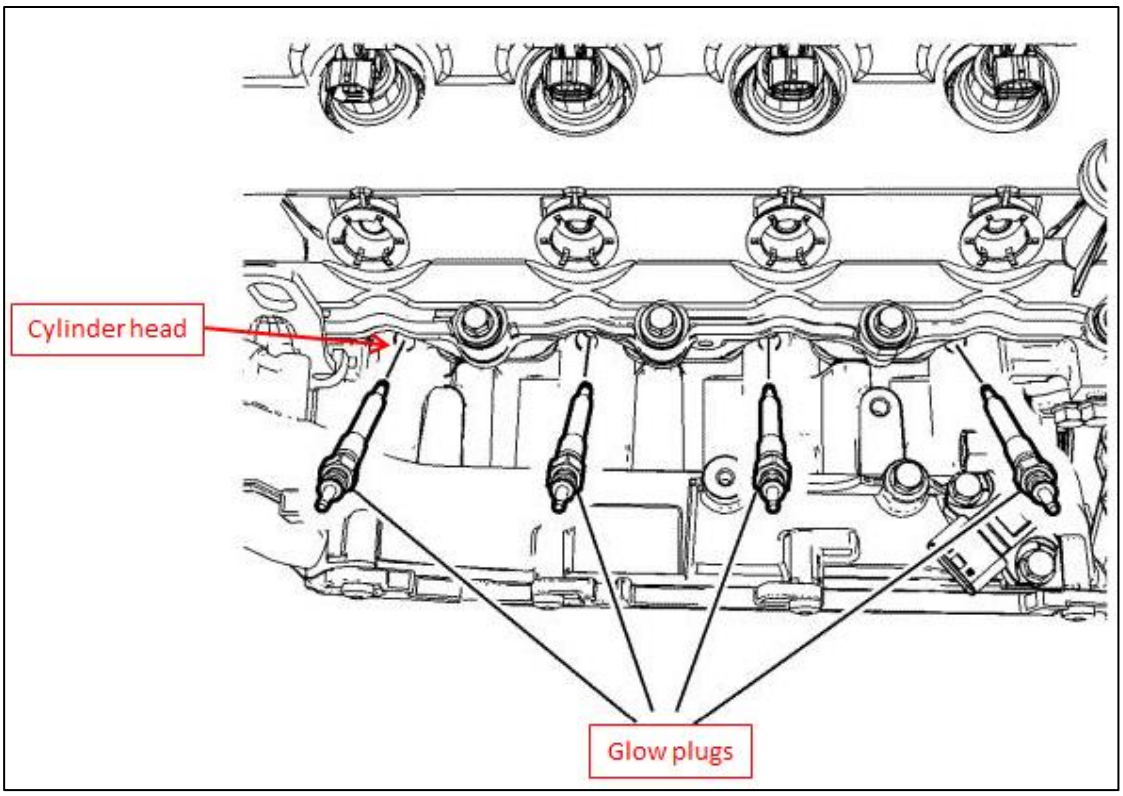

Figure 1-1: Position of the glow plug on a DI diesel engine, the glow plug is inserted into the cylinder head

Different materials and technologies are applied on design of a glow plug. Self-regulating metallic glow plugs, which is amongst the most frequently used glow plug type [32]. As used in the work described in Chapter 4, a self-regulating metallic glow plug with surface temperature of 850°C is

used to investigate the influence of the glow plug on combustion characteristics, as illustrated in Figure 1-2. The voltage is supplied through the connecting terminal at one end of the glow plug, the glow plug is fixed on the cylinder head through a thread, the shell is made of metal and heat tube in the front. Design of the metallic self-regulating glow plug is illustrated in Figure 1-3, as has been interpreted in [33]. The glow plug is able to reach 1000ºC in less than a few seconds. The battery voltage reaches the coils through the central electrode. There is a heating coil heats up very quickly. The heating coil of a self-regulating quick-start glow plug is made of metal. As soon as the glow plug is supplied with current it begins to work and thereby heats up its surroundings. By using different wire diameters or lengths for the construction of heating coils the heating behaviour changes, thus influencing how quickly the glow plug heats up. The control coil is welded to the current-carrying central electrode and the heating coil. As the temperature increases, the electrical resistance of the control coil also increases. In this manner, it reduces the current flow to the heating coil depending on the temperature. Heating tube is made of heat-resistant alloy, together with insulation powder, ensures coils are not subjected to combustion without protection. [33].

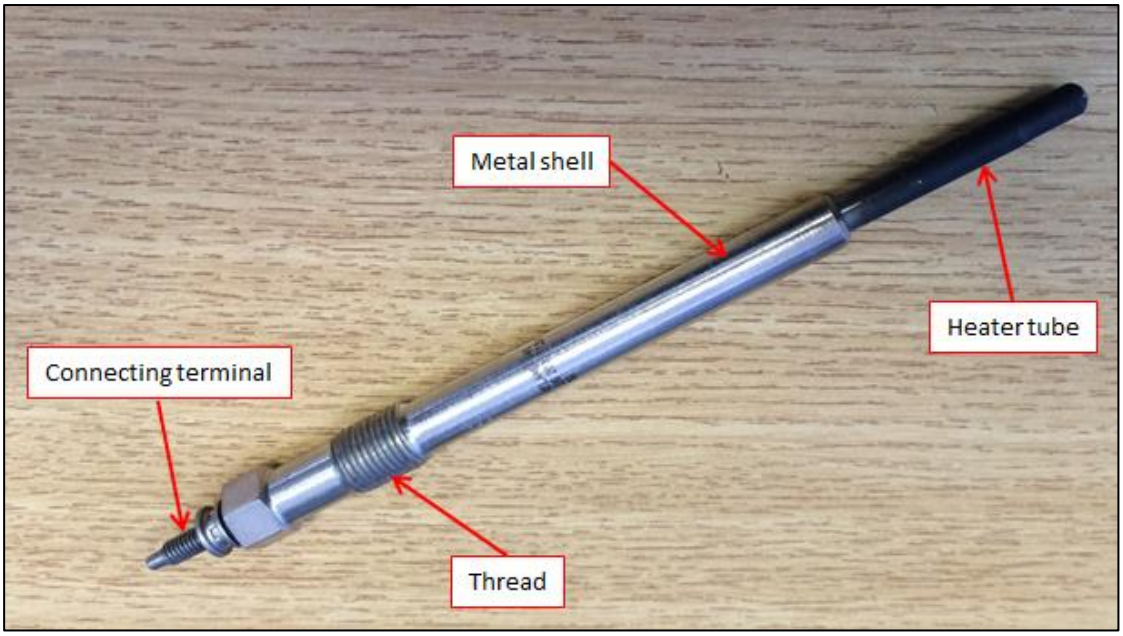

Figure 1-2: Self-regulating metallic glow plug used in this study, as will be used in the work described in Chapter 4

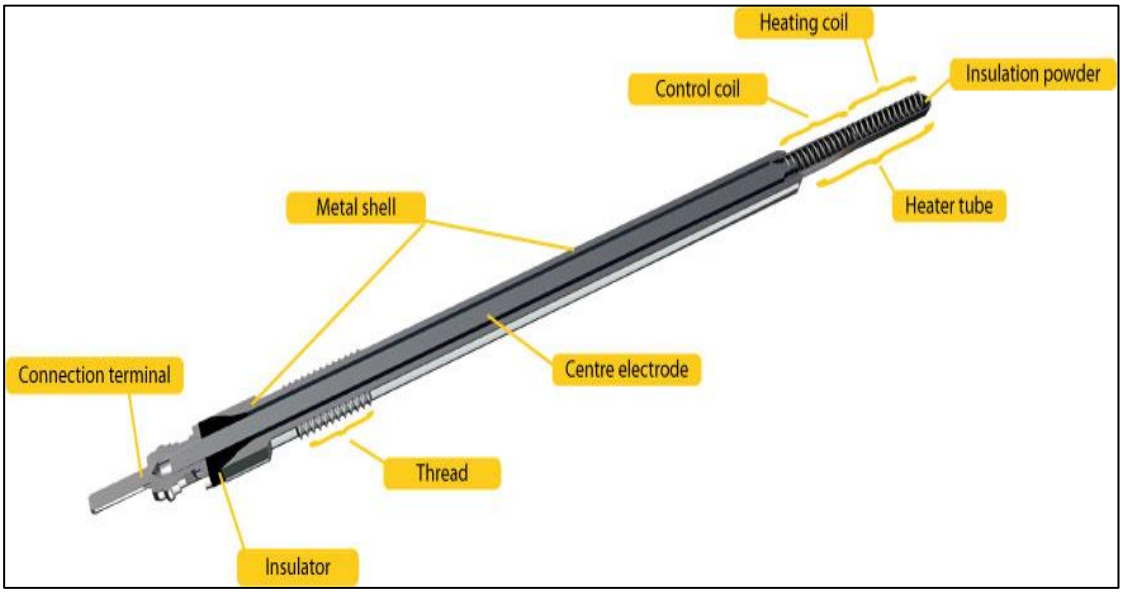

Figure 1-3: Design of a metallic self-regulating glow plug[33]

To investigate the influence of varying glow plug temperature on combustion initiation and development, the other type of the glow plug

used in this study is ceramic high-temperature glow plug, which was specially made by Beru for research use, as illustrated in Figure 1-4. The appearance of ceramic high-temperature glow plug is similar to the metallic self-regulating glow plug, which is also a pencil-shaped piece of metal but with a ceramic tip casing. An R-type thermocouple is embedded into the glow plug to direct measure the core temperature. Voltage from the battery is supplied to the glow plug through the connecting terminal. The heating coil of a ceramic glow plug has an especially high melting point. It is also sheathed in extremely rugged ceramic material. The combination of the heating coil and ceramic sheath enable higher temperatures and extremely short preheating times due to excellent thermal conductivity. As has been examined by MacMillan [3], this ceramic glow plug made by Beru was capable of reaching 1200^{o}C core temperature within 5 seconds. According to Beru [34], the heating element consists of electrically conductive solid ceramic. Because this has a higher specific resistance at the surface than the supply and return conductor material, the glow rod only glows at the tip and therefore reaching high temperatures faster. The glow plug contact consists of an internal and external conductor with an insulator positioned between them as has been shown in Figure 1-5. This ceramic high-temperature glow plug will be used in the work described in Chapter 5, where the internal tip temperature is investigated up to 1200^{o}C.

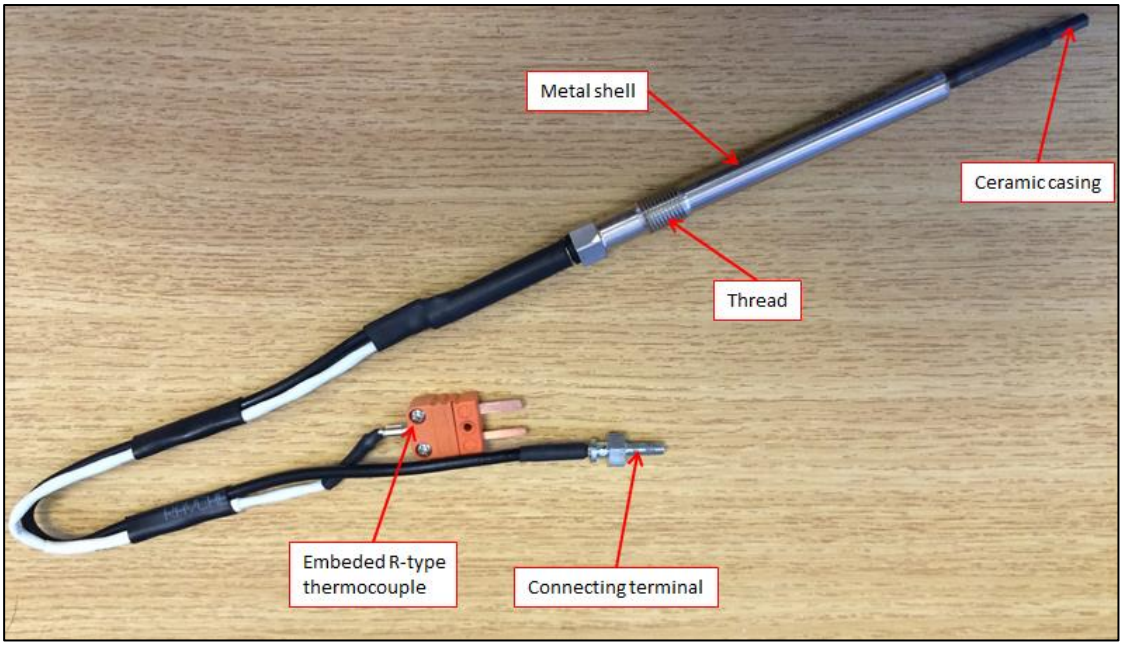

Figure 1-4: Ceramic glow plug used in this study made by Beru, as will be used in the work described in Chapter 5

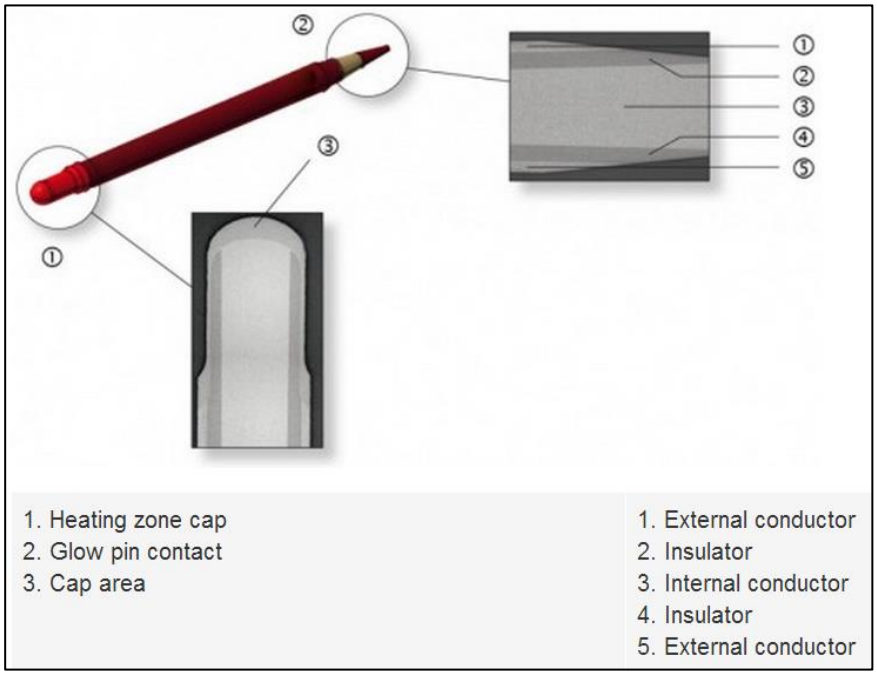

Figure 1-5: Design of a ceramic glow plug heating rod [34]

1.2.3. Combustion Aided by the Glow Plug

The performance of the glow plug during cold start and cold idle for diesel engines has been studied by a number of researchers back to 1960's. Austen and Lyn [15] conducted high speed imaging tests to evaluate the effect of glow plug and concluded that the glow plug works as a combustion initiator rather than heat source. The ignition was found to be originated from the glow plug vicinity and spread downstream of spray. Phatak and Nakamura [35] carried out study on engine cold start and idle performance. It has been reported that glow plug was able to assist engine start down to temperature of -29ºC. Kobayashi et al. [36] investigated time required for the engine to reach idle speed was reduced from 80 seconds to 55 seconds by keeping the electric current of the glow plug even to maintain the glow plug tip temperature after starter motor disengaged. Extended pre-heating and post-heating time is advantageous to achieve quick engine start and stable idling condition. Benefits were magnified if glow plug avoids direct impingement of fuel spray.

More recently, as to meet more and more stringent emission limits whilst keep satisfactory fuel economy, low compression ratio and high boost have been widely adopted by manufactures. Using glow plug is important to mitigate the difficulties caused by engine operating under cold conditions[5, 10]. Combustion behaviour influenced by the glow plug has been studied in several investigations [5-8]. These have shown that the site of initiation is in the vicinity of the glow plug surface and combustion spreads into one on both sprays nearest to the glow plug before the remaining sprays ignite. Both glow plug temperature and the proximity of the spray have been identified as important factors influencing combustion characteristics.

Perrin et al. [10] investigated combustion initiation aided by the glow plug under cold conditions, they found a successful initiation is necessary to satisfy two criteria, a hot source which is the glow plug and well prepared

mixture nearby. Sensitivity of two important parameters: glow plug temperature and glow plug-spray proximity to initiation and development of combustion influenced by the glow plug has attracted attentions of a number of researchers. The impact of spray angle and injector orientation on combustion characteristics has been studied by Pacaud et al. [5], using a diesel engine with a low compression ratio (13.7:1) at test temperatures down to -20°C. They observed that ignition delay could be reduced by increasing spray angle and rotating the injector to change the spray direction by -20º, and concluded that reductions in glow plug tip to spray distance shortened the ignition delay and increased the potential for successful auto-ignition. MacMillan et al. [3] investigated the impact of glow plug temperature on the cycle-by-cycle stability of work output of a common rail diesel engine at low compression ratio. They showed that cold idle stability could be greatly improved through the use of ceramic high-temperature glow plugs. This had the effect of reducing ignition delay and increasing the peak rate of heat release as glow plug temperature increased. In complementary studies, McGhee et al. [4, 11] investigated a range of factors which influence the early stage of diesel spray combustion in a quiescent optical vessel and showed that glow plug temperature and number of pilot of injections have the strongest impact on initiation and early development of combustion. The importance of glow plug temperature and glow plug to spray distance was also recognised by Pastor et al. [9, 12], who suggest these control the initiation of pilot combustion on the nearest sprays which in turn initiates combustion of a subsequent main injection of fuel. Combustion of the first spray propagates to enflame the other sprays, a process aided by the turbulent motion generated by the injection event. They concluded that ignition and combustion in low-temperature conditions starts near the glow plug due to the increased temperature and fuel vapour mass, improving IMEP and combustion stability [29].

1.3. Aims and Objectives

The main aims and objectives are listed as follows:

Investigate the major mechanism for heating spray to vaporize. It could be radiative heat transfer directly from the glow plug or the convective heat transfer from the surrounding hot gas.

- Analytically calculate the rate of heat transfer by convection and radiation separately and then compare the magnitudes of the results.

To determine the threshold in-cylinder temperature for self-sustaining combustion of diesel fuel, and to examine the threshold in-cylinder temperature for CI engines without using a glow plug to perform as good as those using a glow plug.

- Use a single cylinder engine with geometric compression ratio of 15.5 to identify the threshold temperature that enables self-sustaining combustion and sound development without using a glow plug.

Identify the criteria for successful combustion initiated by the glow plug.

- Use a combustion bomb with optical access and the CFD code, ANSYS Fluent 14.0 to investigate factors influencing combustion initiation and vapour/air equivalence ratio required for successful combustion initiation.

Obtain an understanding of the way that combustion system design influences combustion initiation and development aided by the glow plug.

- Develop an initiation delay model to address controlling parameters for behaviour of combustion aided by a glow plug.

Explore the influence of the glow plug on spray vaporization.

- Performing computational studies using the CFD code, ANSYS Fluent 14.0.

1.4. Thesis Layout

The thesis consists of seven chapters. After the introduction, the following chapters are laid out as below:

- A literature review is presented in Chapter 2. Knowledge for diesel combustion characteristics, and spray formation is reviewed. Trend of diesel engine development is also introduced.

- In Chapter 3, test facilities, data acquisition and key response variables are described in Chapter3. The cooling approach, injection control and mathematical derivation of important variables are depicted.

- In Chapter 4, influence of the glow plug on combustion characteristics has been investigated, threshold temperatures for the use of the glow plug have been explored, and influence of injection strategy has been addressed.

- In Chapter 5, the process of combustion initiated by the glow plug has been investigated, criteria for successful initiation have been identified, and an initiation delay model has been developed.

- In Chapter 6, the contribution of radiation to droplet heating has been studied, and the impact of important parameters including glow plug tip surface temperature, glow plug to spray edge proximity and bulk gas temperature on spray vaporization has been evaluated.

- In Chapter 7, discussion and conclusions have been presented as well as proposed future work.

1.5. Contribution to Knowledge

A glow plug has been widely used to assist low compression ratio, DI diesel engines to successfully start and to improve idling stability under cold conditions. This thesis contributes to knowledge of the role of the glow plug and conditions for successful combustion.

The influence of using a glow plug on combustion behaviour was evaluated. Using a glow plug raised engine IMEP, improved combustion heat release and cycle-by-cycle stability up to relatively warm starting temperatures.

A successful self-sustaining reaction is achieved by ensuring a minimum local heat release per unit volume in the vicinity of the glow plug. This study has quantified the minimum gas temperature and the minimum equivalence ratio required for successful combustion initiation.

The role of the glow plug has been examined, temperature of gas was raised above the threshold by the heat released from the glow plug, and spray vaporization was also improved.

The impact of injection strategy on mixture preparation has been addressed. Using multi-pilot injection strategy was beneficial for reaching higher local equivalence ratio in the vicinity of the glow plug.

The research contributions have been summarized into a paper titled' *Initiation and development of combustion under cold idling conditions using a glow plug in diesel engines*' accepted by International Journal of Engine Research on 11/4/2016 in press.

Chapter 2 Literature Review

2.1. Introduction

This chapter is split into six sections. The first and second sections introduce the development of diesel engines for passenger cars. Trend of HSDI engine design has been reported. The third section briefly reviews history of multiple injections and recent applications on improving diesel combustion under cold conditions. The fourth section is a review of diesel combustion characteristics. The fifth section covers physics of diesel spray formation and basics of droplet vaporization. Finally, a summary is presented.

2.2. Overview of Diesel Engine Development

Diesel engines or compression ignition engines (CI engines) were early applications of heavy duty engines with very high compression ratio. This type of engine has been successfully used and operated at railway, marine and power generation plants. Compared with gasoline engines, diesel engines have higher thermal efficiency for reasons which include higher compression ratio but work output is lower than for gasoline engines. Diesel engines also generally operate with quality governing of work output which allows part-load operation without high throttling losses[37-39]. Diesel engines have better torque characteristics and hence can be equipped with optimized transmission system. Vehicles can operate in higher gears for a longer period of time[4].

Diesel engines have been widely used in passenger car application in recent years particularly in Europe. Technologies have been introduced to improve diesel engine efficiency such as direct injection systems together with turbocharger boost, engine downsizing by reducing compression ratio, the high pressure common rail (HPCR) fuel injection, and electronic engine management. Development of fuel injection equipment (FIE) plays important role in improving diesel combustion quality, because common rail allows multiple injection strategies giving to be used greater control over fuel delivery. Accurate, fast, high pressure injection makes spray to atomize, vaporize at correct timing with desired fuel quantity in order to achieve comfortable burn with reduced noise and less emission. Pump-Line-Nozzle, as one of the early fuel injection systems, enables high pressure fuel injection by pressurizing fuel in a pump and distributing to each injector in turn to initiate fuel injection once pressure at the injector exceeds a certain level. The other type was classified as Unit Injection System, where each cylinder was fitted with a unit that consists of a fuel injection pump and nozzle. The actuation of this type of system was achieved by a tappet or a rocker arm driven by camshaft rotation [40]. As

the demands placed on diesel engine fuel injection systems are continually increasing. Higher pressures, faster switching times are required on modern fuel injection equipment. HPCR fuel injection has been developed to adapt flexibility in injection timing, quantity, and strategy. HPCR system is today the most commonly used fuel injection system for modern passenger car and commercial vehicle diesel engines, this system enables separation of fuel injection and pressure generation. The common rail system consists of the main components including the low pressure system comprising the components of the fuel supply system, the high pressure system comprising the high pressure pump, the rail, the injectors and the high pressure fuel lines an ECU for system control. The injector design today is solenoid or piezo-electric type, which permits control of the injection process electronically, safer pressure generation and faster switching time. The common rail system today is capable of providing injection pressure over 2000 bars, a variable start of injection and the possibility of using several pilot/post injections. All these capabilities of HPCR system helps to raise specific power output, lower fuel consumption, reduce noise, pollutant emissions[41]. Exhaust gas recirculation (EGR) is currently the most effective method of reducing emissions of NOx from light-duty diesel engines, since it is particularly beneficial at part load conditions. At part load a diesel engine is operating at a high air to fuel ratio and therefore a large proportion of the intake air charge can be replaced with exhaust gases. EGR reduces the oxygen concentration and increase the heat-absorbing capacity of the inlet charge, thus reducing the peak flame temperatures to lower the formation and emissions of NOx. EGR involves, in effect, the replacement of a small quantity of oxygen and nitrogen in the inlet air to the engine with carbon dioxide and water vapour from the exhaust. Since the specific heat capacity of both CO_2 and water vapour is greater than that for oxygen, the gas temperatures within the engine cylinder during combustion is reduced. Furthermore, by

definition, EGR reduces the exhaust gas mass flow and so lowers the mass of NOx emitted per unit time or distance.

To improve NOx/PM trade-off at part load and achieve higher specific torque and power at full load by using higher boost pressures, engine downsizing by reducing compression ratio has been widely accepted by car manufactures, compression ratio has been decreased from around 19:1 in the 1980's[4] to now typically 16:1 and as low as 14:1 in the case of Mazda's Skyactiv diesel engine [42], together with technological improvements introduced above, demand for light duty diesel engine with smaller compression ratio on passenger cars has been raising over the last decade, primarily due to technology improvements driven by better fuel economy and performance[39, 40], and more and more stringent emission standards for particulate matter (PM), nitrogen oxides (NOx), Improved NVH (Noise, Vibration and Harshness). New cars and light duty vehicles since 1992 have been required to meet emission standards known as 'Euro' standards[43]. The current European exhaust emission requirements regulate four groups of compounds: nitrogen oxides (NOx), carbon monoxide (CO) and particulate matter (PM) and an additional emission element, solid particle number (PN) which became effective since 2011 for all categories of diesel vehicles, emission level tested through the standardized New European Drive Cycle (NEDC). The emission standards are summarized as has been shown in Table 2-1. Legislation is imposing stringent levels particularly on nitrogen oxides (NOx) and particulate matter (PM) for diesel cars as has been shown in Figure 2-1. Euro 6 introduced in 2014 has reduced NOx by 23% and PM by 56% from Euro 5. Car manufacturers start to widely adopt engine downsizing technology to meet the emission standards, which raises adverse effect on cold start and idling.

Table 2-1: EU emission standard for passenger diesel cars

Stage	Year	CO	HC+NOx	NOx	PM	PN
		g/km				#/km
Euro1	1992	2.72	0.97	-	0.14	-
Euro2 (IDI)	1996	1.0	0.7	-	0.08	-
Euro2 (DI)	1996	1.0	0.9	-	0.1	-
Euro3	2000	0.64	0.56	0.5	0.05	-
Euro4	2005	0.5	0.3	0.25	0.025	-
Euro5a	2009	0.5	0.23	0.18	0.005	-
Euro5b	2011	0.5	0.23	0.18	0.005	$6.0x10^{11}$
Euro6	0.5	0.5	0.17	0.08	0.0005	$6.0x10^{11}$

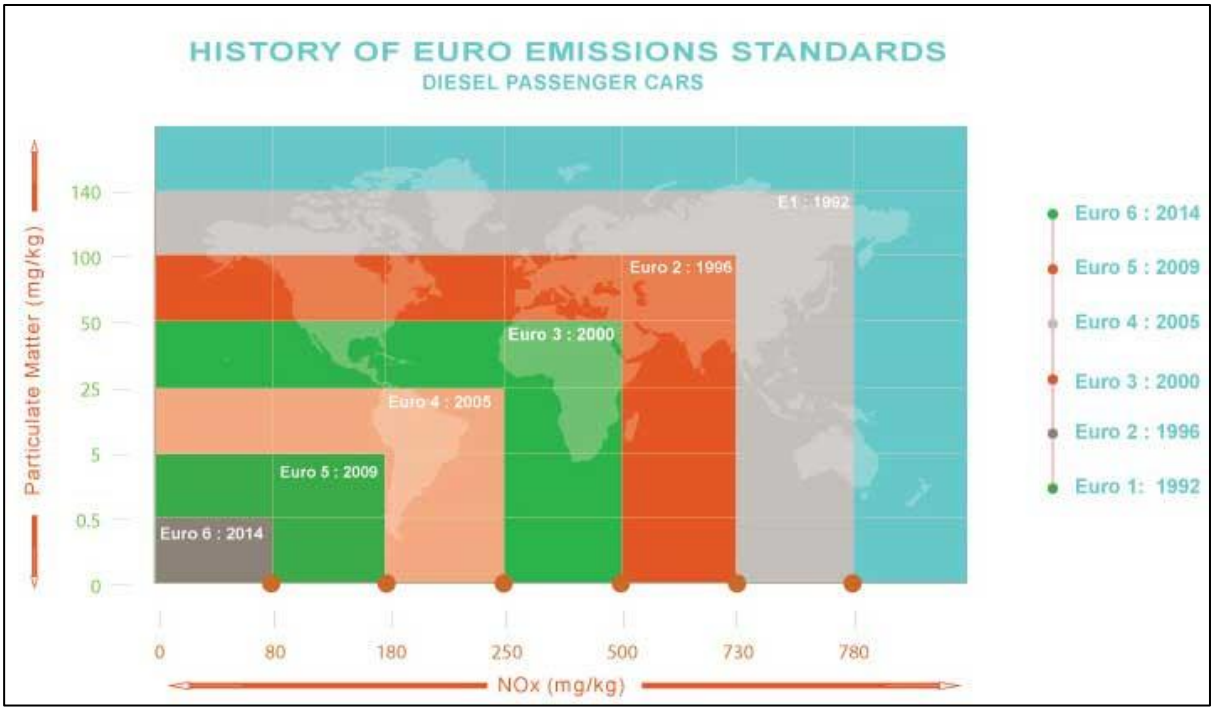

Figure 2-1: History of Euro emission standards for diesel passenger cars[1]

In 2001, in the United Kingdom, diesel vehicles only accounts for 18% of market share of the total new car registrations as shown in Figure 2-2, the number almost tripled by end of 2013. Similar trend was seen among Member States. Belgium, France and Spain have diesel take-up rate at around 65%, while in the Netherlands the rate is much lower, but still accounts for 29%[44].

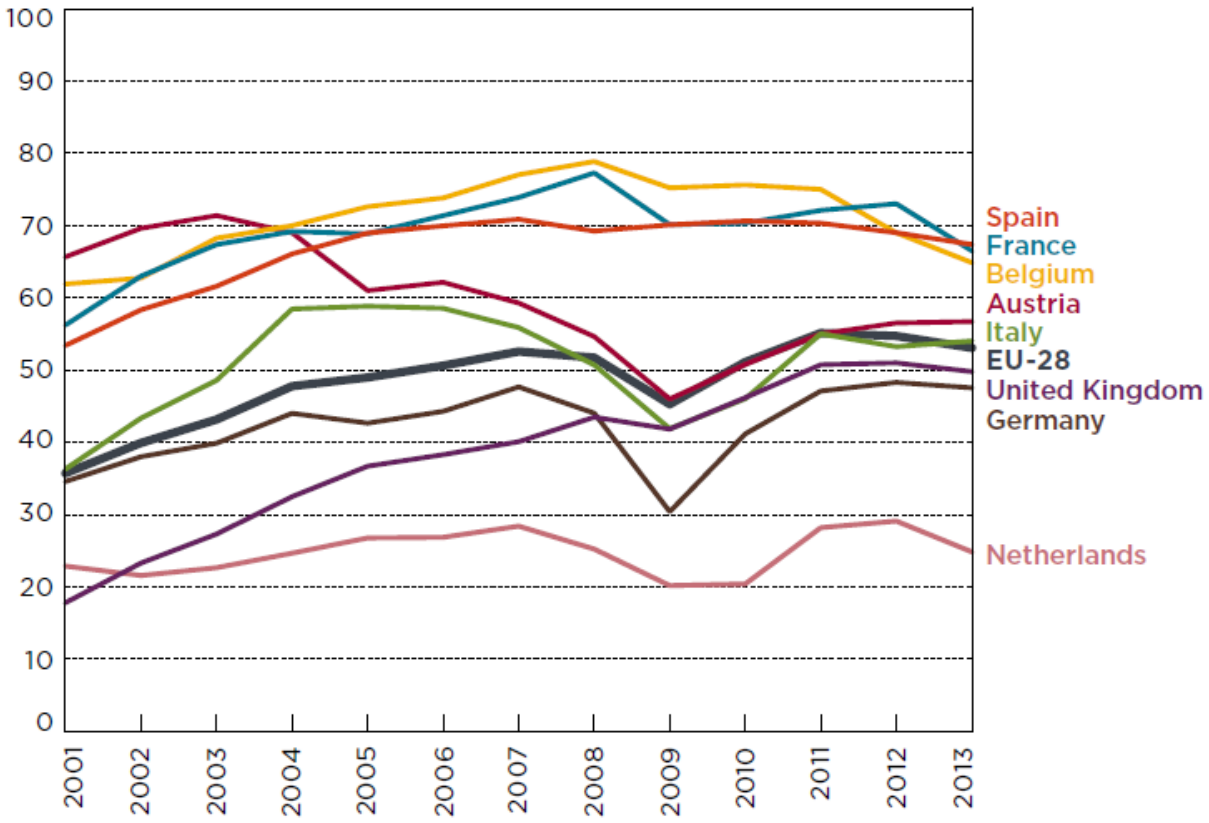

Figure 2-2: Diesel passenger cars market share(percentage) in Europe from 2001 to 2013[44]

Superior fuel economy over spark ignition engines translates into saving CO_2 emissions for reasons which include reduced pumping loss, higher compression ratio and better thermal efficiency. However, the reduction in compression ratio potentially affects other areas of performance, notably cold start and idle behavior. Starting aids such as glow plug is required to mitigate the difficulties of cold start and stable idling. In addition to engine downsizing, many technologies have been developed to mitigate these

emission concerns including those of high pressure injection system, exhaust gas recirculation (EGR) [45, 46] and after- treatment devices. In particular, the new generation of high speed direct injection (HSDI) engines is equipped mostly with a high pressure common rail (HPCR) system capable of multiple injections. The multiple injection strategy with the new common rail injection system has enabled noticeable improvements in the emissions and performances of the DI diesel engine.

2.3. Recent trends in HSDI Diesel Engine Design

During the late 1990s and early 2000s most of the major automobile manufactures developed second-generation four-valve HSDI diesel engines. The move to four-valve per cylinder utilizing two intake and two exhaust, was principally to allow the installation of a central vertical injector to give symmetrical fuel spray plumes for improved air-fuel mixing and equivalence ratio distribution in the combustion chamber. There were also some additional benefits, such as variable swirl levels by port deactivation and a more uniform temperature distribution around the cylinder head flame face, since it is possible to cool the bridges between the exhaust ports. So a new breed of high performance, fuel-efficient diesel engines came onto market. The dramatic increase in performance from light-duty diesel engines over the last 10 years or so has been made possible by three key engine component system developments: first, significant increases in fuel injection system operating pressure, together with greater flexibility of timing and the number of injection events per cycle; second, improvements in turbocharger efficiency with volume production of variable geometry turbochargers, and third, more sophisticated electronic controls for greater flexibility and refinement of the engine systems to provide superior power and response and more acceptable noise levels[47-49].

The HPCR systems have been developed for HSDI engines, the breakthrough features of this type of system are firstly decoupling injection pressure from engine speed, thus allowing injection pressure to be an independent variable; and secondly enabling multiple injections over the speed-load range combined with flexible injection timing. The latter feature provides the opportunity for a pilot injection to control combustion noise over the engine speed range where combustion noise dominates overall engine sound pressure levels. The increase in specific power and improved NOx/PM trade-off led to the downsizing by using higher boost pressures [50-52] as an effective method to improve vehicle performance and emission. The trend has seen compression ratios reduce from around 19:1 in the 1980's [4] to recently typically 16:1 and as low as 14:1 in the case of Mazda's Skyactiv diesel engine [42]. Recently the variable nozzle turbine turbocharger is standard equipment for high-power-density diesel engines and all manufacturers of diesel passenger cars offer high-power output engines using this type of turbochargers since its first introduction by Garrett Turbochargers in 1991 for the Fiat Croma. The main limitation for adopting low compression ratio for mass production is currently cold operation, especially in extreme low temperature starting and running temperature (sub-zero) [5, 11, 30]. Reducing engine compression ratio does not to be problematic till very low temperature thanks to the use of starting aids (glow plugs) and improved injection strategies, however, combustion behaviour tends to be poorer in the phase just after start or when engine is idling[3, 5], very high temperature glow plug and multiple-pilot injections have been proved as effective approaches to improve engine work output and combustion stability under cold idling conditions [11, 23].

2.4. Multiple Injection Technologies

The use of multiple injection was pioneered on larger engines and involved injection modulation or split injection as a good means to reduce NOx and

particulate emissions[53, 54]. First-generation HSDI engines were equipped with HPCR injection systems of the maximum rail pressure, 1350 bar. The HPCR system was limited to two consecutive injections due to the intrinsic limitation of the minimum dwell time of 1.8 ms between two consecutive injections[49]. Pilot injection was mainly used to mitigate combustion noise. Experiments data indicated that apart from noise control, pilot injections allowed the PM-NOx trade-off curves of a diesel engine to shift closer to the origin than with conventional single pulse injections. Reduction of NOx and PM were achieved simultaneously.

Recently, study has shown splitting a single pulse injection into multiple pulses improved combustion stability characterized by coefficient of variation of IMEPg (CoV_{IMEGg}) during the idle phase just after cold start, both fuel conversion efficiency and IMEP were increased [22]. Effect of multiple pilot injections on heat release and ignition characteristics under cold conditions has been reported by[55-57], it has shown that multiple pilot injections offsets the effect of low in-cylinder temperatures on ignition delay deterioration. Influence of multiple injection strategies on engine IMEP and combustion stability was later investigated by [22], they concluded separation between the last pilot injection and the main injection was the most influential parameter on the heat release rate, a separation of 6^{o} CA produced the highest engine IMEP and was always associated with a short ignition delay and strong main combustion development. McGhee [4] has investigated influence of injection strategies and glow plug on engine cold idle stability, the study indicated that increased number of pilot injections has shown more significant benefits on combustion behaviour during cold idling, high glow plug temperature in combination with multiple injections was advantageous to achieve low engine IMEP variation or better stability. To achieve a CoV_{IMEGg} that less than 10%, 20J/^{o}CA of premixed combustion peak was required.

2.5. Diesel Combustion Process

Unlike spark ignition engines, where the air fuel mixture is ignited discharged from a spark plug, in compression ignition engines, air alone is inducted into the cylinder; the fuel is injected directly into the engine cylinder just before the combustion process is required to start. Load control is achieved by varying the amount of fuel injected each cycle; the air flow at a given engine speed is essentially unchanged[37]. Combustion is initiated by means of self-ignition that occurs under high temperature, high pressure conditions.

2.5.1. Introduction to Diesel Combustion Process

Four phases have been summarized in [37] describing the overall process of compression –ignition diesel combustion process. As illustrated in Figure 2-3, ignition delay, premixed or rapid combustion phase, mixing controlled combustion phase and late combustion phase. These four phases were illustrated in a typical heat release rate diagram. Following ignition delay that has been reviewed in earlier section, combustion of the fuel air mixture which is within flammability limits during the ignition delay period occurs rapidly, showing the first peak in heat release rate profile. The third phase is mixing controlled combustion, in this phase, as mixture that prepared in ignition delay has been combusted during the premixed combustion phase, the heat release rate is controlled by the rate at which mixture becomes available for burning. While several processes are involved, liquid fuel atomization, droplet vaporization, mixing, pre-combustion reactions[37], these processes are similar to the process undertaken during physical and chemical delay period, but in mixing controlled phase, the burning rate is primarily controlled by fuel vapour – air mixing process. A second peak in heat release rate profile is usually seen in this phase. The last phase, late combustion phase, where heat release continues at a lower rate into the expansion stroke as charge temperature decreases rapidly. A small fraction of the fuel may not yet

have burned. A fraction of the fuel energy is present in soot and fuel-rich combustion products can still be released[37].

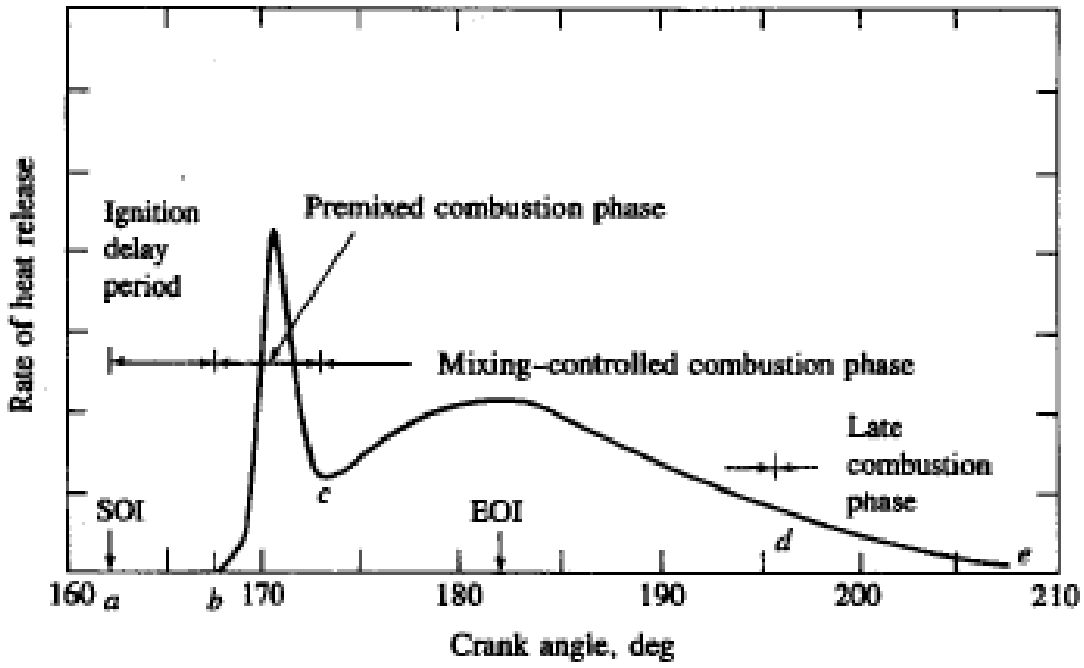

Figure 2-3: Typical heat release rate profile identifying different diesel combustion phases[37]

Ignition delay is the time required for mixture preparation and chemical reactions prior to vigorous hot combustion. This is demonstrated in the next sub-section. During premixed combustion phase, combustion of the fuel which has mixed with air to within the flammability limits during the ignition delay period occurs rapidly in a few crank angle degrees. When this burning mixture is added to the fuel which becomes ready for burning and burns during this phase, a clear spike is present indicating the burning of mixture. Once the fuel and air which premixed during the ignition delay have been consumed, the burning rate is controlled by the rate at which mixture becomes available for burning, i.e., chemical reaction rate is much faster than fuel vapour -air mixing rate, and hence heat release rate is mainly dependent on rate of mixing. The mixing controlled combustion may not reach a second peak shown on the heat release profile and heat release rate during this phase decreases as this phase progresses. Late

combustion phase continues following the mixing controlled combustion burns out remaining fuel as piston moves into the expansion stroke .

2.5.2. Ignition Delay

Ignition delay is the period between the start of the fuel injection and the start of the ignition. While start of fuel injection can be accurately measured at the time when the injector needle lifts off its seat, depends on criteria used, there are three ways to define the start of ignition: Illumination delay, pressure rise delay and heat release delay[58, 59]. Illumination delay is the time between the start of injection and the first appearance of detectable flame. Pressure rise delay is the time between the start of injection and a measurable rise of pressure due to combustion events. Heat release delay is defined as time between the start of injection and the moment when heat release rate turns negative to zero[24], or 2.5J/^{o}CA in some studies[4]. During this ignition delay period, diesel self-ignition is enabled once physical and chemical processes proceed to a proper level. Physical process can be generally classified into spray atomisation, droplet vaporization and fuel-air mixing[37]. Chemical process is basically a series of oxidisation reactions in the fuel, air and residual gases as well as cracking of hydrocarbon chains, producing more volatile species[3]. Two-stage ignition chemistry is typically used to interpret reactions processed during chemical delay[60]. At lower temperatures (800-1000K), a pool of ketohydroperoxide radicals builds and then rapidly breaks down at the end of the first stage of ignition, forming another pool of hydrogen peroxide (H_2O_2). The temperature rise associate with the first stage of ignition terminates the pooling of ketohydroperoxides, but the H_2O_2 pool continues to build as the temperature gradually increases. When the temperature reaches approximately 1200K, the H_2O_2 pool breaks down to release hydroxyl (OH) radicals that promote rapid oxidation during the hotter second-stage ignition and premixed burn [49]. The first-stage ignition happens at

different times for different equivalence ratios, as the mixtures with a wide range of equivalence ratios within diesel spray, the effect of net heat release due to first-stage ignition is decayed. Besides, temperature rise in cylinder is in a very rapid rate due to fuel vapour mixing with high temperature in-cylinder gas, which leaves a relatively short period to first-stage ignition, as a consequence of time limitation for the radical pools to build, effect of first-stage ignition is weak. Release of hydroxyl (OH) due to second-stage ignition can be detected optically as chemiluminescence, because OH generation represents rapid promotion of oxidation and leading to premixed burn, detection of OH can be treated as the end of the ignition delay. A more straightforward way to detect the end of ignition delay is appearance of luminous soot emission. Following the rapid oxidation process alongside release of OH, the premixed burn increases the temperature in the jet, and the resulting hot, partially oxidized mixtures synthesize polycyclic aromatic hydrocarbon (PAH) soot precursors that go on to form soot.

Ignition delay has attracted interest of a number of researchers and engineers because of its direct impact on the intensity of heat release immediately following self-ignition [62][62][62][62][62][62][62, 63]. Atomization turns liquid fuel into smaller droplets, followed by droplet vaporization. Air entrainment takes place where fuel vapour generated at droplet surface mixes with air surrounded to form combustible mixture. This combustible mixture will be ignited once mixture is well prepared and temperature of the wake is above self-ignition temperature[64]. Time taken to cover physical and chemical process is termed physical ignition delay and chemical ignition delay respectively. Numerous steady-state ignition delay correlations have been proposed based on experimental data in constant volume bombs, steady flow reactors, rapid compression machines and engines[61], many of those correlations use an Arrhenius expression that has been shown in Equation 2-1.

$$\tau_{ID} = AP^{-n}\exp(\frac{E_a}{RT})$$

Equation 2-1

Where τ_{ID} is ignition delay, P and T are pressure and temperature, E_a is activation energy, R is universal gas constant, and A, n are multiplying factor and adjustable constant respectively.

Based on the semi-empirical equation developed by Wolfer [65] back to 1938, Waston [66] developed an ignition delay model based on experimental work on a diesel engine under steady state conditions, the activation energy term and universal gas constant that has been shown in Arrhenius expression has been integrated into a fixed constant of 2100, the expression of the ignition delay correlation has been shown in Equation 2-2.

$$\tau_{ID} = 3.45P^{-1.02}\exp(\frac{2100}{T})$$

Equation 2-2

Where A and n have been replaced by two constants, 3.45 and -1.02, shows ignition delay period has inverse dependence on charge pressure.

2.6. Features of Spray Formation

The fuel is introduced into the combustion chamber of a diesel engine through one or more nozzles with a large pressure differential between the fuel supply line and the cylinder[37]. The spray is formed once the liquid is injected into gaseous condition from an injector. The injected liquid begins to interact with charge instantly leading to the decomposition and detachment from the periphery of the jet. Smaller droplets are formed, droplet vaporization takes place and fuel vapour mixes with air. These processes, breakup, atomization, droplet vaporization and mixing are of great importance for the mixture preparation[67].

Spray momentum turns up the turbulence just after the fuel injected into gaseous environment. The liquid is internally and externally undergone various forces, results in the generation of droplets with various diameters[68]. Arcoumanis [69] classified the regimes of the breakup into three types, breakup caused by external air forces where fuel air interaction and air drag force is dominant, breakup caused by turbulence where the magnitude of the jet radial velocity caused by the turbulence in the nozzle is high and inertial force overtakes the restoring force, and the last one, breakup caused by internal cavitation where growth and decomposition of the air foams lead to jet breakup[70]. Diesel engine sprays are usually of the full-cone type. See Figure 2-4 for a schematic drawing of a full-cone spray. At first, there is an intact liquid core from nozzle hole exit. The fuel consists of ligaments which disintegrate into smaller size droplets. The entire break up process is split up into two categories: primary break up and secondary break up.

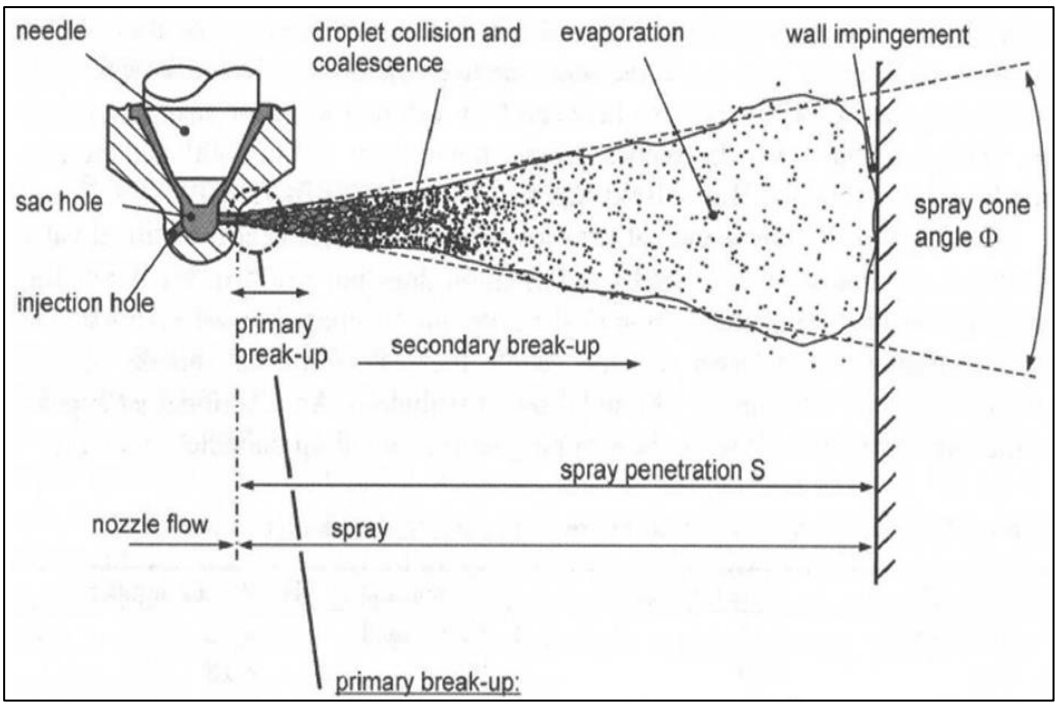

Figure 2-4: Illustration of full cone spray, primary breakup and secondary breakup[71]

2.6.1. Fuel Jet Breakup

Process of liquid jet disintegrating into small droplets are categorised by two sequential breakup mechanisms. The first breakup process is called primary breakup, which mainly deals with the breakup of the intact liquid core into droplets and the Secondary breakup is the process that turns droplets into smaller size, characterized by droplet sizes [71, 72].

In the process of primary breakup, inertial force, surface tension force and viscous force of particles are of particular importance. The primary breakup process can be characterized by three dimensionless numbers. Weber number (We) is a dimensionless number that is used to measure the relative importance of the particle's inertia compared to its surface tension, referring to the ratio of inertial force to surface tension force. Higher value of Weber number indicates stronger air drag force. While a small value means inertial force is weak compared with tension force, which is unfavourable to spray breakup. Weber number is expressed in Equation 2-3.

$$We_l = \frac{d_0 \rho_g u^2}{\sigma_l}$$

Equation 2-3

Where d_0 is diameter of the nozzle hole, ρ_g is gas density, u is jet velocity and σ_l is liquid surface tension.

Reynolds number (Re) is a dimensionless number that is used to characterize turbulence. Refers to the ratio of inertial force to viscous force, Reynolds number is expressed in Equation 2-4.

$$Re = \frac{\rho_l l_c u_d}{\mu_l}$$

Equation 2-4

Where l_c is characteristic length, μ_l is liquid dynamic viscosity.

Ohnesorge number (Oh) is a dimensionless number that relates the viscous force to inertial and surface tension force. Refer to ratio of Weber number to Reynolds number, as expressed in Equation 2-5.

$$Oh = \frac{\sqrt{We}}{Re}$$

Equation 2-5

Reitz [73] categorized the regimes into four categories, an example has been shown in Figure 2-5.

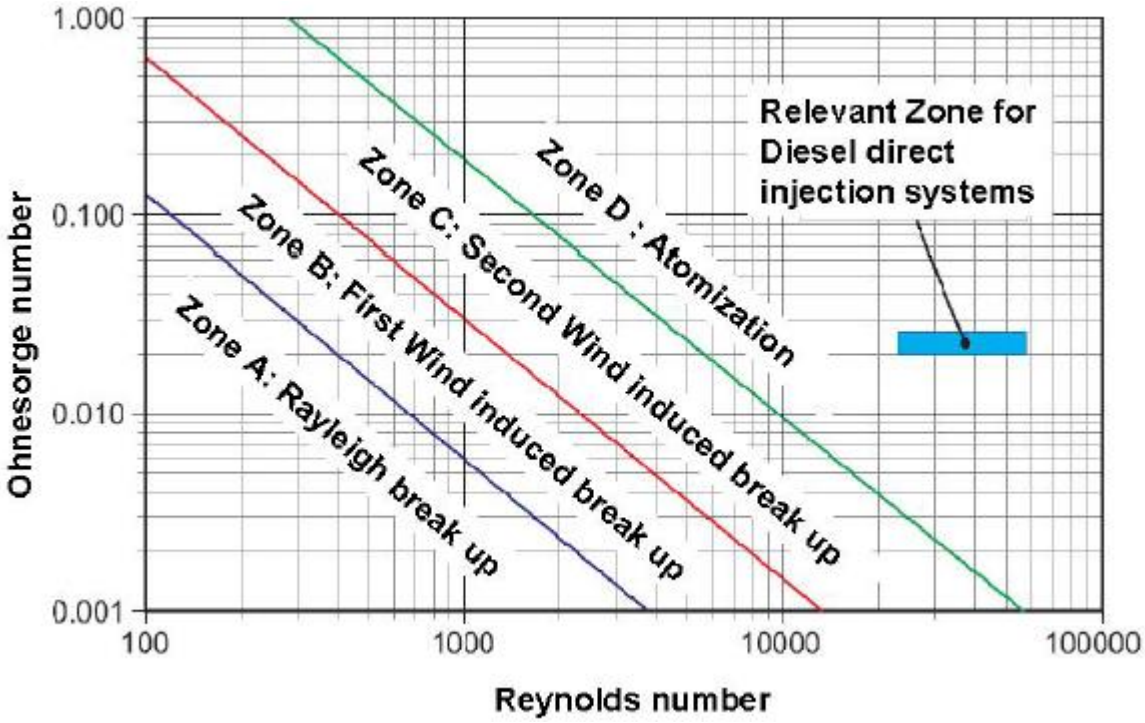

Figure 2-5: Ohnesorge diagram: classifying four primary breakup regimes[74]

Morphology of spray under these four breakup regimes are shown in Figure 2-6.

1. Rayleigh jet breakup

Rayleigh breakup regime occurs at low jet velocity. External drag force dependent on relative velocity between liquid and gas is small, breakup is

primarily due to axisymmetric oscillations initiated by liquid inertia and surface tension forces[75].

2. First wind-induced breakup

External drag force becomes important as the spray jet velocity increases, liquid inertia and surface tension forces are amplified as well. Breakup regime transfers from Rayleigh jet breakup regime into first wind-induced breakup regime as a result of increased Weber number.

3. Second wind-induced breakup

The flow is more turbulent and breakup regime transfers into second wind-induced breakup regime as a result of spray jet velocity continue to increase. Instable growth of short wavelength surface waves initiated by the turbulence and amplified by external drag force[75].

4. Atomization

In this regime, the liquid state becomes completely atomized after the liquid being injected out from the nozzle. It has been illustrated in Figure 2-5 that spray jet breakup regime for modern direct injection diesel engine application is always in atomization regime.

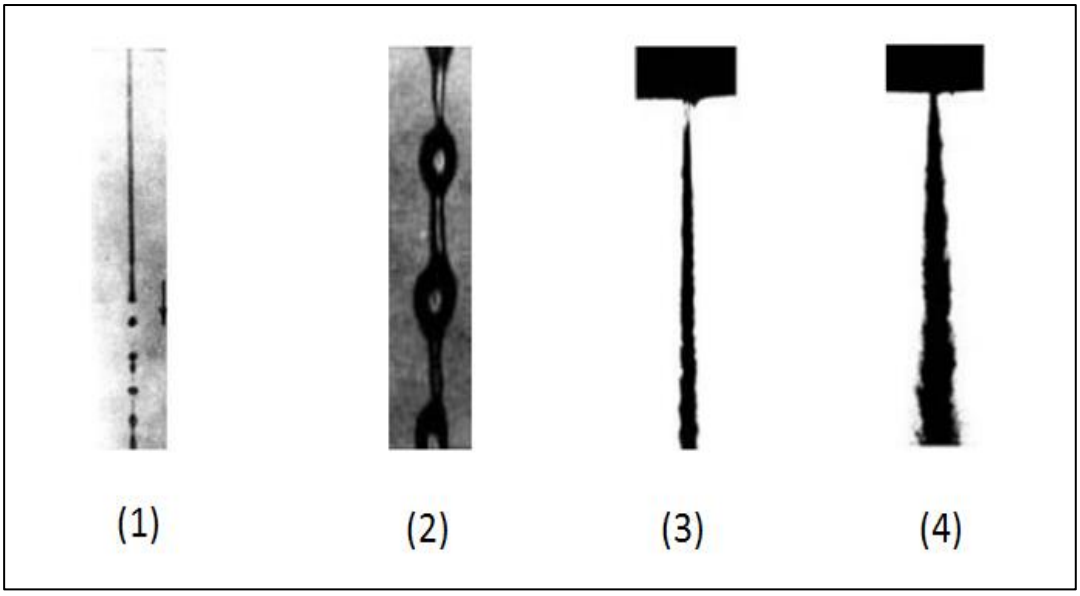

Figure 2-6: Morphology of spray under four breakup regimes[73]

Droplets that created after the process of primary breakup are usually not stable and hence are subject to further breakup. This subsequent breakup process is generally referred to as secondary breakup. The secondary breakup is dominated by aerodynamic forces, relative velocity between gas and droplet is therefore essential in the breakup mechanism. Spray jet breakup including primary breakup and secondary breakup has been illustrated in Figure 2-7.

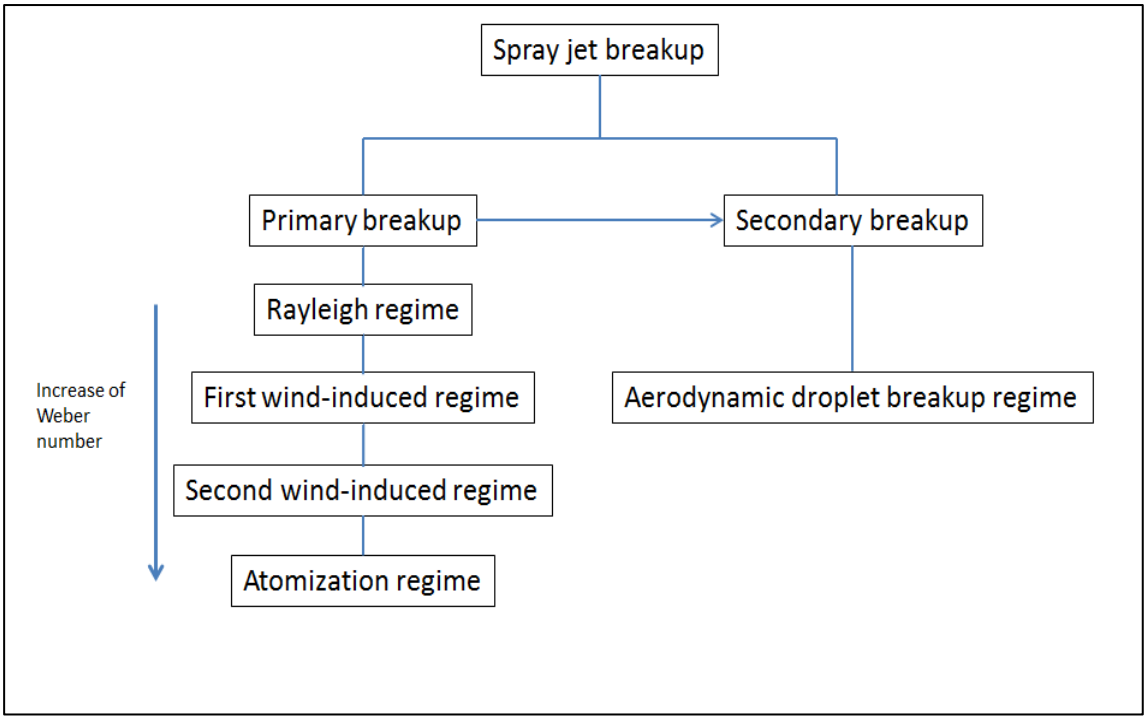

Figure 2-7: Diagram illustrating primary and secondary breakup

The Sauter Mean Diameter (SMD) characterizes a single droplet with the same volume to surface area ratio as the ratio of the respective quantities integrated over the whole droplet size distribution present in a real spray[37, 76]. The SMD is the diameter of the droplet that has the same surface/volume ratio as that of the total spray.

$$SMD = \frac{\int d^3 dn}{\int d^2 dn}$$

Equation 2-6

Where dn is the number of droplets with diameter d in the range of $d - d(\frac{d}{2}) < d < d + d(\frac{d}{2})$. The integration is usually carried out by summing over an appropriate number of drop size groups.Elkotb [77] has developed a model that considered properties of both liquid and gas phase. Expression has been shown in Equation 2-7.

$$SMD = 3.085 {v_l}^{0.385} {\sigma_l}^{0.737} {\rho_l}^{0.737} {\rho_g}^{0.06} \Delta P^{-0.54}$$

Equation 2-7

Where v_l is liquid kinetic viscosity, σ_l is surface tension, ΔP is pressure drop.

Varde [78] has taken into account the diameter of the injection nozzle hole in predicting SMD, correlation has been shown in Equation 2-8.

$$SMD = 8.7 d_0 (ReWe)$$

Equation 2-8

Where D_n is injector nozzle diameter, Re and We are Reynolds number and Weber number respectively.

Merrington [79] has studied liquid jet breakup. Droplet size distribution curves have been empirically obtained by a static nozzle directed vertically downward in an enclosed spray tower. Lefebvre [80] developed a correlation based on work by Merrington [79] considering the effect of orifice diameter, the correlation of SMD has been expressed in Equation 2-9.

$$SMD = \frac{500 {d_0}^{1.2} {v_l}^{0.2}}{V_{inj}}$$

Equation 2-9

Where v_l is the kinetic viscosity of the liquid and V_{inj} is the injection velocity.

Hiroyasu [81] provided an empirical correlation that has taken into account of typical diesel fuel properties, as shown in Equation 2-10.

$$SMD = 2.33 \times 10^{-3} \Delta P^{-0.135} {\rho_g}^{0.121} {m_l}^{0.131}$$

Equation 2-10

Where ΔP is the pressure drop between rail pressure and charge pressure, ρ_g is gas density and m_l is mass of fuel injected.

Hiroyasu [72] later considered the effect of fuel properties, spray momentum experimentally, correlation has been given in Equation 2-11 and Equation 2-12.

$$SMD = MAX({D_{SM}}^{LS}, {D_{SM}}^{HS})$$

$$SMD^{LS} = 4.12.d_0.Re^{0.12}We^{-0.75}(\frac{\mu_l}{\mu_g})^{0.54}(\frac{\rho_l}{\rho_g})^{0.18}$$

Equation 2-11

$$SMD^{HS} = 4.12.d_0.Re^{0.38}We^{-0.32}(\frac{\mu_l}{\mu_g})^{0.37}(\frac{\rho_l}{\rho_g})^{-0.47}$$

Equation 2-12

Where μ_l and μ_g are dynamic viscosity of liquid and gas respectively. $SMD = MAX$ () denotes a larger value of these two equation.

Small droplet size is favourable to vaporization since convective heat transfer has been enhanced due to increased surface area to volume ratio. Convective heat transfer also increases with increasing velocity of moving droplets because convective heat transfer coefficient tends to increase with increasing Reynolds number. Droplet velocity can be estimated as rate of spray penetration which is dependent mainly on pressure differential between injection pressure (rail pressure) and charge pressure. High injection pressure leads to smaller droplet with fast moving velocity, which means both droplet heating and vaporization can be improved. The secondary breakup concerns the breakup of droplets due to aerodynamic forces that are included by the relative velocity between the droplets and the surrounding gas. On the gas-liquid interface instable growth of waves occurs. While in the same time surface tension counteracts the disintegration process. Similar to the first wind-induced regime for the liquid core the gas Weber number is the relevant dimensionless quantity to identify the process, with the difference that nozzle diameter d_0 in Equation 2-3 is replaced by droplet diameter d [75] and jet velocity is

replaced by relative velocity between droplet and surrounding gas. Gas Weber number is expressed in Equation 2-13.

$$We_g = \frac{d\,\rho_g {u_{rel}}^2}{\sigma_l}$$

Equation 2-13

Secondary breakup can be modelled using WAVE breakup model of Reitz [82], which is more appropriate model for high- Weber number flows (Weber number is greater than 100) than Tayler analogy breakup model. WAVE breakup model considers the breakup of the droplets to be induced by the relative velocity between the gas and liquid phases. The model assumes that the time of breakup and the resulting droplet size are related to the fastest-growing Kelvin-Helmholtz instability, derived from the jet stability analysis. The wavelength and growth rate of this instability are used to predict details of the newly formed droplets[83].

2.6.2. Spray Tip Penetration

Spray tip penetration in design of DI engines has been studied extensively due to its importance on air utilization and fuel-air mixing rate. In this section, a number of widely used correlations will be reviewed. The research can be traced back to 1960's. Wakuri et al. [84] used momentum theory to develop the fuel spray model by assuming that relative velocity between fuel droplets and entrained air can be neglected and the injected liquid droplet momentum is transferred to the homogeneous fuel droplet-entrained air mixture for the density rate range of 40-60[76]. The model has been expressed in Equation 2-14.

$$S = 1.189 {C_a}^{0.25} \left(\frac{\Delta P}{\rho_g}\right)^{0.25} \left(\frac{d_0 t}{\tan(\theta)}\right)^{0.5}$$

Equation 2-14

Where C_a is the coefficient of contraction, ΔP is pressure difference between fuel injector pressure and ambient gas pressure, ρ_g is the gas density, d_0 is nozzle diameter and θ is the spray cone angle.

Dent et al. [85] developed a spray tip penetration model based on jet mixing theory, the model is different from others for considering gas temperature effects (T_g), as has been expressed in Equation 2-15.

$$S = 3.07\left(\frac{\Delta P}{\rho_g}\right)^{0.25}(d_0 t)^{0.5}(\frac{294}{\mathrm{T}_g})^{0.25}$$

Equation 2-15

Hiroyasu and Arai [72] proposed a model which are derived from data obtained during their previous study [86] and from applying the jet disintegration theory by Levich [87]. They used two different equations, one from the beginning of the injection to the jet breakup time, where the penetration is proportional to time and regardless the influence of ambient temperatures. The other one occurs at times exceeding the jet breakup time, where the penetration is proportional to the square root of time[76], as expressed in Equation 2-16 and Equation 2-17. t_b is breakup time.

$$S = 0.39\left(\frac{2\Delta P}{\rho_g}\right)^{0.25} t \quad 0 < t < t_b$$

Equation 2-16

$$S = 2.95\left(\frac{\Delta P}{\rho_g}\right)^{0.25}(d_0 t)^{0.5} \quad t > t_b$$

Equation 2-17

2.6.3. Spray Cone Angle

Spray cone angle, as has been illustrated in Figure 2-4, is defined as the angle formed by two straight lines drawn from the injector tip to the outer periphery of the spray[80]. Spray cone angle generally shows drastic increases after the very appearance of the plume, and then almost keeps

constant[88, 89]. In this section, a number widely used correlation will be reviewed. Arai et al. [90] proposed a model considering injector nozzle diameter, rail pressure and ambient gas properties:

$$\theta = 0.05(\frac{\rho_g \Delta P {d_0}^2}{{\mu_g}^2})^{0.25}$$

Equation 2-18

Although the effects of various factors are expected to be influential, Wakuri et al. [91] found that the ratio of liquid density and gas density was the only factor that affected the spray cone angle:

$$\theta = 2\arctan(0.427\left(\frac{\rho_g}{\rho_f}\right)^{0.35})$$

Equation 2-19

Hiroyasu and Arai [72] investigated the influences of fuel viscosity and the injection pressure on spray cone angle. It was reported that with the increase of the jet speed, the angle initially increased, reached a peak value and stabilized at a constant value. The rate of increase and the peak value were dependent on fuel viscosity. As has been shown in Figure 2-8, they proposed an empirical equation for the spray cone angle which includes some characteristics of the nozzle:

$$\theta = 83.5\left(\frac{l_0}{d_0}\right)^{-0.22}(\frac{d_0}{d_{sac}})^{0.15}(\frac{\rho_g}{\rho_l})^{0.26}$$

Equation 2-20

Where d_{sac} is the diameter of the sack chamber.

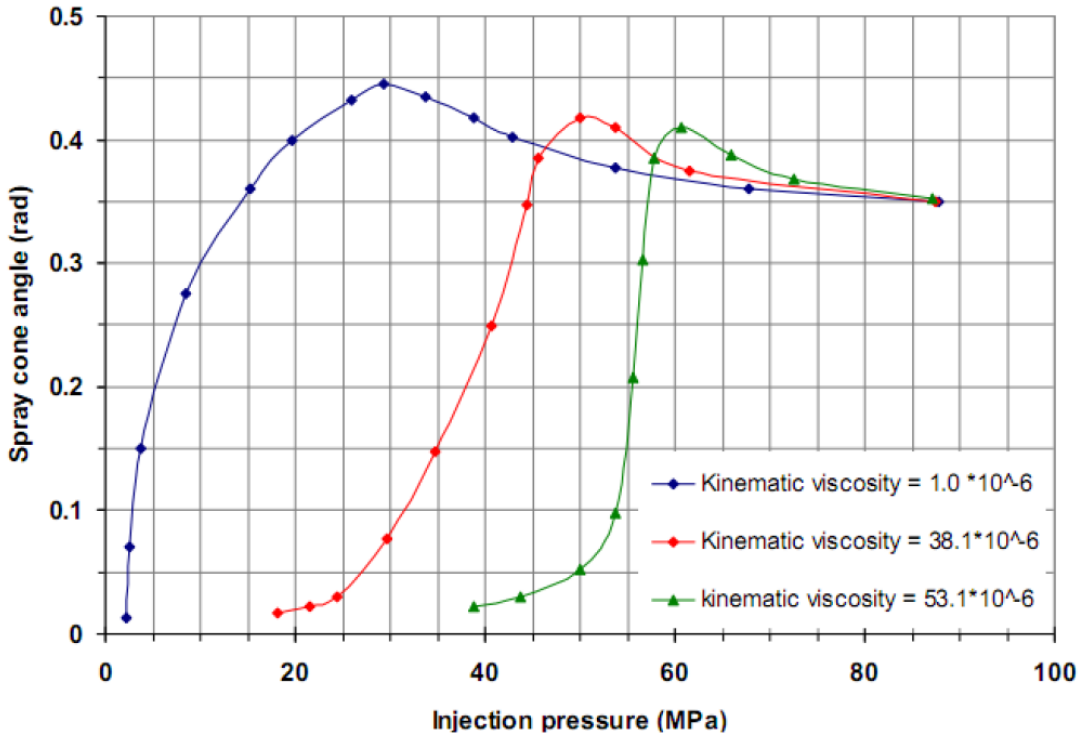

Figure 2-8: The effect of injection pressure and fuel viscosity on the spray cone angle [72]

2.6.4. Droplet Vaporization

Single droplet model describing heating and vaporization of spherically symmetric moving droplets have been carried out extensively since the first steady state model of a liquid droplet vaporization in a stationary gas environment by Spalding [92], more efforts have been made to introduce effective of convective heat and mass transfer between the droplet surface with gas when there is relative velocity between the droplet and the gas[93]. Hydrodynamic models that are widely used to predict droplet behaviour, progress has been continuously made through the years, Abramzon and Sirignano [94], Yal, Abdel-Khalik and recently Ghiaasiaan [95], Sazhin [96-98]. Models including both liquid phase models and gas phase models have been investigated and compared in terms of the trade-off between model accuracy and computational cost [96]. Models used to predict droplet heat and mass transfer in terms of the interaction with glow plug will be interpreted later in this section.

An introduction to droplet vaporization modelling has been presented in this section, materials used were primarily taken from [96, 99] where a detailed review regarding droplet heating and vaporization was included. The liquid phase model dealing with heat transfer in terms of droplet heating, suggested by Sirignano [100], the following classification of the models for heat transfer inside droplets, in the order of increasing complexity:

1. Models based on assumption that the droplet surface temperature is uniform and does not change with time;
2. Models based on the assumption that there is no temperature gradient inside droplets (infinite thermal conduction of liquid, the ITC models);
3. Models taking into account finite liquid thermal conductivity, but not the re-circulation inside droplets (conduction limit);
4. Models taking into account both finite liquid thermal conductivity and the re-circulation inside droplets via the introduction of a correction factor to the liquid therjal conductivity (effective conductivity models, the ETC models);
5. Models describing the re-circulation inside droplets in terms of vortes dynamics (vortex models);
6. Models based on the full solution of the Navier-Stokes equation;

The first group of models allows the reduction of the dimension of the system via the complete elimination of the equation for droplet temperature, although this group of models are widely used for the analytical studies of droplet vaporization and thermal ignition of fuel vapour/air mixture [101-103], however, this group of models are believed to be over-simplified for most practical engineering problems. Groups (5) and (6) have not been used and are not expected to be used in most of CFD codes due to their complexity. Groups (2-4) have been adopted in

most cases in engineering approximations or incorporated into CFD codes. The infinite thermal conductivity model, assuming no temperature gradient inside droplets so that droplet surface temperature can be found from the energy balance equation [96]

$$\frac{1}{3}\pi d^3 \rho_l c_l \frac{dT}{dt} = \pi d^2 h(T_{g\infty} - T_d)$$

Equation 2-21

This equation merely indicates that all the heat supplied from gas to droplet is spent on raising the temperature of the droplet and radiation plays no role in droplet heating, thermal radiation to droplet is small and decreases with decreasing droplet radius, it has a straightforward solution that is widely adopted, as shown in Equation 2-22, The ITC model has been extensively used and discussed in various applications in conjunction with the mass transfer equation in recent publications [104-109], and is also adopted in many CFD commercial code for heat transfer calculations, for instance, ANSYS Fluent [83].

$$T_d = T_{g\infty} + \left(T_{d0} - T_{g\infty}\right)\exp\left(-\frac{6ht}{c_l \rho_l d}\right)$$

Equation 2-22

Droplet vaporization can be understood as a process including two main phases as described in [96]:

1. Detachment of fuel molecules from the surface of the droplet into gas in the immediate vicinity of droplets (evaporation proper)
2. Diffusion of fuel vapour from the surface of droplet into the ambient gas

The first process has been ignored in the most engineering modelling by researchers due to its extremely complicated mathematical modelling and

the second process has been paid particular attention. The assumption has been made that fuel vapour in close proximity of fuel droplet surface is always saturated. Hence the rate of fuel vaporization is equal to the rate of fuel diffusion from the droplet surface to ambient gas. These are well known as the hydrodynamic models of droplet vaporization. While models which are taking into account of the first process are named kinetic models. Hydrodynamic model was used in this study to investigate droplet vaporization.

Vaporization rate or rate of diffusion from droplet surface can be expressed in Equation 2-23 that has been widely accepted [94, 96-99, 110].

$$\dot{m}_d = \pi \rho_g D_{Fa} d Sh_0 \ln(B_M + 1)$$

Equation 2-23

Where ρ_g is average density of vapour air mixture, D_{Fa} is binary diffusion coefficient of fuel vapour in air ($\overline{\rho_g}$ and D_{Fa} can be obtained following calculation presented in Appendices A and B in [98]). Sh_0 is non-dimensional number, Values for Sh_0 depend on the gas phase model selected. B_M is termed Spalding mass transfer number, is expressed in Equation 2-24.

$$B_M = \frac{Y_s - Y_\infty}{1 - Y_s}$$

Equation 2-24

Where Y_s and Y_∞ is the mass fraction of vapour at droplet surface and at large distances from the droplet respectively. Fuel mass fraction can be determined from saturation pressure on droplet surface which can be calculated using Clausius- Clapeyron equation [111]. For evaporating moving droplets, Sh_0 can be approximated [80, 112] below in Equation

2-25, the expression have been applied in many CFD codes, for instance, ANSYS Fluent [83].

$$Sh_0 = 2(1 + 0.3Re^{\frac{1}{2}}Sc^{\frac{1}{3}})$$

Equation 2-25

Where Re is Reynolds number; Sc, is Schmidt number.

2.7. Summary

The market share of diesel engine powered light duty passenger vehicles rose rapidly and currently account for more than 50% in Europe. This is due to reasons which include dramatic improvements in specific power and reduced emissions. This has been achieved by higher fuel injection pressures, flexible control of injection strategy, higher boost pressure using sophisticated turbocharger design, refined exhaust gas recirculation systems and development of engine downsizing. However, there remain areas in need of further improvement, particularly at reduced ambient air temperatures during engine cold idling and warming up. Recent investigations indicated using multi-pilot strategy and high temperature glow plug are effective approaches to mitigate these problems. Increasing number of pilot injections means reduction in the main injection if total fuelling level is the same, this will sacrifice idle speed control which is mainly achieved through main injection. The use of the glow plug becomes essential and a deeper understanding of the role of the glow plug and parameters influencing its function is urgently needed. In this thesis, the role of the glow plug will be explored experimentally using a single cylinder engine unit and an optical vessel, CFD simulation will also be used to understand interactions between the glow plug and the diesel spray.

Chapter 3 Test Facilities, Data Acquisition and Simulation Models

3.1. Introduction

In this chapter, rig setup and data processing for engine tests and optical tests are described, key variables are identified, and simulation models used in ANSYS Fluent are introduced.

Experimental facilities used for engine tests which are described in Chapter 4 have been introduced. This covers the specification of the single cylinder test engine, rig setup, injection control, instrumentations and data acquisition as well as test procedure are included. To investigate the influence of the glow plug on engine cold performance, a cooling system capable of chilling engine operating temperature down to sub-zero has been used. ATI version software was used to control injection parameters and communicate with engine ECU. Temperatures, pressures, crankshaft positions were monitored and recorded by a dSpace modular hardware system and post-processed using Matlab software. Key response variables converted from experimental values taken as in-cylinder data have been introduced, heat release rate, stability indicator and gross indicated mean effective pressure have been mathematically derived. An optical investigation has been performed in Chapter 5 to explore the process of combustion initiation. An optical vessel has been used combined with a high speed camera. Rig setup and data processing has been introduced in section 3.4. Spray models used in ANSYS Fluent 14.0 are depicted in section 3.5.

3.2. Engine Setup

3.2.1. Single Cylinder Rig

The single cylinder rig as shown in Figure 3-1 has been used to carry out experiments investigating the role of the glow plug at cold start and idling. Using a single cylinder eliminates interactions between cylinders which might influence gas exchange characteristics and a smaller capacity of cooling tower and dynamometer can be used, and additionally, the simplicity of the rig offers ease of accessibility and maintenance. This engine is a Hydra unit manufactured by Ricardo and the piston assembly, cylinder head and crankshaft were taken from a Ford 2.2 Puma upgraded DI diesel engine. The test facility has been used in several earlier studies by various researchers[3, 4, 40]. Specifications for this single cylinder DI diesel test engine including information of injection system is given in Table 3-1. An 8-hole piezo-electric injector was provided as part of HPCR fuel injection equipment, which is capable of 6 reliable injections per cycle under high pressure of 2000 bar. Carcal 740-B5-A diesel fuel was used in the engine tests (Chapter 4) and the optical studies (Chapter 5), properties are given in Table 3-2.

Figure 3-1 Single cylinder rig

Table 3-1: Specifications for single cylinder unit

Bore	86 mm
Stroke	94.6 mm
Displacement	0.55 litre
Compression ratio	15.5:1
Injection system	2000 bar Bosch high pressure fuel pump, common rail, centrally mounted piezo-electric injector with 8 holes (120μm diameter)
Valves	4 per cylinder, 2 intake/exhaust
Swirl ratio	1.5

Table 3-2: Fuel properties

Property	Unit	Spec Min	Spec Max	Result	Method
Cetane Number		52	54	54	ASME D613
Cetane Index		50		54.7	ASME D4737
Density at 15ºC	g/ml	0.833	0.837	0.8331	ASME D4052
Viscosity at 40º	mm2/sec	2.3	3.3	2.6	ASME D445
Gross Calorific Value	MJ/kg			44.58	IP12
Net Calorific Value	MJ/kg			41.73	IP12

The engine is mounted on a test bed and connected to a David McClure swing frame DC dynamometer with rated capacity of 60Kw at 4500rpm. The rotational speed was controlled by a Control Techniques Mentor II DC drive unit, which is able to keep constant speed against varying engine torque through the cycle.

3.2.2. Rig Setup and Injection Control

The self-regulated glow plug with a tip diameter of 4.5mm capable of surface temperature of 850°C has been used on the single cylinder engine unit in the experiments. In separate optical investigation of which reported in Chapter 5, a ceramic type glow plug has been used on the combustion bomb in the optical studies. Power source for the glow plug, ECU and current clamp was a 12 V battery connected to a trickle charger. In order to achieve cold test conditions, a F+R VP45WC chiller was used to chill the coolant, 50/50 mixture of water and BS6580 ethylene antifreeze, capable of chilling down to -30°C. In practice, coolant was circulated around the engine to chill the engine down. The fuel was directly chilled by using a radiator with coolant circulating it. Coolant also flows around the fuel rail to ensure low fuel temperature throughout fuel delivery to injector. Oil was also kept chilled by flowing around the engine. An 80 litre plenum

before the intake manifold was chilled using an atmospheric cooling radiator to provide a reservoir of low temperature intake air. Coolant flows through a water jacket around the intake manifold to keep low air temperature. To remain low temperatures, insulating jackets were placed over the engine.

A Watlow Industries 3 kW immersion heater was used to directly increase the temperature of the coolant fluid, and two Eltron Chromalox sump mounted heaters for the oil after a day of testing. Due to lacked heat produced from the single cylinder engine compared to complete engine setup, heaters are necessary to offer heat to assist the single cylinder to achieve typical warm operating conditions. A Carter M3 series cooling tower was used for heat rejection other than a radiator. A schematic of the coolant system layout is presented in Figure 3-2. When cold tests are running, cold circuit valves switched on, coolant comes out from engine, flows into chiller and flows back to engine. When hot tests are running, hot circuit valves switched on, coolant comes out from engine, flows into cooling tower and flows back to engine.

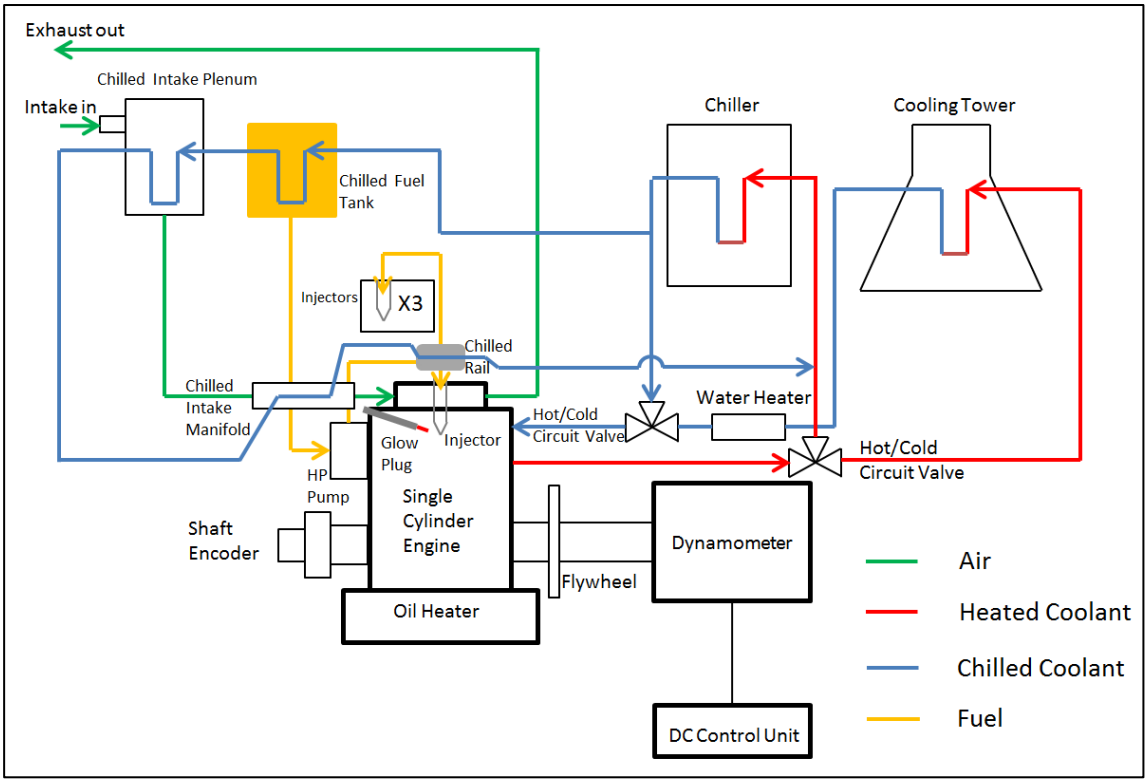

Figure 3-2: Cooling system layout

ATI vision software which is an integrated calibration and data acquisition tool that collects signals from the engine's ECU. Control of injection parameters such as injection strategy including injection timing, separation, number of injections, injection quantity and rail pressure was achieved by using the software. Because there is only one cylinder, so injection quantity denoted in ATI in mg/stroke refers to mass of fuel injected per cylinder per cycle in unit of mg.

3.2.3. Instrumentations and Data Acquisition

Intake air, exhaust air, coolant, fuel and oil were monitored using sheathed TC limited K-type Chomel-Alumel thermocouples. Those thermocouples were calibrated from temperature of 0ºC in a crushed ice water bath and up to 100ºC in a thermostatic oil bath with 10ºC interval to ensure sufficient accuracy and operating range. Thermocouple which measured exhaust temperature was specially calibrated up to temperature of 300ºC.

Pressure monitoring was achieved using various pressure transducers mounted around engine. Engine in-cylinder pressure was measured using a Kistler 6125B quartz pressure transducer with high measurement accuracy rated at peak pressure of 250 bar. This pressure transducer was selected also because its high resistance to thermal shock. A Kistler 5011 charger amplifier was connected to this transducer to amplify signal to range of 0-10V. This type of sensor is piezo-electric, therefore signal drifts with little or no change in pressure. Hence, the signal was referenced at bottom dead centre (BDC) of intake stroke with signal from the intake manifold pressure transducer to give a baseline. The Kistler transducer (to measure in-cylinder pressure) was calibrated using a Budenberg deadweight calibration bench to 0.05% accuracy. A Kulite pressure transducer capable of measuring pressure up to 2200 bar was used to measure fuel rail pressure. Similarly, aims to input signal within range of 0-10V so that dSpace data acquisition system can process, a Kulite amplifier was used to amplify signals from this transducer. A 7 bar Kulite pressure transducer monitored oil pressure, along with two 4 bar Kulite transducers for intake and exhaust manifold pressures. These transducers output signals to in-house amplifiers (0-10 V) and then input to the dSpace system. All these pressure transducers were calibrated using the Budenberg hydraulic deadweight calibration bench.

A Hohner Automation optical shaft encoder capable of 0.5º CA resolution was used to firstly, monitor crankshaft position, and secondly to trigger data acquisition since TDC signal was required to initiate various in-cylinder calculations. Output one digital pulse every half degree means 720 pulses per revolution and 1440 pulses per cycle were received by data acquisition. Small errors in TDC measurement can result in large calculation errors in IMEP [113] so that an accurate measurement was needed. An AVL 402 dynamic probe was used to align piston top dead

centre (TDC) with encoder TDC marker. The shaft encoder was set to within 0.2º CA compared to TDC measured using AVL 402 dynamic probe.

A dSpace modular hardware system was used for data acquisition from the engine sensors and for engine control. The unit consists of three A/D boards, a Control Area Network (CAN) board and a single processor that runs the uploaded Simulink model. The time trigger boards were used to capture data at various sampling rate. The hardware triggered boards allow data at crank angle resolution and the A/D converter boards that were used to convert analogue signals to digital signals. Engine variables that were captured using various sensors were processed in Simulink model and displayed on screen for users to monitor. Data monitored were also recorded for post-processing using MatLab. Communications among engine, dSpace and ECU are illustrated in Figure 3-3.

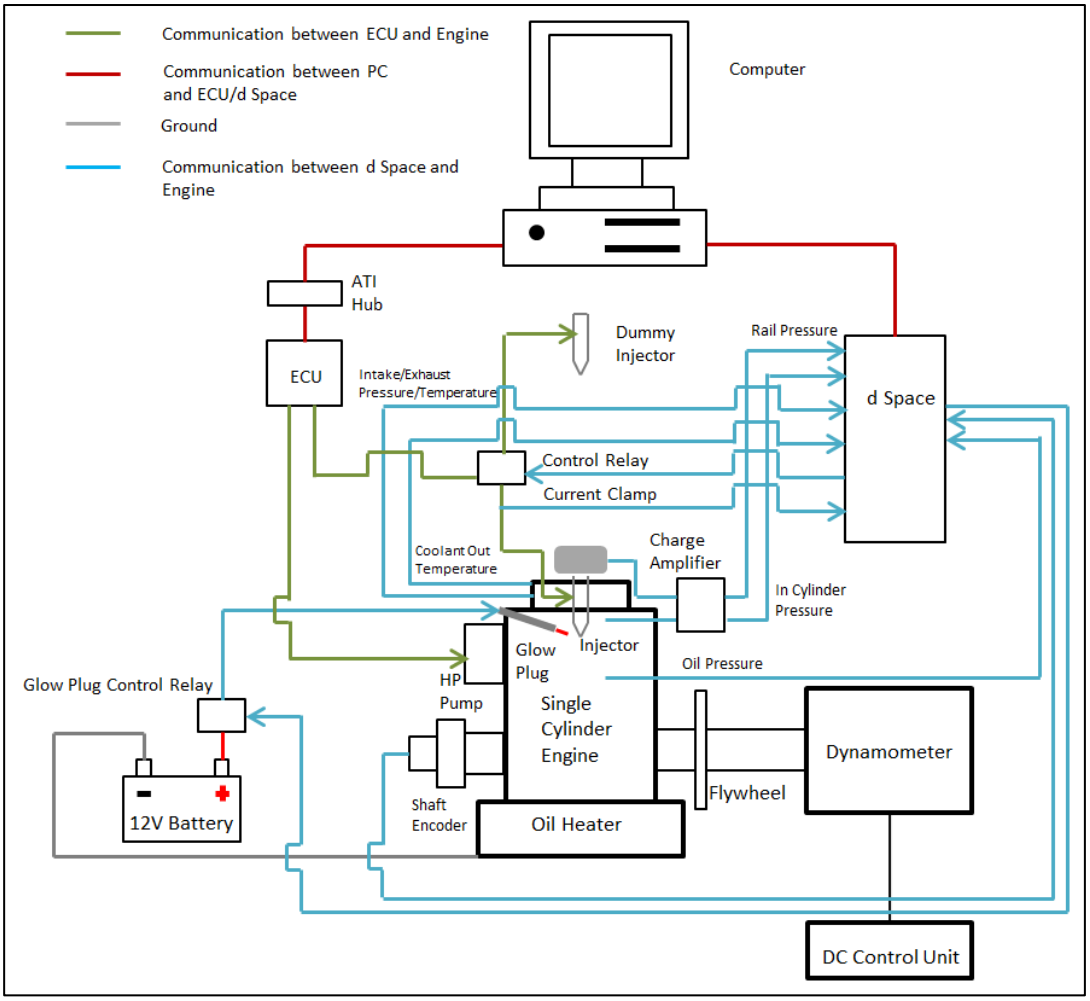

Figure 3-3: Electrical signal communication illustration

3.2.4. Test Procedure

The test was planned on daily base. In order to achieve target engine temperature, engine was soaked for 3 hours at the start of the day. The engine- out coolant temperature monitored has been defined as engine test temperature. Test procedures can be summarized as below:

1. Program ATI for the desired injection strategy and rail pressure.
2. Turn on glow plug (if needed) for a pre-glow period of 7.5s and remained on during test.
3. Start dynamometer, engine was motored for 15 cycles. The purpose was to ensure both engine speed and rail pressure achieved target and stabilized during test.

4. Engaged fueling on the 16th cycle and continued for 40 consecutive cycles.
5. Motored engine after end of test for 2 minutes to draw purge air through the cylinder.
6. Ran fully warmed conditioning tests to maintain repeatable cylinder conditions for subsequent tests.
7. 3 tests were run at same condition. 15 minutes interval between tests to allow the engine returns to cold state condition. The last two repeat tests. Results of all three tests were presented in same figure to show consistency of experimental outputs.
8. Adjust soak temperature to target, starts test after engine test temperature achieved target temperature and maintained.
9. At end of the day, turned on oil heater and coolant heater, ran the engine around 45 minutes under fully warm operating conditions. The purpose was to clean the engine of any potential soot build-up, fuel impinged on the cylinder walls and potential water and ice build-up. Due to the cold conditions and poor combustion efficiencies at cold temperatures, the oil and oil filter were changed on a weekly basis to avoid significant build-up of fuel that could potentially negatively affect the lubricating properties.

MacMillan [3] suggested that 20 tests per day are feasible with the conditioning technique employed, after which stability decreases in the peak compression pressure before injection on this engine. McGhee [4] recommended 15 tests per day on this engine showed good repeatability and allowed for a sufficient amount of data collection witout sacrificing accuracy of the results. In this investigation, maximum tests number of 15 per day was accepted.

3.3. Key Response Variables for Engine Tests

Various temperatures, pressures, engine speed were monitored throughout experiment. Two key variables are of particular importance in terms of analyzing engine performance. The first one is Indicated Mean Effective Pressure (IMEP). IMEP is defined as the work per cycle per unit of swept cylinder volume, so it is used as a parameter that allows comparing engine performance regardless of engine displacements. Similar to indicated work, IMEP was categorized to gross IMEP (IMEPg) and Net IMEP (IMEPn) [37]. IMEPn refers to work delivered to the piston over the entire four stroke cycle per unit of cylinder swept volume; IMEPg refers to work delivered to the piston over compression and expansion stroke per unit of cylinder swept volume. The difference is the pumping work between intake stroke and exhaust stroke. IMEPg is more suitable to be used as an indicator to measure the engine performance since combustion variations in cylinders cause wave motion in intake and exhaust pipes that leads to potential cycle-by-cycle fluctuations in pumping work. And as emphasized in [4], the pumping work in practice was small and trends in net and gross IMEP data were very similar. The second key response variable is heat release rate. Heat release rate is defined as the rate at which the chemical energy of the fuel is released into sensible internal energy. Net heat release rate will be used here. Net heat release rate equals the rate at which work is done on the piston plus the rate of sensible internal energy of the cylinder contents. Both two key response variables are derived from in-cylinder pressure that measured by Kistler 6125B quartz pressure transducer. IMEPg and GHRR will be derived and explained in the following sections.

3.3.1. Indicated Mean Effective Pressure

IMEPg is the work done on the piston covering period from BDC at intake stroke to BDC at expansion stroke divided by swept volume. IMEPg can be

expressed by Equation 3-1. Volume in the cylinder at any time in the cylinder is required to solve this integral.

$$IMEPg = \frac{\int_{BDC_{intake}}^{BDC_{expansion}} pdV}{V_s}$$

Equation 3-1

Heywood [37] introduced a method to calculate the cylinder volume at any crank position θ. The angle θ that is defined in Figure 3-4, the connecting rod stroke can be related to twice of crank radius. The cylinder volume V at any crank position θ can be expressed in Equation 3-2.

$$V = V_c + \frac{\pi B^2}{4}(l + a - s)$$

Equation 3-2

Where V_c is the clearance volume. And s can be expressed in Equation 3-3.

$$s = acos\theta + \sqrt{(l^2 - a^2 sin^2\theta)}$$

Equation 3-3

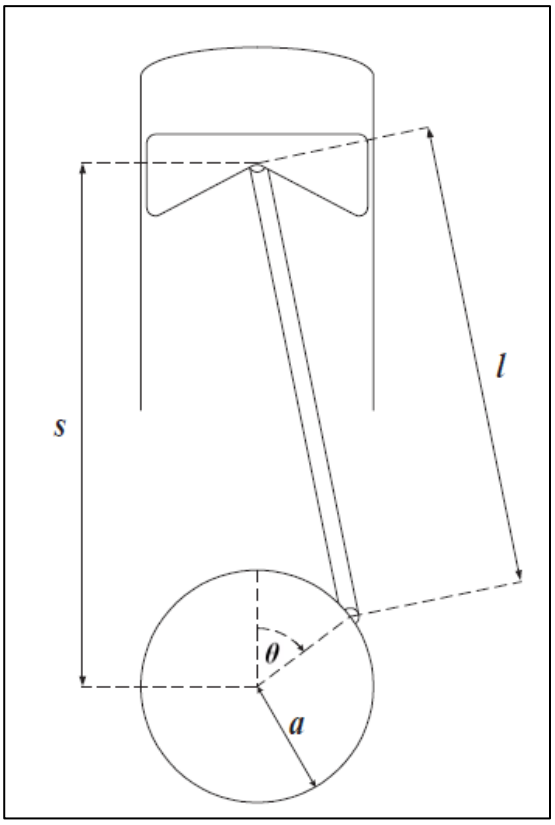

Figure 3-4: Geometry of cylinder, piston, connecting rod, and crankshaft where s is distance between the crank axis and the piston pin axis, L=stroke, l=connecting rod length, a=crank radius, θ is crank angle

3.3.2. Combustion Stability Indicator

Coefficient of variation in IMEPg (CoV_{IMEPg}) was used to indicate cycle-by-cycle variability in combustion work output, as accepted in literature [114-116], defined as ratio of standard deviation of IMEPg to mean value of IMEPg over total fired cycles. Since 10 cycles were investigated in this study, $StD_{IMEPg40}$ is expressed in Equation 3-4.

$$StD_{IMEPg10} = \sqrt{\frac{1}{n-1}\sum_{i=1}^{10}(IMEP_{g,i} - IMEP_{fit,i})}$$

Equation 3-4

Although tests were continued for 40 firing cycles, the data used in this study was restricted to the first 10 of these. Over a larger number of

cycles, the effects of surface temperature and fuel accumulation in the combustion system are increasingly significant. The extension of the test run aided the detection of any test problems and contributed to conditioning the engine for later tests.

CoV_{IMEPg} is expressed in Equation 3-5.

$$CoV_{IMEPg} = \frac{StD_{IMEPg10}}{\overline{IMEPg}} \times 100$$

Equation 3-5

Where $\overline{IMEPg}$ is mean value of IMEPg over the first 10 fired cycles.

3.3.3. Heat Release Rate

In engine investigation reported in Chapter 4, net heat release rate is analyzed. The first law of thermodynamics was used to derive net heat release rate as shown in Equation 3-6.

$$\frac{dQ_{net}}{d\theta} - p\frac{dV}{d\theta} + \sum_i \dot{m}_i h_i = \frac{dU}{d\theta}$$

Equation 3-6

Where $dQ_{net}/d\theta$ is the heat transfer rate across the system boundary into the system, $pdV/d\theta$ is the rate of work transfer done by the system due to system boundary displacement, $\dot{m}_i$ is the mass flow rate into the system across the system boundary at location i, h_i is the enthalpy of flux i entering or leaving the system and U is the energy of the material contained inside the system boundary. For the single cylinder engine which employs direct injection system, to be considered as a single open system, the only mass flows across the system boundary while intake and exhaust valves are closes is fuel and crevice flow. The occupied volume compared to cylinder volume is too small so that can be neglected, and Equation 3-6 becomes Equation 3-7.

$$\frac{dQ_{net}}{d\theta} = \frac{dU}{d\theta} + p\frac{dV}{d\theta}$$

Equation 3-7

The apparent net heat release rate, $dQ_{net}/d\theta$, which is the difference between the apparent heat release rate and the heat transfer rate to the walls equals the rate at which work is done on the piston plus the rate of change of sensible internal energy of the cylinder contents.

The sensible internal energy U can be expressed in Equation 3-8.

$$\frac{dU}{d\theta} = mC_v\frac{dT}{d\theta}$$

Equation 3-8

From the ideal gas law where

$$pV = mRT$$

Equation 3-9

Differentiate in terms of θ, Equation 3-9 becomes Equation 3-10.

$$\frac{d(pV)}{d\theta} = mR\frac{dT}{d\theta}$$

Equation 3-10

Substitute Equation 3-8, Equation 3-10 into Equation 3-7, we have Equation 3-11.

$$\frac{dQ_{net}}{d\theta} = p\frac{dV}{d\theta} + \frac{C_v}{R}\frac{d(pV)}{d\theta}$$

Equation 3-11

After rearrangement, Equation 3-11 becomes Equation 3-12, replace C_v/R in terms of γ which is ratio of specific heats: C_p/C_v . Equation 3-12 becomes Equation 3-13.

$$\frac{dQ_{net}}{d\theta} = \left(1 + \frac{C_v}{R}\right)p\frac{dV}{d\theta} + \frac{C_v}{R}V\frac{dp}{d\theta}$$

Equation 3-12

$$\frac{dQ_{net}}{d\theta} = \left(\frac{\gamma}{\gamma - 1}\right) p \frac{dV}{d\theta} + (\frac{1}{\gamma - 1}) V \frac{dp}{d\theta}$$

Equation 3-13

It has been shown in equation (3.13) that net heat release rate is calculated from instantaneous in-cylinder pressure, cylinder volume and γ. In-cylinder pressure was measured at 0.5º CA resolution and cylinder volume was calculated based on method described in section 3.3.1. Value of γ depends on charge temperature and composition can be correlated to charge temperature that was calculated using perfect gas law given that in-cylinder pressure and cylinder volume are known. Brunt and Platts [117, 118] proposed a correlation expressed in Equation 3-14 that followed previous work [119] offer good accuracy over wide range of charge composition for diesel engine operation.

$$\gamma = 1.44 - 1.2 \times 10^{-4} T + 10^{-8} T^2$$

Equation 3-14

3.4. Rig Setup and Data Processing for Optical Vessel Tests

Process of combustion initiation is difficult to be studied using the engine rig because it occurs before the pressure becomes measurable. To explore the criteria for successful combustion initiation, an extension of the investigation has been carried out by using a quiescent combustion bomb with optical access; the work will be covered in Chapter 5.

3.4.1. Optical Test Facilities and Data Processing

The initiation and early development of combustion was investigated. Test facilities and data acquisition are described in this section. Studies of initiation by glow plug were carried out using an unstirred, quiescent combustion bomb. The volume of the bomb is large compared to the clearance volume of the engine cylinder. This has optical access through a

quartz window giving a view normal to the plate in which the injector and glow plug were mounted. The spacing between the injector and glow plug was the same as in the engine. The internal volume of the bomb is roughly cylindrical with a length of 190mm and a bore of 100mm. This is large compared to the clearance volume of the engine, and the bomb is used here only to examine the initial development of combustion which effectively takes place at constant pressure. The experimental facility is shown schematically in Figure 3-5. The same design of HPCR fuel injection system and Continental fuel injector was used as employed on the engine. The injector was of the piezo-electric type, with 8 nozzle holes. The holes have a diameter of 120μm.

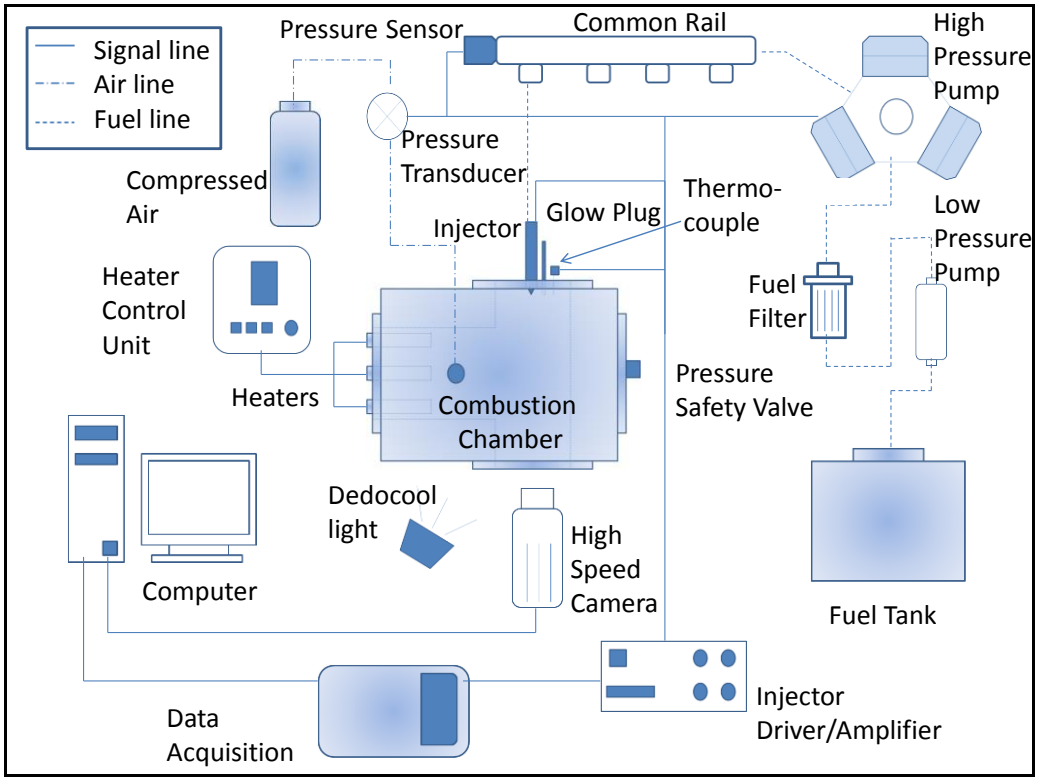

Figure 3-5: Schematic of the rig architecture

The ECU has been replaced by a USB-6351 X- series Data Acquisition system (DAQ) which acquires data from various sensors as shown in Figure 3-6, National Instruments' LabView codes were programmed to control and monitor experimental parameters. Pressure of the fuel as well as the injection parameters (duration and timings) were controlled in a

PID modular installed in LabView software, Adjustments are made by Pulse Width Modulation (PWM) signal that sent from DAQ to Pressure Control Valve (PCV) on the high pressure pump to regulate fuel pressure to stabilize at a target set point, 400 bar in this study. PWM signal was sent from DAQ to injector to control injector opening/closing. Injector nozzle opening time that represented by duty cycles of PWM signal, which controls opening time of injector nozzle for each injection quantity were calibrated.

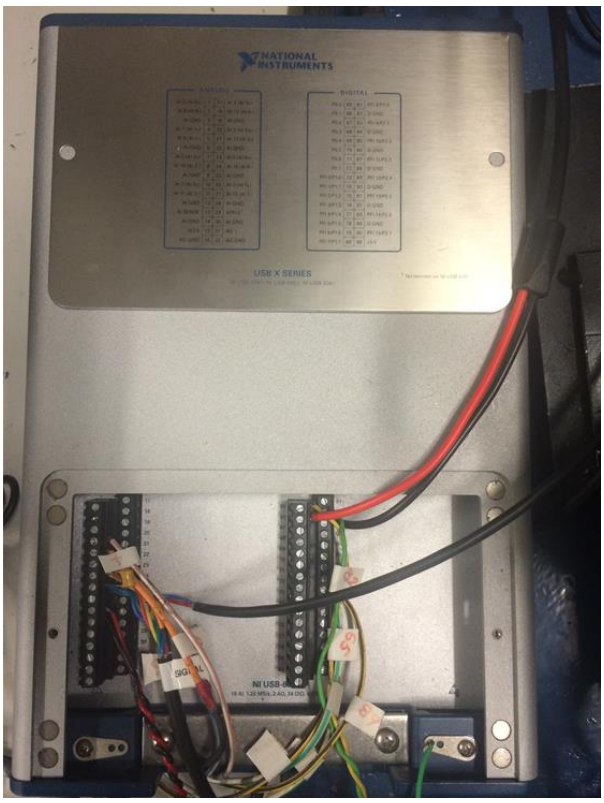

Figure 3-6: USB-6351 X-series DAQ system

Calibration experiment was carried out to work out the relationship between injection duration and fuel mass injected. Fuel was collected in a cotton wool filled container to trap spray mass injected from injector. Mass of container was weighted using an Oertling scales, accurate to 1/10000th of a gram before and after collecting fuel mass. The mass was then divided by the total number of injections, giving a mass per injection.

Calibration was carried out covering various injector nozzle opening time that was controlled via LabView code, as shown in Figure 3-7.

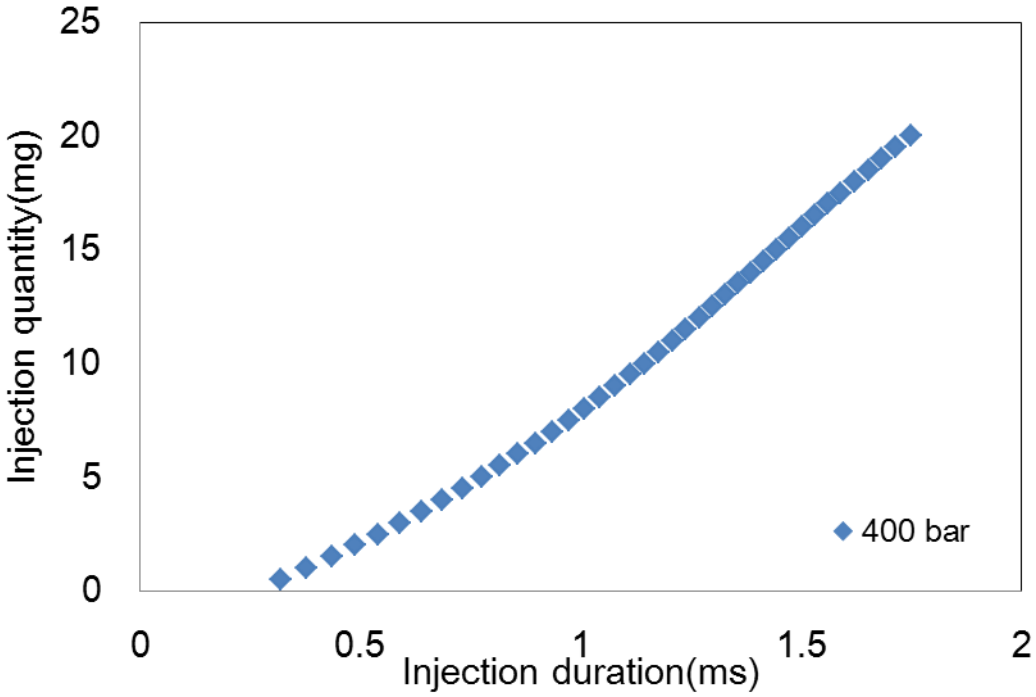

Figure 3-7: Injection flow characteristics calibration at a rail pressure of 400bar

Pressure in combustion bomb was raised by compressing fresh air. A maximum limit of 75 bars piezo- resistive Kulite pressure transducer was calibrated to measure vessel pressure and monitored via LabView software. A 50 bar safety valve was installed to release excessive compressed air for safety concern. Three Watlow cartridge heaters with closed loop temperature control were used to heat the air in the combustion bomb. They each provided 350W of heat input, allowing the maximum bulk air temperature to reach just over 200ºC. The conditions created inside the bomb were not fully representative to those in an engine due to the large volume, but low temperature, quiescent environment is ideal to look insight the combustion initiation and early stage development. K- Type thermocouples were utilized to measure bulk air temperature. Position of thermocouple tip is adjustable so that temperature of air near glow plug

can be measured. Ceramic type glow plug manufactured by Beru with 3.3 mm tip diameter for research was used in the optical studies, temperature of this type of glow plug is controllable by voltage supplied, glow plug tip surface temperature is controlled at desired level throughout tests. The surface temperature was related to this internal temperature through calibration experiments conducted separately in quiescent air with a thermocouple in good contact with the surface, as shown in Figure 3-8. Typically the surface temperature was about 100ºC lower than the core temperature of the glow plug. An R-type thermocouple is embedded into the glow plug tip to output the core temperature. All experimental settings were monitored via the LabView software.

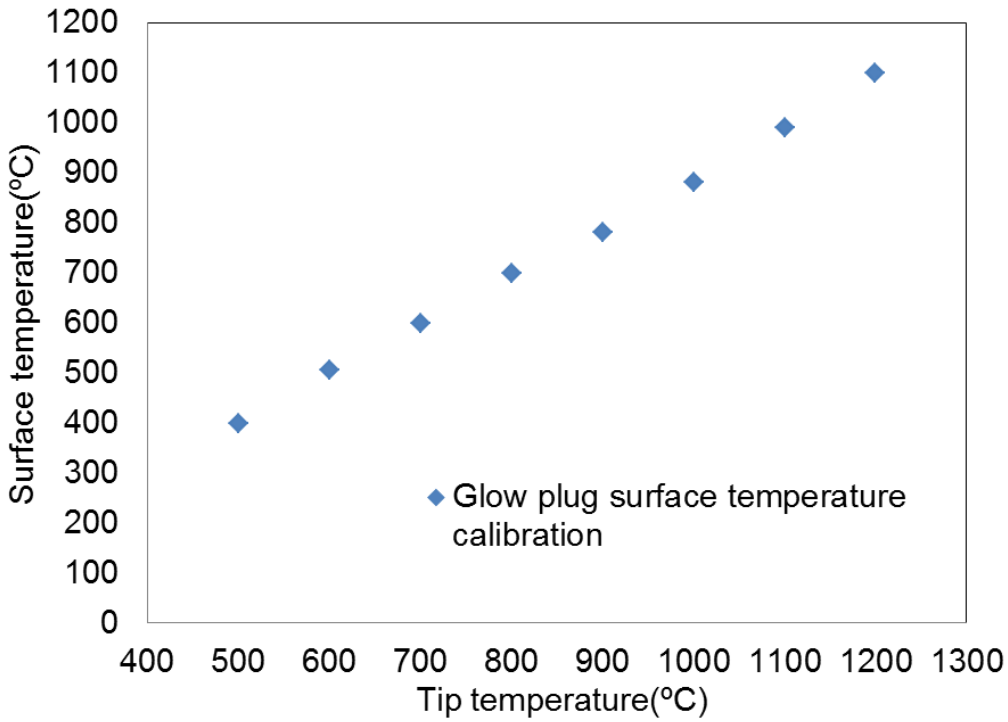

Figure 3-8: Calibration of glow plug surface temperature versus internal tip temperature

A CAD drawing showing the key dimensions is given in Figure 3-9, in this setup, fuel is delivered in eight sprays but only the two sprays passing nearest to the glow plug, one to each side, are capable to be ignited. To

investigate influence of glow plug-spray proximity on ignition, a plate was designed and manufactured to allow the injector to rotate around its longitudinal axis, incorporating graduation marks to measure angular rotation as has been shown in Figure 3-10.

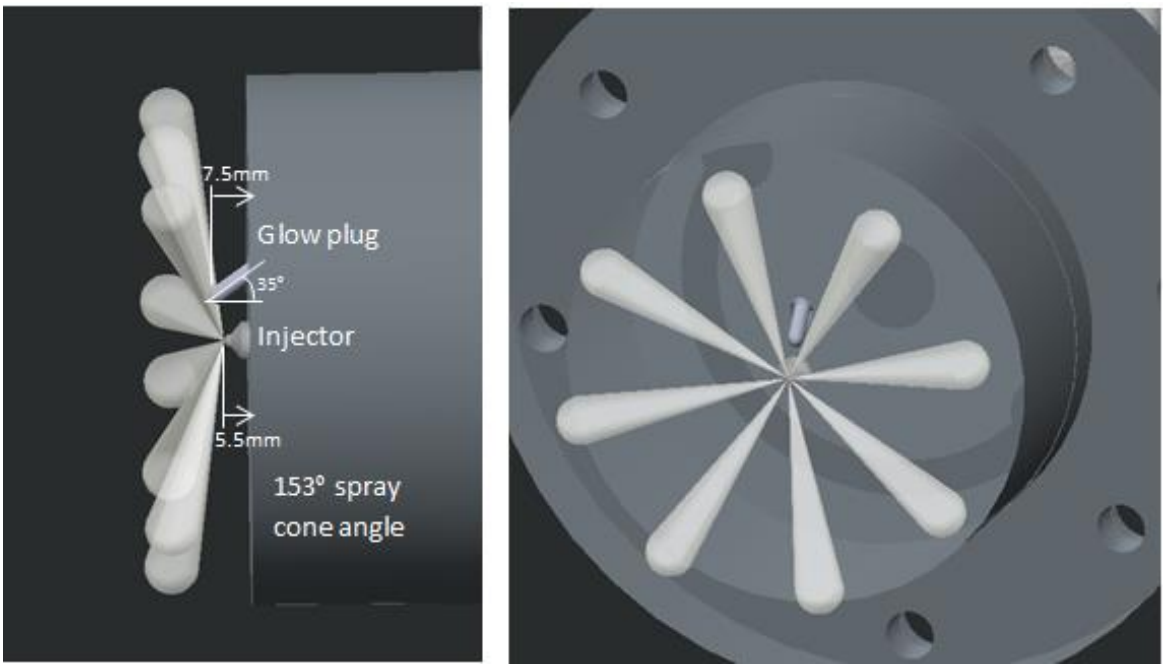

Figure 3-9: Key dimensions showing configurations among spray, glow plug and injector

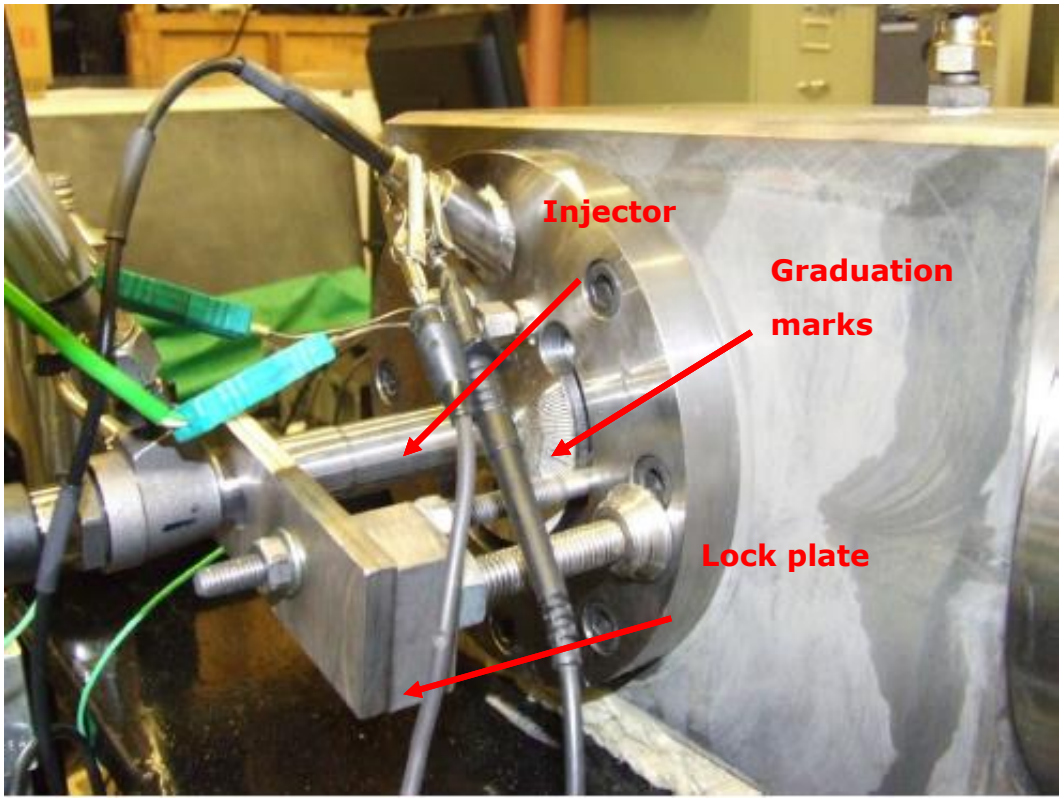

Figure 3-10: plate was designed and manufactured to allow the injector to rotate around its longitudinal axis, incorporating graduation marks to measure angular rotation

The injector could be rotated through a small angle to vary the distance between the glow plug surface and the two adjacent fuel sprays. A standard procedure is followed, loose the lock plate by losing the nut which pushes the lock plate, carefully rotate the injector to the desired angular position which is confirmed by the graduation mark, at last, tighten the nut to fix the lock plate.

The distance between the visible edge of the nearest fuel spray and the glow plug tip was determined from a CAD model of the installation and verified by the analysis of video images. In this study, the distance between the glow plug tip surface and visible edge of the spray was measured from 3D CAD model. 3D measurement of the distance was taken from a CAD model created using Creo 2.0 software, the dimension of the bomb, injector, glow plug are consistent with experimental setup. 3D measurement has been verified by comparing to 2D measurement

where the distance between the glow plug and visible edge of the spray was scalded based on tip diameter of the glow plug, as shown in Figure 3-11 and Figure 3-12.

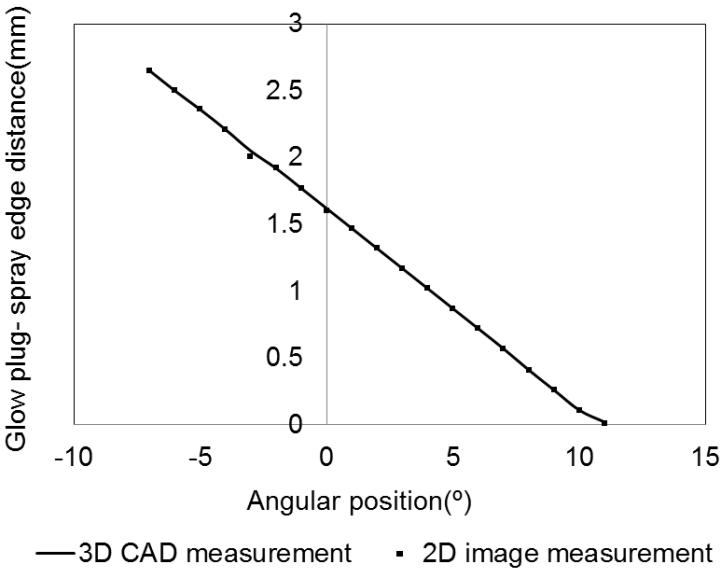

Figure 3-11:2D and 3D measurements for glow plug to spray edge distance

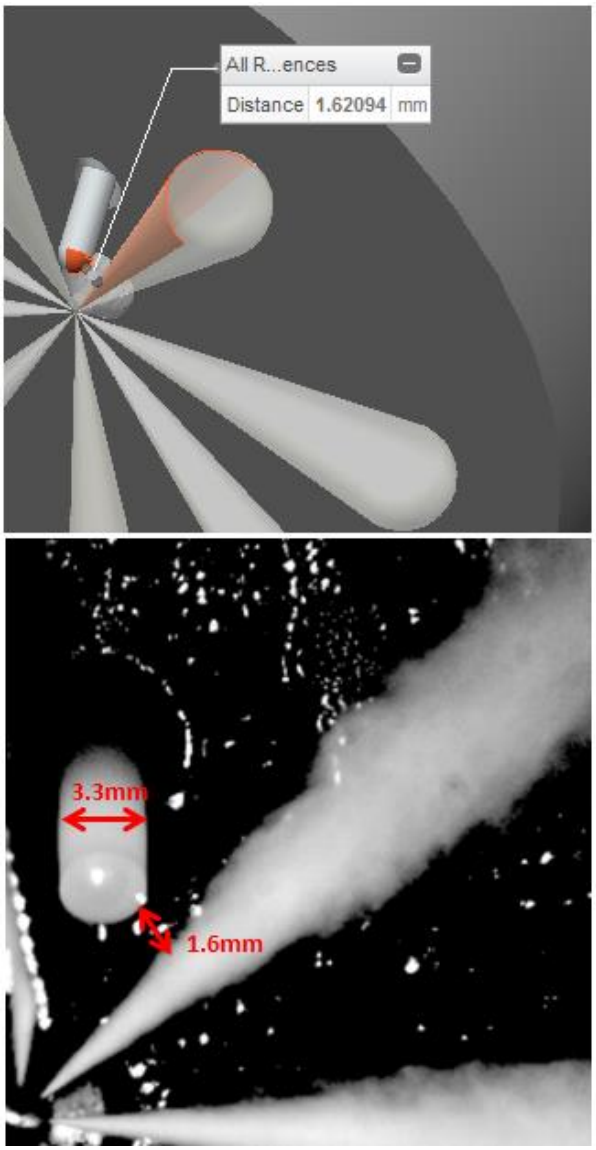

Figure 3-12: 3D and 2D measurements of distance between the glow plug tip surface and visible spray edge, conditions: bulk temperature=200°C, glow plug surface temperature=900°C, pressure=38 bar, rail pressure=400 bar

A LabView code was programmed to monitor the signals in real time. For the image acquisition system, The camera used was a Phantom V12.1 CMOS high speed camera capable of 6,242 frames per second at a maximum resolution of 1280x800 pixels, camera was set up with fixed focal length, 105mm with an aperture of f/3.5 and exposure time of 100 µs, which allowed sufficient luminosity of the combustion even whilst provided a good depth of field. A 5V TTL signal was sent to the camera from the DAQ to provide a rising edge to trigger the camera. To

compensate dark view attributed relatively smaller aperture, and also provide a clearer view for observation of spray, one dedocool tungsten light was used to illuminate the area of interest.

3.4.2. Luminous Natural Flame

It is well known that some natural flame emission occurs prior to the first detectable combustion induced pressure rise and some natural flame emission occurs prior to this time. Natural light emissions during diesel combustion are due to chemiluminescence and soot luminosity. Both techniques were widely used to research combustion, providing a convenient, nonintrusive measure of transient combustion phenomena[4]. Chemiluminescence is a process that releases relatively weak natural light emission. This emission arises from specific molecules that are raised to an excited state by exothermic chemical reactioins and then subsequently decay back to equilibrium energy levels by emitting a photon[120]. Chemiluminescence emission occurs in specific wavelength bands that are characteristic of the emitting molecules that responsible for the chemiluminescence change for different combustion regimes and provide information about the nature of the reactions and the fuel air mixture[121]. Chemiluminescence emission therefore indicates spatial and temporal information of early reactions during diesel autoignition[120]. However, chemiluminescence signal is too weak to be captured by conventional high speed cinematography, moreover, signals appear in non-visible wavelengths, intensified devices and additional filters are required in the set up. The other commonly used optical diagnostics is soot luminosity. This soot luminosity arises from the thermal or 'grey-body' temperatures by the combustion process. Although chemiluminescence continues to occur throughout the combustion event, the intense yellow emission from the soot dominates over the weaker chemiluminescence once soot formation is underway[120, 122]. This strong luminosity appears in visible range of wavelengths, and much easier to be detected by using

conventional high speed cinematography. The initial rise of soot luminosity generally correlates to some degree with the pressure-indicated ignition timing[120]. Soot luminosity imaging has been widely used to investigate diesel combustion in early time [37, 123], some also attempted to use luminosity imaging to gain insight into the location and timing of diesel autoignition [37, 124-126]. More recently, soot luminosity were used to investigate diesel combustion at cold condition using a glow plug [4, 9]. The soot luminosity imaging technique has been used in this investigation, luminous soot emissions were used to provide an indication of reaction sites.

3.5. Spray Models Used in ANSYS Fluent 14.0

A detailed CFD investigation on factors influencing spray vaporization will be presented in Chapter 6. Fuel vapour- air equivalence ratio should be above a minimum level to produce a positive IMEPg if gas temperature is above threshold, however, both engine test and optical test could not reveal information relating to mixture composition, ANSYS Fluent 14.0 has been therefore used and models for spray injection is described in following sections.

3.5.1. Discrete Phase Model

CFD has been used to investigate the local droplet vaporization in the vicinity of the glow plug. A mesh containing a number of control volumes or cells is used to provide the finite approximation for the spatial domain, the transport equations are solved using such a mesh for the fluid phase is termed an Eulerian approach. Lagrangian approach, as used in this study to track the moving particles.

The Lagrangian discrete phase model in ANSYS Fluent follows the most widely used Euler- Lagrangian approach[83, 127], the gas has been modelled using an Eulerian coordinates and diesel spray has been modelled into computational parcels, each contains a certain number of

droplets, are described by Lagrangian coordinates. The dispersed liquid phase (droplets) can exchange momentum, mass and energy with the fluid phase. Single component $C_{10}H_{22}$ was used to represent light diesel fuel [128, 129] in this study. In the discrete phase model, two-way coupling of the phases and droplet collision and coalescence are enabled, the spray origin, spray direction, initial fuel temperature, nozzle diameter and mass flow rate are prescribed.

3.5.2. Turbulence Model

The spatially symmetric spray that penetrates into a non-convective, quiescent environment has been modelled. Turbulence is present as the high speed spray is introduced. The standard k-ε model in ANSYS Fluent was used with default settings to solve two separate variables, the turbulent Kinect energy k and its dissipation rateε. Standard k-ε model was chosen because it is known to yield reasonably realistic predictions of major mean-flow features in most situations including fuel spray injection into quiescent environment [130, 131].

3.5.3. Injection Model

The injection model used in this study is a solid cone injection model in ANSYS Fluent. The model requires a spray cone angle, the direction of the injection as well as the coordinates of the point where the injection initiates is defined, the direction of a droplet to be injected into the domain is then calculated by multiplying the spray cone angle and a random number with value between 0 and 1, this angle obtained is the angle between the direction of the droplet injected and the direction of the set spray. The spray cone angle has been measured in high speed image recording the spray penetration, as shown in Figure 3-13, the spray cone angle measured in this study was 16^{o},as has been reviewed in section 2.5.3, spray cone angle is influenced by the gas temperature, however, in this study, where the pressure difference between the rail pressure and

pressure was same, the spray cone angle was not changed markedly at different bulk gas and glow plug temperatures.

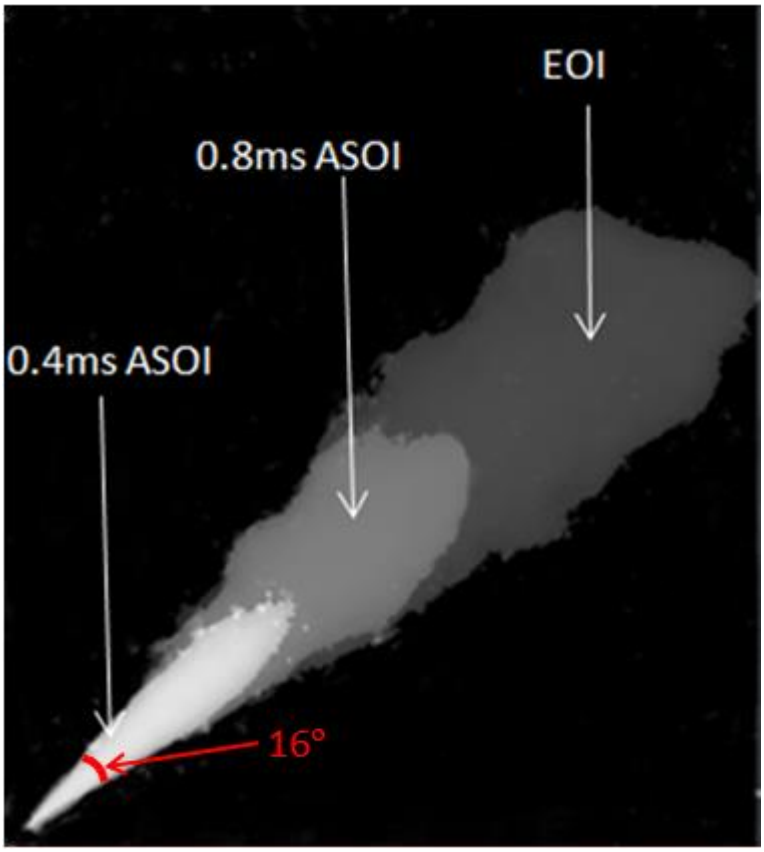

Figure 3-13: Measurement of spray cone angle in high speed image showing spray penetration

The droplet initial velocity is dependent on the rail pressure and the pressure in the bomb, in this case, initial velocity of droplets are calculated given that mass flow rate and the diameter of the nozzle hole is known, as shown in Equation 3-15.

$$V_{inj} = \frac{\dot{m}_l}{\rho_l \pi (\frac{d_0}{2})^2}$$

Equation 3-15

Where

$\dot{m}_l$= mass flow rate (kg/s)

ρ_l= liquid fuel density (kg/m3)

d_0= nozzle hole diameter (m)

In this case, spray primary breakup is modelled by providing initial droplet size distribution obeying Rosin-Rammler distribution that was chosen in ANSYS Fluent 14.0, which will be introduced in section 3.5.5.

3.5.4. Particle Motion Models

Once the droplet initial conditions were provided the particle motion will be tracked with Newton's second law. ANSYS Fluent predicts the trajectory of a discrete phase droplet by integrating the force balance on the particle, which is written in a Lagrangian reference frame[83]. This force balance equates the particle inertia with the forces acting on the droplet, and can be expressed in Equation 3-16.

$$\frac{d\vec{u}_d}{dt} = F_D(\vec{u} - \vec{u}_d) + \vec{F}$$

Equation 3-16

Where $\vec{F}$ refers to additional acceleration arises attributed to pressure gradient in the fluid. In case when non-combusting sprays are applied, this contribution is small.

F_D is the drag force per unit droplet mass, and can be expressed in Equation 3-17.

$$F_D = \frac{3\mu C_D Re}{4\rho_l d^2}$$

Equation 3-17

Reynolds number is expressed in Equation 3-18.

$$Re = \frac{\rho_g d|\vec{u} - \vec{u}_d|}{\mu}$$

Equation 3-18

Where μ is the molecular viscosity of the gas, $\vec{u}_d$ and u is droplet velocity and gas velocity respectively, ρ_l and ρ_g is droplet density and gas density respectively, d is droplet diameter. Because the gravitational force is too

small compared to the drag force attributed to small droplet size, the gravitational force is neglected in this study. ANSYS Fluent offers several models available for the drag coefficient C_D, in this study, the drag coefficient is determined from the dynamic drag model that accounts for the effects of droplet distortion, linearly varying the drag between that of a sphere and a disk.

The interaction of droplets with the individual turbulent eddies cannot be resolved by the flow field. In ANSYS Fluent 14.0, the dispersion of particles due to turbulence in the fluid is predicted using the random walk model includes the effect of instantaneous turbulent velocity fluctuations on the droplet trajectories through the use of stochastic methods. The fluctuating velocity components are discrete piecewise constant functions of time. Their random value is kept constant over time given by the characteristic lifetime of the eddies[83].

3.5.5. Breakup Models

Process of liquid jet disintegrating into small droplets are categorised by two sequential breakup mechanisms. The first breakup process is called primary breakup, which mainly deals with the breakup of the intact liquid core into droplets and the Secondary breakup is the process that turns droplets into smaller size, characterized by droplet sizes [71, 72].

3.5.5.1. Primary Breakup

Droplet size distribution due to primary breakup is closely related to nozzle state. Primary breakup is very complex and difficult to be modelled, in this study, initial droplet size distribution is provided as inputs to mimic the effect of primary breakup. In ANSYS Fluent 14.0, a two-parameter Rosin-Rammler method, characterized by the most probable droplet size and a spread parameter is used to predict initial droplet size distribution. The Rosin-Rammler distribution function is based on the assumption that an exponential relationship exists between the droplet diameter. The most probable droplet size is obtained is the Sauter mean diameter (SMD)

predicted in this study based on model developed by Elkotb [77], as shown in Equation 3-19.

$$SMD = 3.085 {v_l}^{0.385} {\sigma_l}^{0.737} {\rho_l}^{0.737} {\rho_g}^{0.06} \Delta P^{-0.54}$$

Equation 3-19

Where v_l is liquid kinetic viscosity, σ_l is surface tension, ΔP is pressure drop. The value of spread parameter was determined to be 2, mass fraction of droplets versus droplet diameter is illustrated in Figure 3-14. The minimum droplet size (1μm), the maximum droplet size (80 μm) and the mean droplet size (27 μm) are required as user-defined variables in ANSYS Fluent 14.0 to give the droplet size distribution illustrated in Figure 3-14.

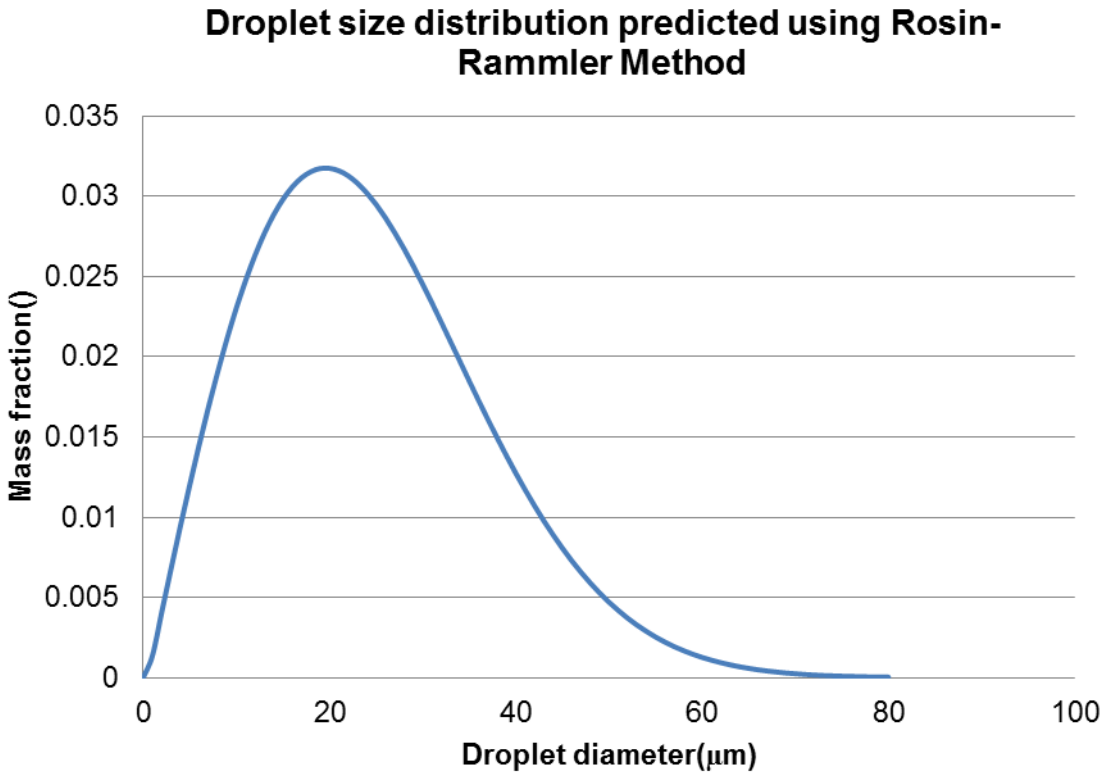

Figure 3-14: Droplet size distribution predicted using Rosin-Rammler distribution, the most probable droplet size is obtained as the SMD, value of the spread parameter is 2

3.5.5.2. Secondary Breakup

WAVE breakup model is used other than TAB (Taylor analogy breakup) model in this study is because WAVE breakup model is more appropriate for high-Weber number flows (Weber number is greater than 100)[73], for applications such as high pressure fuel injection as to be modelled in this investigation where the Kelvin-Helmholtz instability is believed to dominate droplet breakup, WAVE breakup model is chosen. In the WAVE breakup model, breakup of droplet is calculated by assuming that the radius of the newly formed droplets is proportional to the wavelength of the fastest-growing surface wave on the parent droplet, as expressed in Equation 3-20.

$$d = 2B_0\Lambda$$

Equation 3-20

Where d is droplet diameter, Λ is corresponding wavelength and B_0 is the model constant set equal to 0.61 in ANSYS Fluent 14.0 based on the work of R.D.Reitz [82]. The rate of change of droplet radius in the parent parcel is characterized by Equation 3-21.

$$\frac{da}{dt} = -\frac{(a - d/2)}{t_b}, d \leq 2a$$

Equation 3-21

Where a refers to radius of parent droplet, t_b is the breakup time, is given by Equation 3-22.

$$\tau = \frac{3.726B_1 a}{\Lambda\,\Omega}$$

Equation 3-22

Where Ω is the maximum growth rate, B_1 is model constant with default value in ANSYS Fluent 14.0 of 1.73 based on the work by Liu et al. [132].

Expressions of ∧ and Ω are functions of Weber number and Ohnesorge number. Values of B1 vary between 1 and 60 depending on the injector properties. Parametric studies of B1 have been conducted by Haran et al. [133], they have concluded that B1 dictates the period for particles breakup, which affects the spray penetration, and a value of 20 was found to accurately predict the diesel spray behaviour. In this study, model coefficient B1 was set equal to 20.

3.5.6. Droplet Heating and Vaporization Models

Droplet heating is controlled by two ways, convective heat transfer with heat input from surrounding gas and radiative heat transfer directly from the glow plug. Infinite thermal conduction (ITC) model which ignores temperature gradient inside the droplet so that heat supplied to droplet raises temperature of the whole droplet as has been shown in equation below. The ITC model has been widely used in various applications in conjunction with the mass transfer equation in recent publications [104-109].

$$\frac{1}{6}\pi d^3 \rho_l c_l \frac{dT}{dt} = \dot{Q}_d^c + \dot{Q}_d^r = \pi d^2 h\left(T_{g\infty} - T_d\right) + \dot{Q}_d^r$$

Equation 3-23

Where

$\dot{Q}_d^c$ = convective heat transfer rate (W)

$\dot{Q}_d^r$ = rate of radiative heat transfer (W)

d = diameter of droplet (m)

ρ_l = liquid fuel density (kg/m^3)

c_l = heat capacity of fuel (J/kg-K)

h = convective heat transfer coefficient (W/K-m^2)

$T_{g\infty}$ = gas temperature (K)

T_d= droplet temperature (K)

Black body radiation was attempted in this study to characterize radiative heat transfer which makes emissivity equals 1. Radiation is assumed to disperse from the glow plug tip which has been regarded as a sphere heat source, assume heat was transferred from a much larger sphere to a smaller sphere, shape factor was introduced to account for portion of amount of heat arriving on droplet, radiation shape factor can be formulated [134] in Stefan- Boltzmann law as shown below.

$$\dot{Q}_d^r = \sigma A_{GP}^s ({T_{GP}^s}^4 - {T_d}^4) F_{12} F_e = \sigma A_{GP}^s ({T_{GP}^s}^4 - {T_d}^4) \times (1 - \sqrt{1 - \left(\frac{d}{2L}\right)^2})(1 - \sqrt{1 - \left(\frac{D}{2L}\right)^2})(\frac{2L}{D})^2$$

Equation 3-24

Where

$F_{12=}$ radiation shape factor from glow plug to droplet

Fe= emissivity (=1)

σ =Stefan-Boltzmann constant

$\boldsymbol{T_{GP}^s}$= glow plug tip surface temperature (K)

$\boldsymbol{A_{GP}^s}$=surface area of glow plug tip (m^2)

d = droplet diameter (m)

L = distance between centroid of glow plug tip and centroid of droplet (m)

D = diameter of glow plug tip (m)

A heat transfer analysis has been carried out in this section to investigate the importance of radiative heat transfer from the glow plug to the droplet. The analysis was based on a non-evaporating, static droplet, the droplet is exposed to the glow plug, assume the droplet is 1.3mm distant from the glow plug surface, the glow plug surface temperature is 973K(700°C). Gas temperature near the glow plug is predicted and is used to calculate convective heat transfer. Radiative and convective heat transfer has been

worked out, because the droplet is static and the Nusselt number equals 2 [94, 96-99] and convective heat transfer coefficient is obtained. The convective and radiative heat transfer was calculated based on 300K droplet surface temperature. Convective heat transfer rate is calculated using Equation 3-25 and radiative heat transfer is calculated using Equation 3-24. The convective heat transfer coefficient can be correlated to the Nusselt number, droplet diameter and thermal conductivity of fuel.

$$\dot{Q}_d^c = \pi d^2 h\left(T_{g\infty} - T_d\right) = \pi d^2 \times \frac{Nuk_l}{d} \times \left(T_{g\infty} - T_d\right) = \pi d Nuk_l\left(T_{g\infty} - T_d\right)$$

Equation 3-25

Where

Nu= Nusselt number (=2, when the static condition is assumed [94, 96-99])

k_l= thermal conductivity of fuel (W/m-K)

As illustrated in Figure 3-15 and Figure 3-16, convection and radiation was calculated and presented respectively. The calculation was conducted based on the typical droplet size range due to high pressure diesel injection from 20μm to 100μm[37], the distance between the glow plug surface to the droplet was analyzed in range from 0.5mm to 2.5mm. As indicated in Equation 3-25, in this calculation, non- evaporating droplet is assumed with constant temperature and the droplet is at static condition, when the droplet is placed at a location with fixed distance to the glow plug, thermal conductivity of the droplet, temperature difference between gas and the droplet and Nusselt number are fixed, as a result, convective heat transfer rate is proportional to droplet diameter. In Figure 3-15, gas temperature is higher when the distance between the glow plug and droplet is shorter, convective heat transfer rate is higher, convective heat transfer increases linearly with droplet size increasing. Radiative heat transfer from the glow plug to the droplet is calculated and presented in

Figure 3-16, radiative heat transfer rate is higher when the distance is shorter between the glow plug and when the droplet and droplet size is larger.

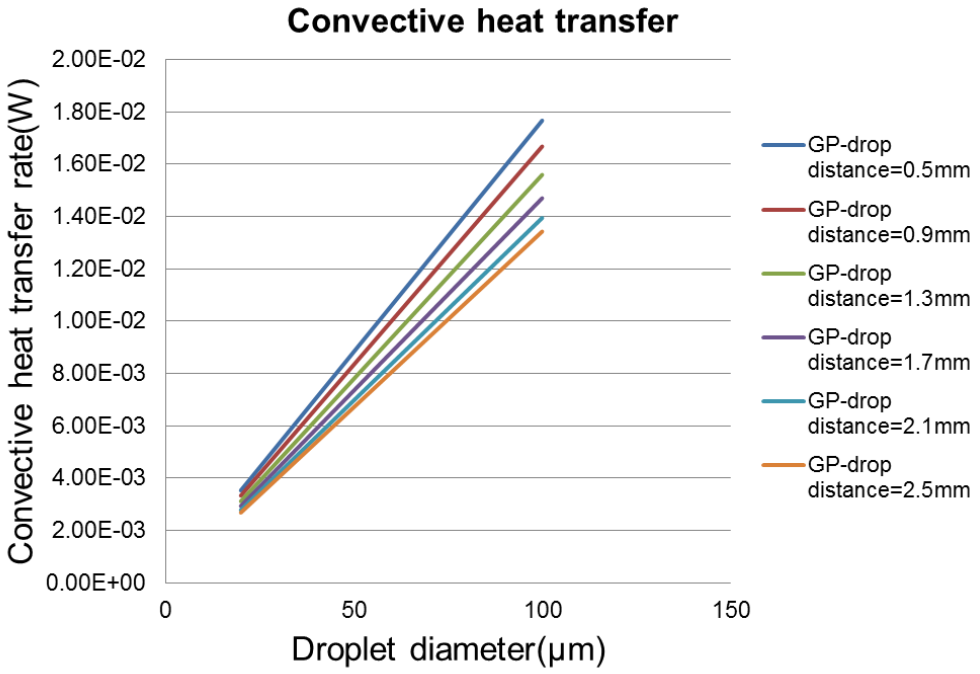

Figure 3-15: Rate of convective heat transfer from gas to droplet

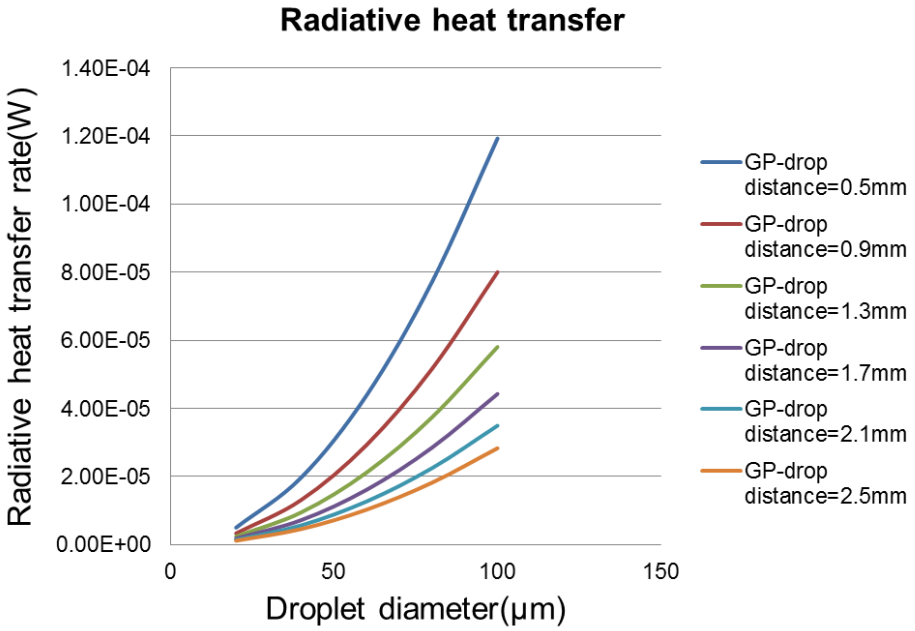

Figure 3-16: Rate of radiative heat transfer directly from the glow plug to droplet

The radiative heat transfer rate is two orders smaller than convective heat transfer rate, the ratio of the radiative heat transfer rate to the sum of the radiative heat transfer rate and convective heat transfer rate is calculated. It has been shown in Figure 3-17 that the contribution of radiation directly from the glow plug is larger when the distance between the glow plug and the droplet is shorter and the droplet size is larger. Generally, the contribution of radiation in droplet heating is no more than 1%, which is negligible in practice compared with convective heat transfer. Heat transfer to the droplet is dominated by convective heat transfer which is dominated by gas temperature.

The effect of radiation is neglected so that Equation 3-23 becomes Equation 3-26.

$$\frac{1}{6}\pi d^3 \rho_l c_l \frac{dT}{dt} = \pi d^2 h\left(T_{g\infty} - T_d\right)$$

Equation 3-26

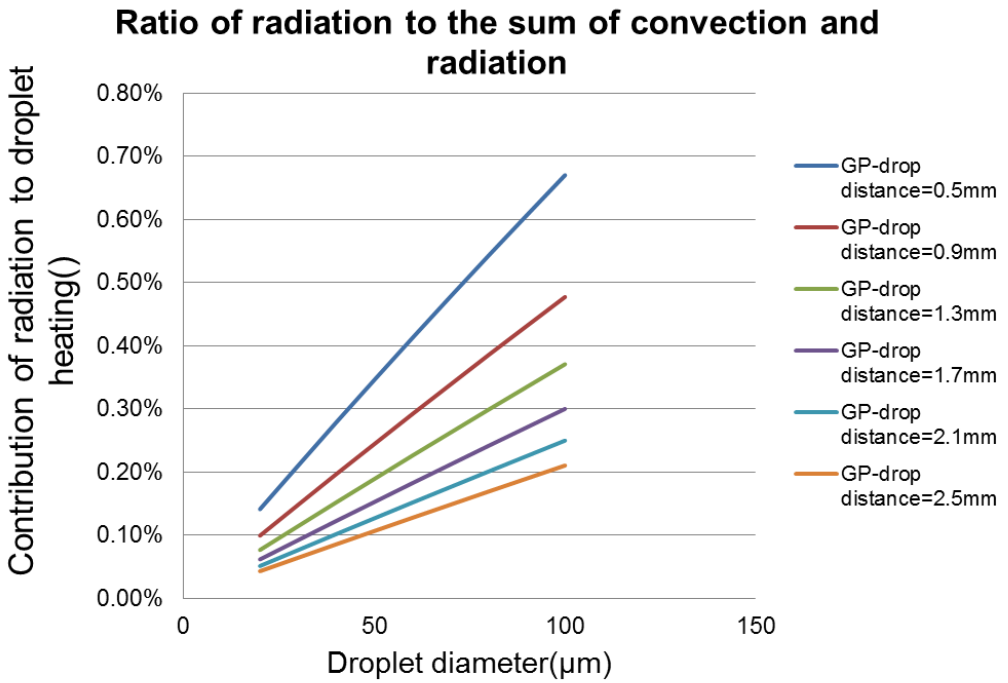

Figure 3-17: Ratio of radiation to overall heat transfer (convection plus radiation), radiative heat transfer from the glow plug is negligible

In ANSYS Fluent 14.0, Equation 3-27 is used to characterize heat exchange between the surrounding gas and the droplet until the temperature of the droplet reaches boiling temperature. When the droplet temperature reaches the boiling point, a boiling rate equation is applied [83, 135]:

$$\frac{d(d)}{dt} = \frac{4k_g}{\rho_l c_g d}\left(1 + 0.23\sqrt{Re}\right) In\left[1 + \frac{c_g(T_g - T_d)}{h_{fg}}\right]$$

Equation 3-27

Where

k_∞=thermal conductivity of the gas (W/m-K)

$c_{p,\infty}$=heat capacity of the gas (J/kg-K)

The boiling temperature is user-defined variable that is consistent with the average pressure in the region where the droplet vaporizes, the boiling temperature can be estimated by using Clausius- Clapeyron equation

assuming saturation pressure on droplet surface is equal to environment pressure [111].

When the droplet surface temperature is below boiling point, droplet vaporization is modelled by convection controlled mass transfer equation [94, 96-99, 110]:

$$\dot{m}_d = \pi \rho_g D_{Fa} d Sh_0 \ln(B_M + 1)$$

Equation 3-28

Where

$\dot{m}_d$=vaporization rate (kg/s)

ρ_g=average density of vapour air mixture (kg/m^3)

B_M=Spalding mass transfer number

Sh_0=Convective Sherwood number

D_{Fa}=binary diffusion coefficient (m^2/s)

In ANSYS Fluent 14.0, the binary diffusion coefficient is user-defined variable. Sazhin et al. [98] provided a method to estimate values of binary diffusion coefficient under various temperatures, based on the single component fuel $C_{10}H_{22}$ that was used in this study to represent light diesel, the binary diffusion coefficient can be fitted as a second order polynomial function according to gas temperature as has been shown in Figure 3-18.

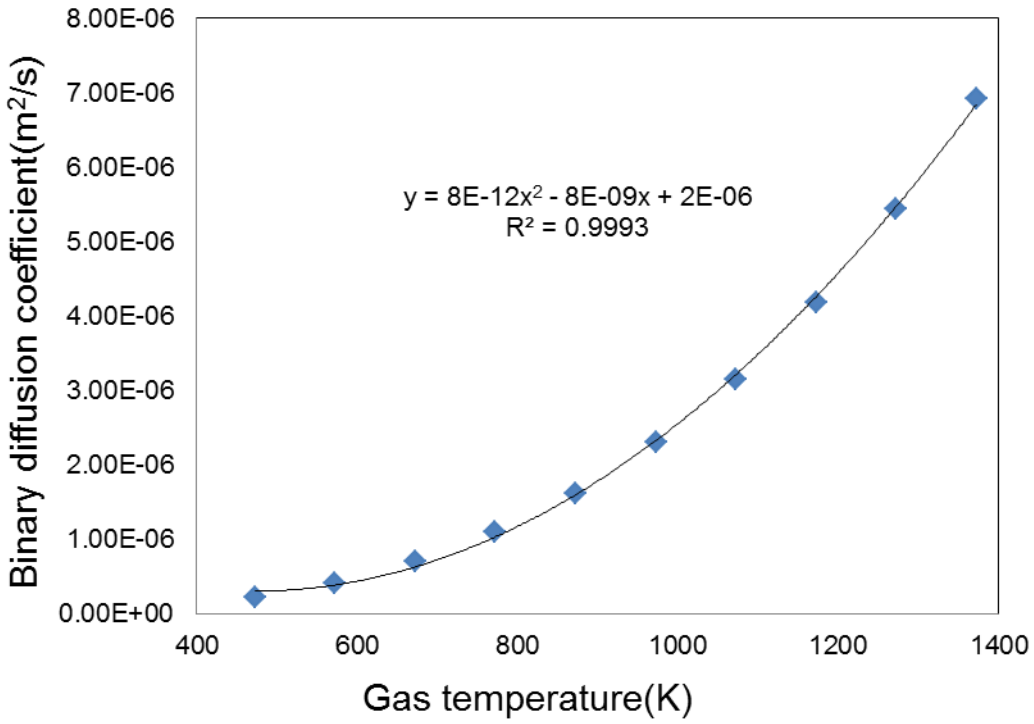

Figure 3-18: Binary diffusion coefficient against gas temperature, polynomial form is used as a user-defined input in ANSYS Fluent 14.0 spray model

3.6. Summary

A single cylinder research engine that was used to investigate combustion characteristics aided by a glow plug has been described. A specially made cooling system which is capable of chilling the coolant and the intake air to mimic cold temperature conditions down to -30ºC was used. In-cylinder pressure, as an essential parameter that was used to analyze combustion behavior was monitored and captured using a Kistler 6215B quartz transducer rated at 250 bar peak pressure. A Kulite pressure sensor was used to capture charge pressure at BDC of the intake stroke as a reference pressure to account for the drift of the piezo-electric in-cylinder pressure sensor. All thermocouples and pressure transducers that used to capture temperature and pressure around the engine have been calibrated prior to tests. Key response variables have been demonstrated, calculations of net heat release rate, gross mean effective pressure (IMEPg) have been

described, and coefficient of variation of IMEPg (CoV_{IMEPg}) has been introduced to quantify combustion stability at cold idle.

Chapter 4 Influence of the Glow Plug on Combustion Initiation and Development

4.1. Introduction

In this chapter, the influence of the glow plug on combustion initiation and development under idling conditions is determined. In section 4.2, the influences of the glow plug on engine combustion behavior including the engine work output, heat release rate, fuel utilization and cycle-by-cycle combustion stability are investigated. In section 4.3, the threshold in-cylinder temperature for a self-sustaining reaction is determined experimentally. The range of in-cylinder temperatures that engine requires the glow plug to improve combustion development is studied. In section 4.4, the influences of injection strategies on the glow plug performance are demonstrated. Finally, the main conclusions are presented.

4.2. Influence of the Glow Plug on Combustion Characteristics

4.2.1. Influence of the Glow Plug on Work Output

The aim of the work reported in this section was to investigate the influence of the glow plug on engine work output. Tests have been carried out using the single cylinder engine at test temperature range from 3°C to 17°C. Tests were carried out each with and without the glow plug switched on. Three tests were repeated at same test condition. Combustion stability under cold start and idling conditions have been shown to be improved by using up to four pilot injections [4, 11, 20], although this reduces the proportion of total fuel delivered in the main injection, and can make idle speed control through fueling control more difficult. At the mildly cold test temperatures used in the work reported in this chapter, an injection strategy combining twin pilots and a main was used as an appropriate compromise. The effect of injection timings has been evaluated by McGhee [4], who concluded that the highest IMEPg and lowest cycle-by-cycle variation of IMEPg were achieved around -8°CA ATDC for all injection strategies. The effect of injection separation has also been investigated and reducing injection separation from 10 to 6°CA was shown to improve cycle-by-cycle variation of IMEPg by raising IMEPg and reducing StD_{IMEPg}. This was also supported by Payri [22]. In this investigation, injection separation between was 6°CA and the start of the main injection was at -8°CA ATDC. Injection strategies and other test parameters are given below in Table 4-1. The tests were carried out with a metallic glow plug installed in the engine. The tip surface temperature of the glow plug was measured in still air to stabilize at 850ºC.

Table 4-1: Test parameters

Parameter	Base line	Sweep
Soak temperature(°C)	3	3-17
Glow plug tip surface temperature(°C)	850	Glow plug switched on/off
Injection quantity(mg)	2, 2, 6	-
Injection timing(°CA ATDC)	-20, -14, -8	-
Engine speed(rpm)	1000	-
Rail pressure(bar)	400	-

A standard engine test procedure was followed: The glow plug was powered on and the engine was motored for 15 engine cycles before enabling fuel injection to allow the target speed and fuel rail pressure to be achieved before enabling fuel injection. Fuel injection was initiated on cycle 16 and continued for 40 consecutive cycles after which the test was ended. Post- test, results from the first 10 firing cycles were analysed in this study, because over a larger number of cycles, the effects of surface temperature and fuel accumulation in the combustion system are increasingly significant. The extension of the test run aided the detection of any test problems and contributed to conditioning the engine for later tests. The engine was motored for two minutes to draw purge air through the cylinder before cold soaking the engine in preparation for the next test. Generally, tests at the same conditions were repeated three times. Fully-warm engine conditioning tests were run daily to condition the engine and maintain repeatable cylinder conditions for subsequent tests.

Gross IMEP is defined as the work per cycle per unit of swept cylinder volume over compression and expansion strokes. Values of gross IMEP has been used to measure engine performance. Ensemble averaged IMEPg of

the first firing cycles have been used to characterize engine work output at start-up and idling conditions in this section. Values of IMEPg measured with glow plug switched on and off were presented in Figure 4-1, it can be observed that with the glow plug switched on, IMEPg is generally between 2 bar and 2.5 bar and shows a trend of slight increase as soak temperature increases, this indicates the engine is capable to overcome the friction and maintain stable idling. IMEPg with the glow plug switched off is negative when the soak temperature is lower than 4°C, indicating the occurrence of engine misfire, IMEPg with the glow plug switched off shows a clear trend to rise with incremented soak temperatures, at soak temperature higher than 8°C, positive IMEPg is guaranteed. IMEPg is found always lower with glow plug switched off than the IMEPg with the glow plug is switched on at all test temperatures covered. The difference in work output becomes smaller as a consequence of soak temperature rise. Although upper test temperature was limited as the highest ambient temperature in the laboratory was reached, extrapolation implies work output is continuously improved by using the glow plug until soak temperature reaches 20°C.

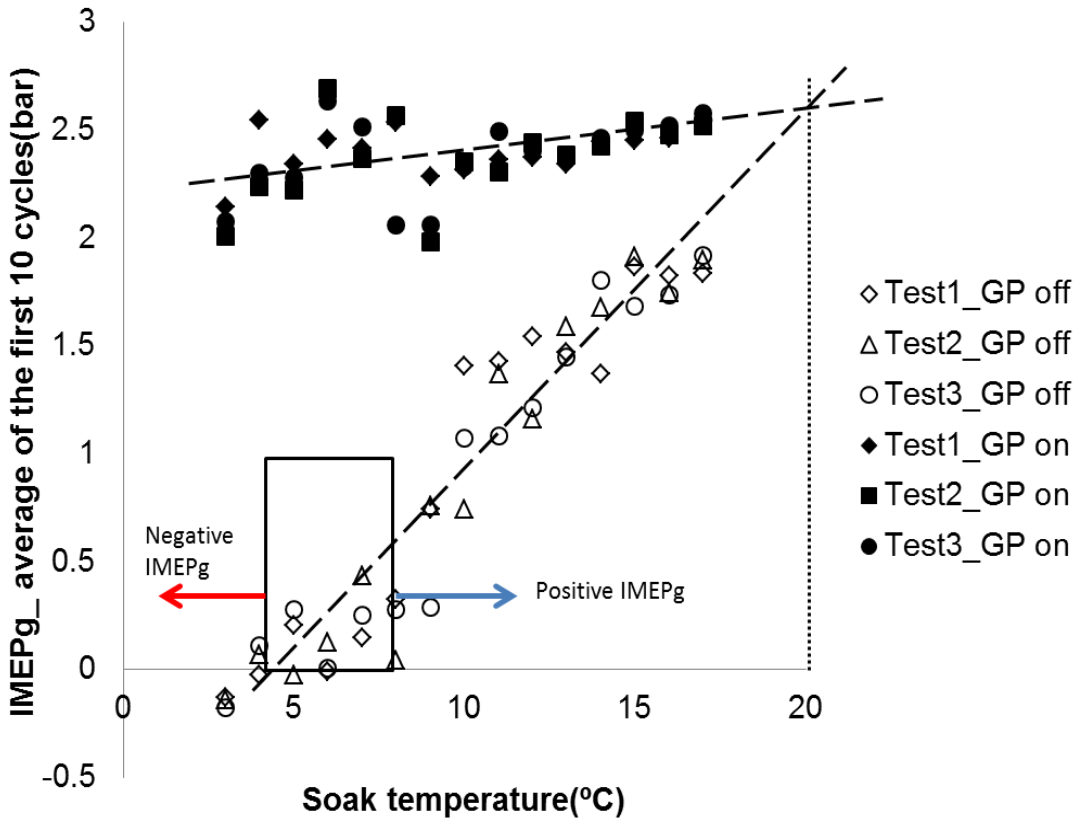

Figure 4-1: IMEPg comparison between cases with glow plug switched on and off over a test temperature range of 3°C to 17°C, test parameters refer toTable 4-1

As illustrated in Figure 4-1, when the glow plug is switched off, IMEPg is always negative at soak temperature below 4°C, and always positive at soak temperature above 8°C. At the temperature range between these two, IMEPg is close to zero. To study this transient range, values of IMEPg with the glow plug switched off over the first 10 cycles for three test temperatures, 3ºC, 6ºC and 9ºC have been shown in Figure 4-2 to Figure 4-4.

IMEPg for the first 10 cycles at soak temperature of 3ºC has been illustrated in Figure 4-2 with the glow plug switched off, it has been shown that IMEPg is generally negative with a few occasional cycles showing positive IMEPg, however, the value is very close to zero. Cycles with

negative values of IMEPg indicate occurrence of engine misfire, and irreversibility during compression and expansion processes.

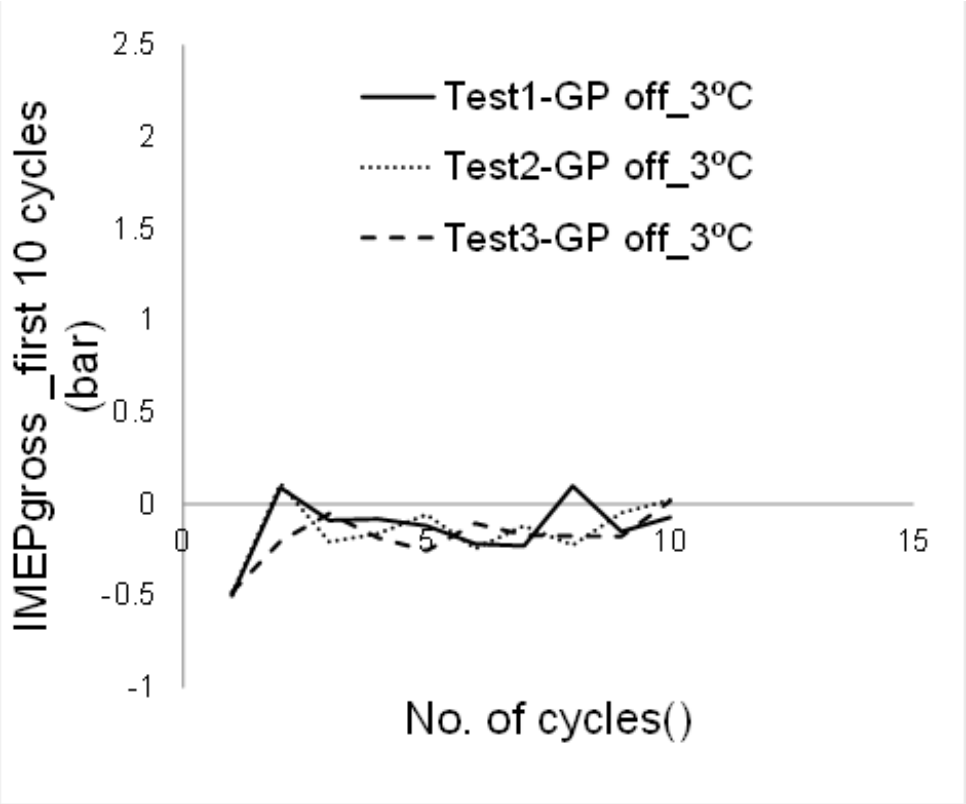

Figure 4-2: Averaged gross IMEP over the first 10 cycles. Three tests per each glow plug state off, at soak temperature of 3ºC

In Figure 4-3, IMEPg with the glow plug switched off from three tests undertaken at soak temperature of 6ºC has been shown. IMEPg in the first 10 cycles are low and close to zero, but still with a few cycles showing negative values, which indicates positive work output is possible to be generated but misfire still exists.

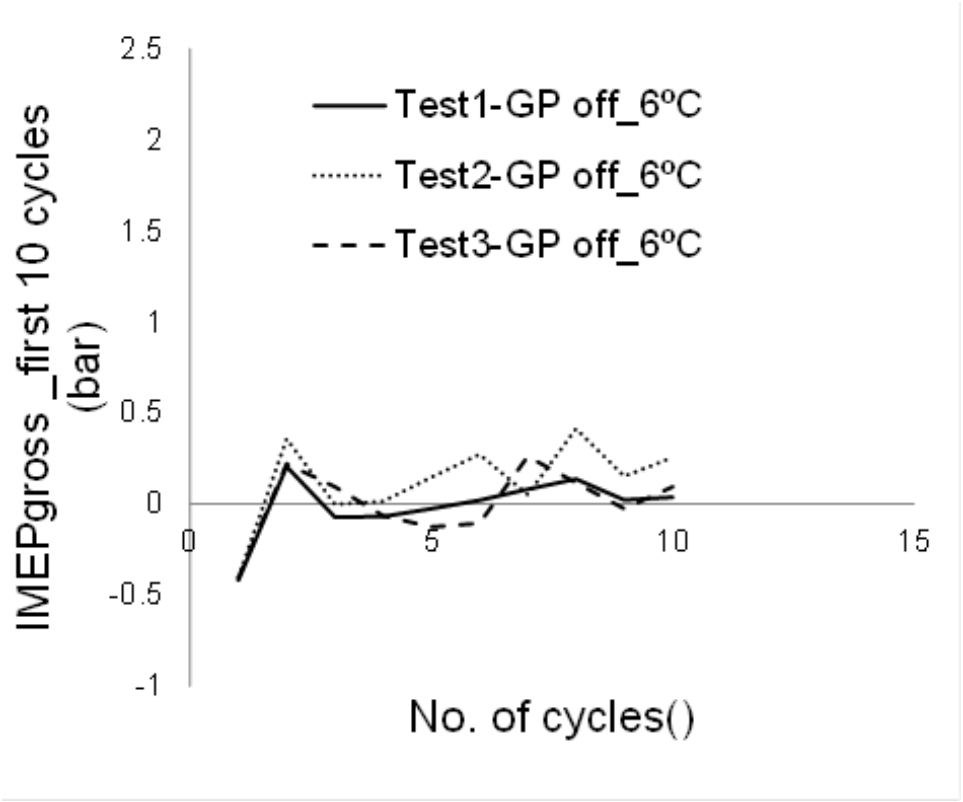

Figure 4-3: Averaged gross IMEP over the first 10 cycles. Three tests per each glow plug state off, at soak temperature of 6ºC

At soak temperature of 9ºC, as has been shown in Figure 4-4, for tests with the glow plug switched off, IMEPg are positive in all 10 cycles for three tests, but still low at around 1 bar. It is indicated that at 9°C soak temperature, self-sustaining combustion is successfully initiated and positive work output is guaranteed in the first 10 cycles in all three tests.

It is worth mentioning that at soak temperature of 9° C, the IMEPg of the first 10 cycles are around 1 bar, which is insufficient to achieve stable idling[16], although self-sustaining combustion in the engine combustion chamber can be successfully initiated.

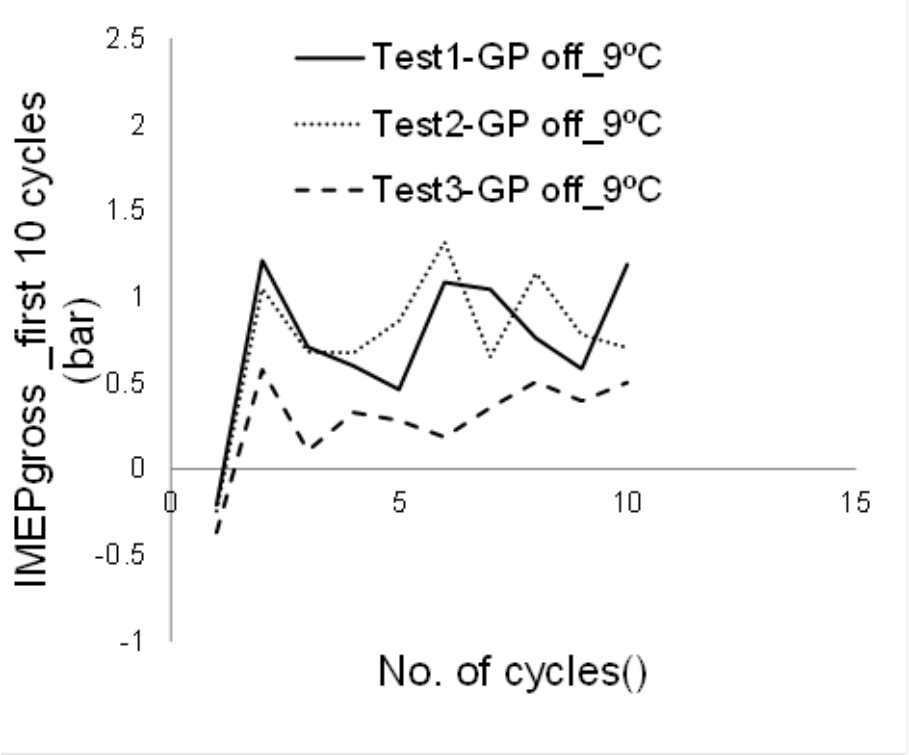

Figure 4-4: Averaged gross IMEP over the first 10 cycles. Three tests per each glow plug state off, at soak temperature of 9ºC

4.2.2. Influence of the Glow Plug on Heat Release Rate

As presented in the previous section, with the glow plug switched off, IMEPg is negative at soak temperature below 4ºC, IMEPg becomes positive when the soak temperature is above 8ºC, IMEPg increases as soak temperature rises. In this section, heat release rate based on three soak temperatures 3ºC, 9ºC and 17ºC were chosen to be analyzed in this section in order to identify the phenomena responsible for desirable or undesirable combustion characteristics.

As illustrated in Figure 4-1, current clamp was used to initiate injector to inject fuel spray and was used here to indicate pilot/main injections. At soak temperature lower than 4ºC, IMEPg without assistance from the glow plug is negative, while IMEPg with the glow plug switched on is around 2 bar. Ensemble averaged net heat release rate at 3°C soak temperature against crank angle after TDC has been shown in Figure 4-5, current clamps refer to injection timings for the pilot injections and the main injection. Heat release rate reduces after the start of each injection,

indicating heat consumption attributed to droplet vaporization. With the glow plug switched on, a strong and clear premixed spike and diffusion burn is observed. The peak value for premixed phase and mixing controlled phase combustion is similar around 15 J/° CA. With the glow plug switched off, heat release rate is zero and rises weakly without any initial spike.

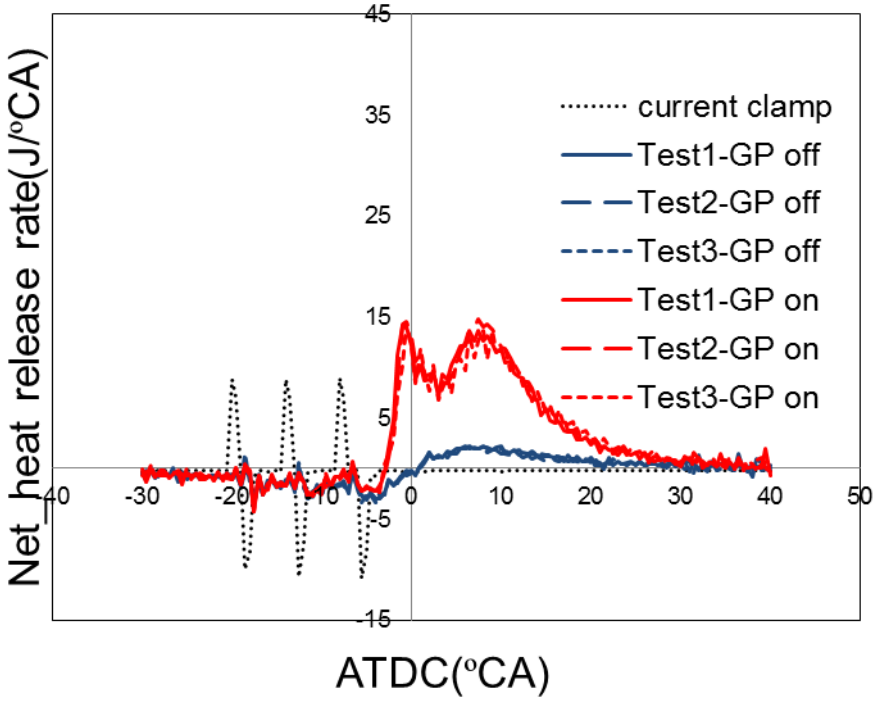

Figure 4-5: Ensemble averaged net heat release rate over the first 10 cycles with/without glow plug assistance at 3°C soak temperature

Also shown in Figure 4-1, at soak temperature of 9ºC, without assistance from the glow plug, IMEPg is positive at approximately 1 bar, this is insufficient to overcome engine friction and achieve stable idling in a short time, but it is evidenced that combustion is successfully initiated. Ensemble averaged net heat release rate over the first 10 cycles against crank angle after TDC has been shown in Figure 4-6. With the glow plug switched on, heat release rate rises strongly showing a premixed spike of

15 J/°CA. Mixing controlled combustion shows a peak of 25 J/°CA, 10 J/°CA higher than that is observed in Figure 4-5 when the soak temperature is 3ºC. With the glow plug switched off, heat release rate rises slowly up to 7J/°CA without any initial premixed spike.

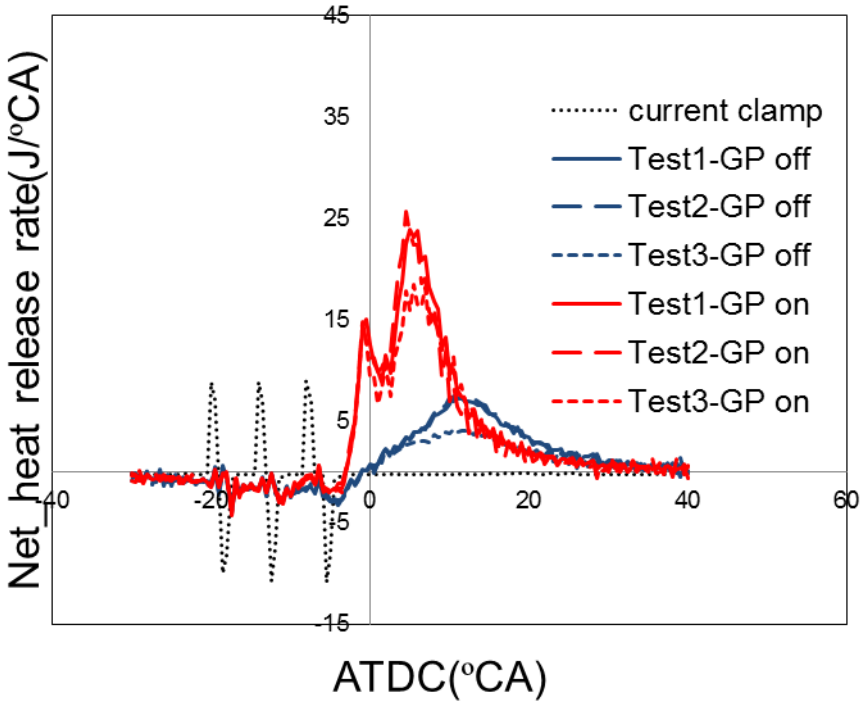

Figure 4-6: Ensemble averaged net heat release rate over the first 10 cycles with/without glow plug assistance at 9°C soak temperature

The glow plug influences combustion development at soak temperature above 9°C until 20°C. Ensemble averaged net heat release rate over the first 10 cycles against crank angles after TDC at the highest test temperature, 17°C, has been shown in Figure 4-7, with the glow plug switched on, before the start of the main injection, higher heat release rate is observed compared to that with the glow plug switched off, suggesting that when the glow plug is on, pilot combustion is strong enough to promote detectable pressure rise. After the start of the main injection, heat release rate reduced attributed to droplet vaporization, a premixed spike of 15 J/ºCA is observed, a strong mixing controlled

combustion with peak value of 40 J/ºCA is detected. With the glow plug switched off, heat release rate initially rises slowly until 4 ºCA after TDC where a quick rise of heat release rate is observed, a single peak heat release profile is observed with the highest value of 24 J/ºCA. At 17ºC soak temperature, established self-sustaining combustion is definitely ensured, although there is no premixed spike with the glow plug switched off, this indicated that premixed combustion is a result of flame propagation initiated from local combustion induced by the glow plug.

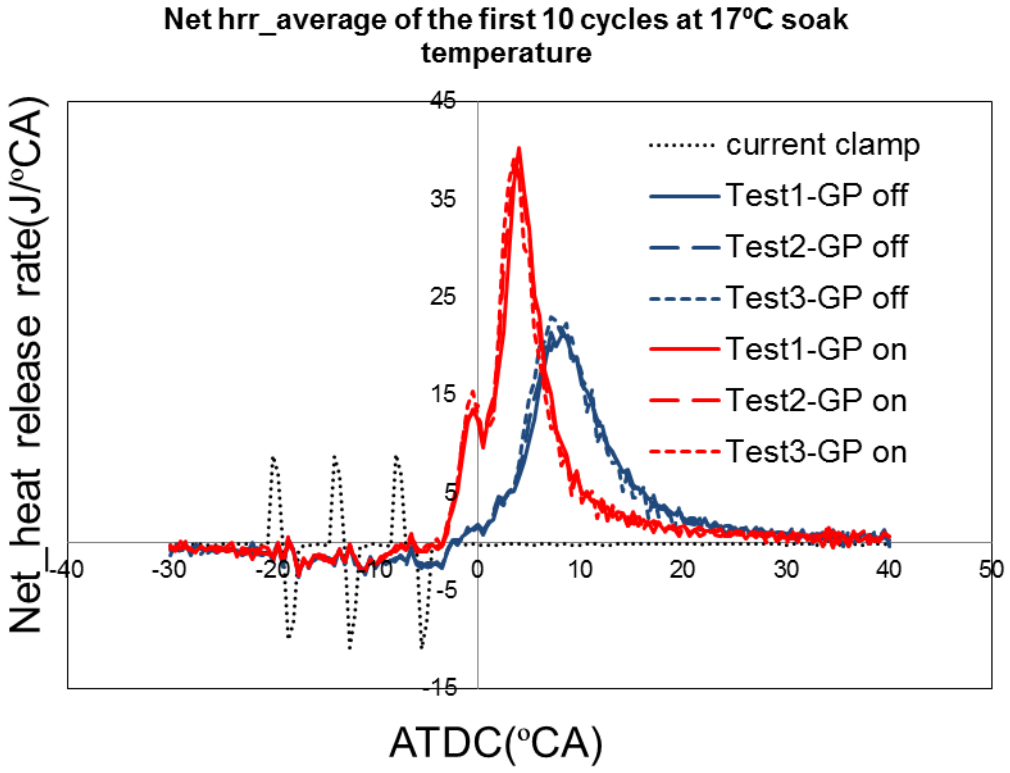

Figure 4-7: Ensemble averaged net heat release rate over the first 10 cycles with/without glow plug assistance at 17ºC soak temperature

4.2.3. Influence of the Glow Plug on Fuel Utilization

In this section, net cumulative heat release is examined to explore the influence of the glow plug on fuel utilization. Assuming heat transfer losses to the walls are unchanged, higher cumulative heat release for a given fueling indicates an increase in combustion efficiency. The influence of the

glow plug on fuel utilization was investigated over a range of test temperatures up to 17°C.

Ensemble averaged cumulative heat release over the first 10 cycles is higher with the assistance of the glow plug covering all test temperatures as can be observed in Figure 4-8. The advantage diminishes at higher test temperatures until 20°C. This is considerably higher than the temperature of 9°C at which reliable self-ignition can be achieved without the glow plug.

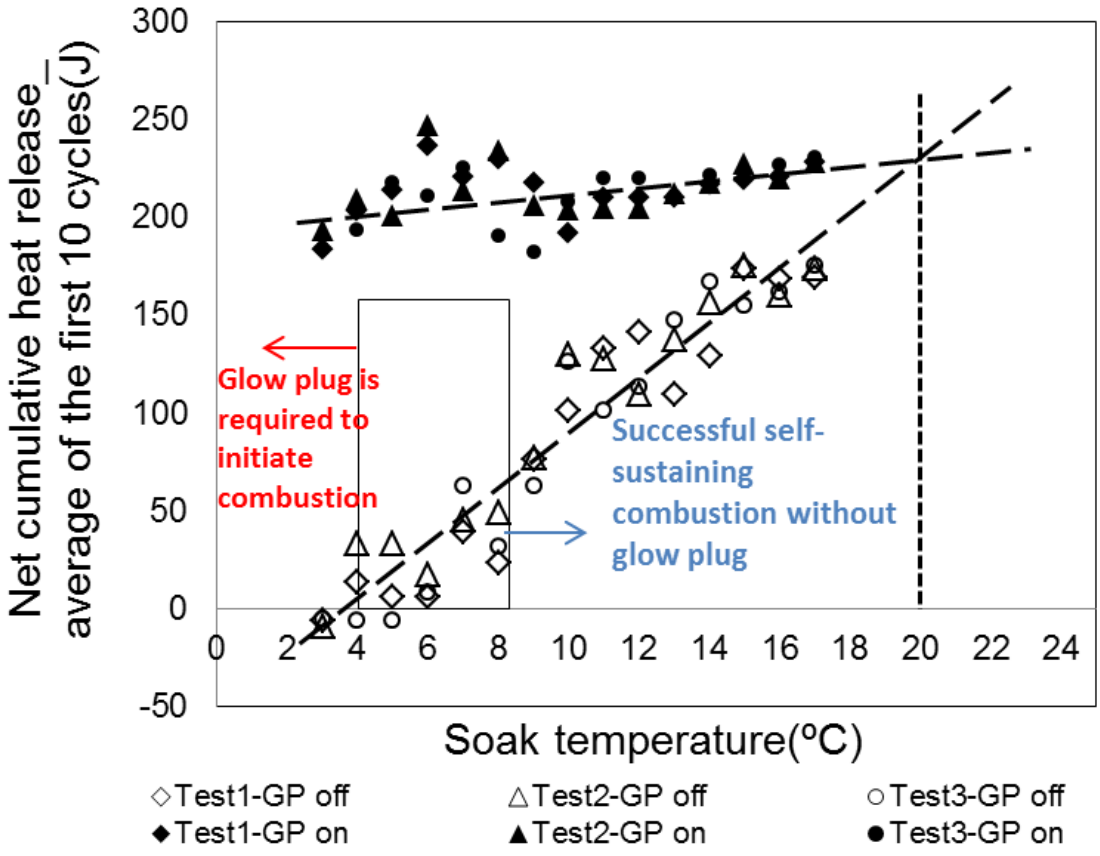

Figure 4-8: Comparison of net cumulative heat release between glow plug switched on and off.Test parameters refer to Table 4-1

The ratio of cumulative heat release values for the glow plug switched off and on has been shown in Figure 4-9. As illustrated in Figure 4-9, the ratio increases steadily to between 0.7 and 0.8 at the highest test temperature (17ºC), from close to zero at 4ºC. At lower temperatures, the glow plug is required to achieve reliable initiation and detectable heat release.

At ambient temperature of 20°C, in-cylinder temperature at start of main injection is around 430°C according to Figure 4-14, this temperature is 17°C higher than the threshold temperature (413°C) required to get fuel self-ignited. This continuing benefit over initiation indicates spray vaporization must be improved attributed to the heat input from the glow plug. The glow plug enhances the early development of the combustion by producing a strong premixed spike, which influences following mixing controlled combustion.

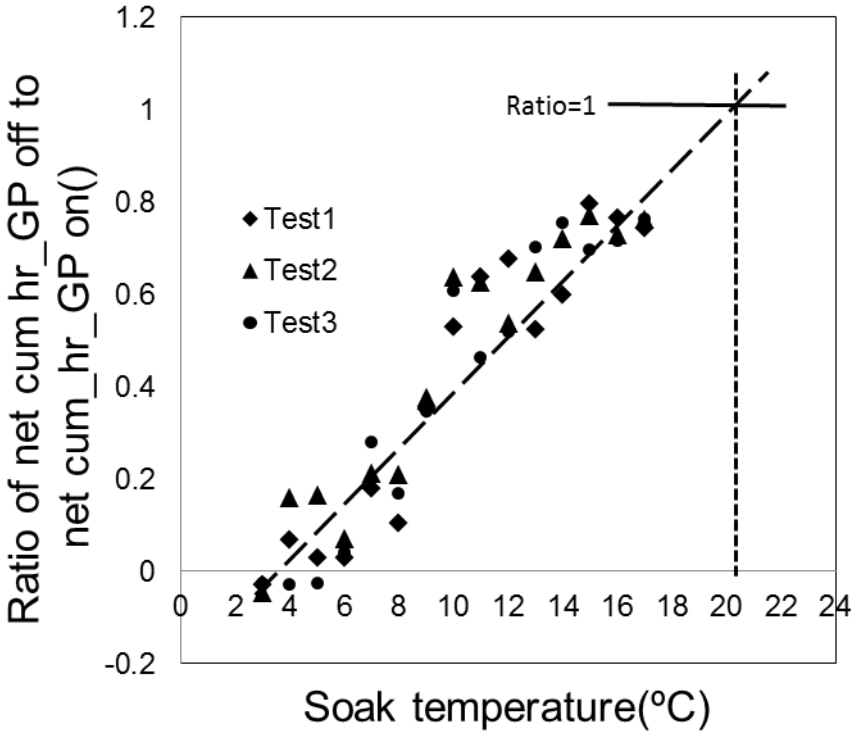

Figure 4-9: Ratio of cumulative net heat release with glow plug switched off to switched on. Test parameters refer to Table 4-1

4.2.4. Influence of the Glow Plug on Combustion Stability

The cycle-by-cycle variations in IMEPg and cumulative heat release are represented by the standard deviations given in Figure 4-10 and Figure 4-11 respectively. Standard deviations of IMEPg over the first 10 fueled cycles have been in Figure 4-10. Standard deviation of IMEPg with the assistance of the glow plug is significantly lower, approximately 50% than that with the glow plug switched off. Standard deviations of cumulative

heat release over the first 10 cycles have been shown in Figure 4-11. Across the temperature range covered, with the glow plug switched on, the standard deviation of the cumulative heat release is substantially lower, by up to half of that with the glow plug switched off. The benefit is less clear in the standard deviation of cumulative heat release for temperatures below 8ºC than that in the standard deviation of gross IMEP, when most variation arises in the later stages of the burn.

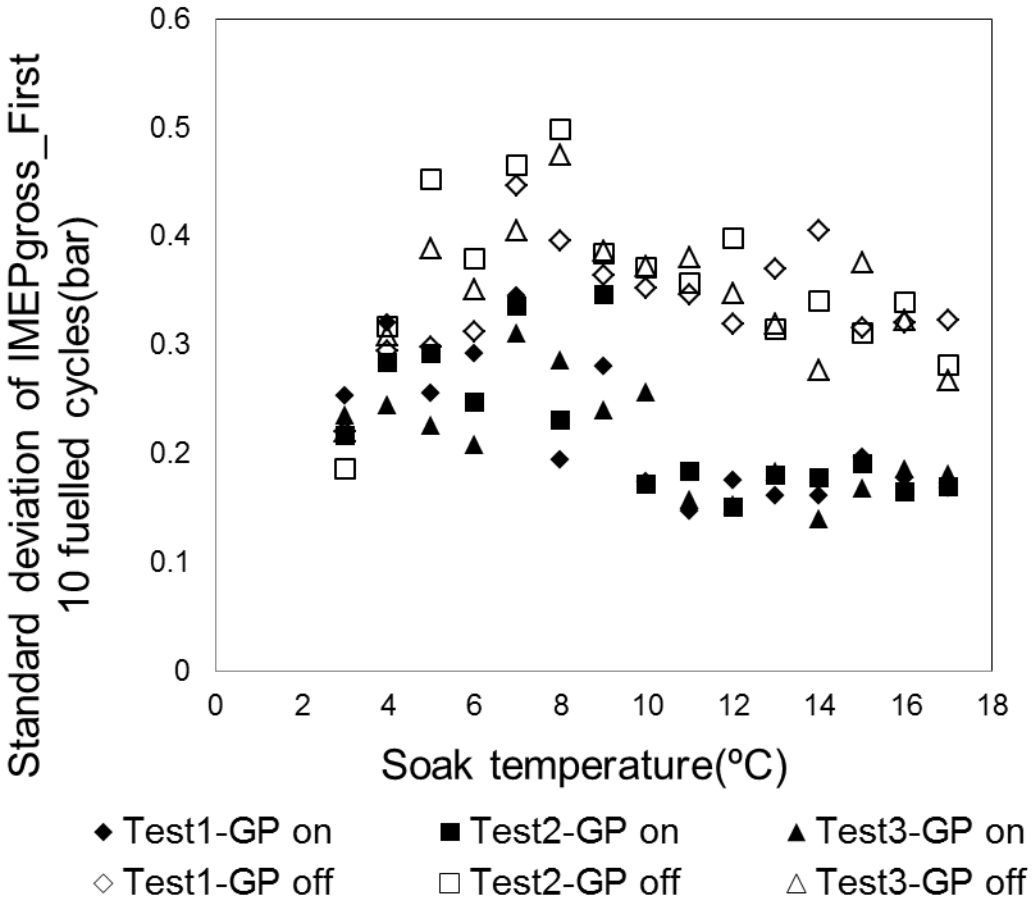

Figure 4-10: Standard deviation of IMEPg over the first 10 fuelled cycles. Test parameters refer to Table 4-1

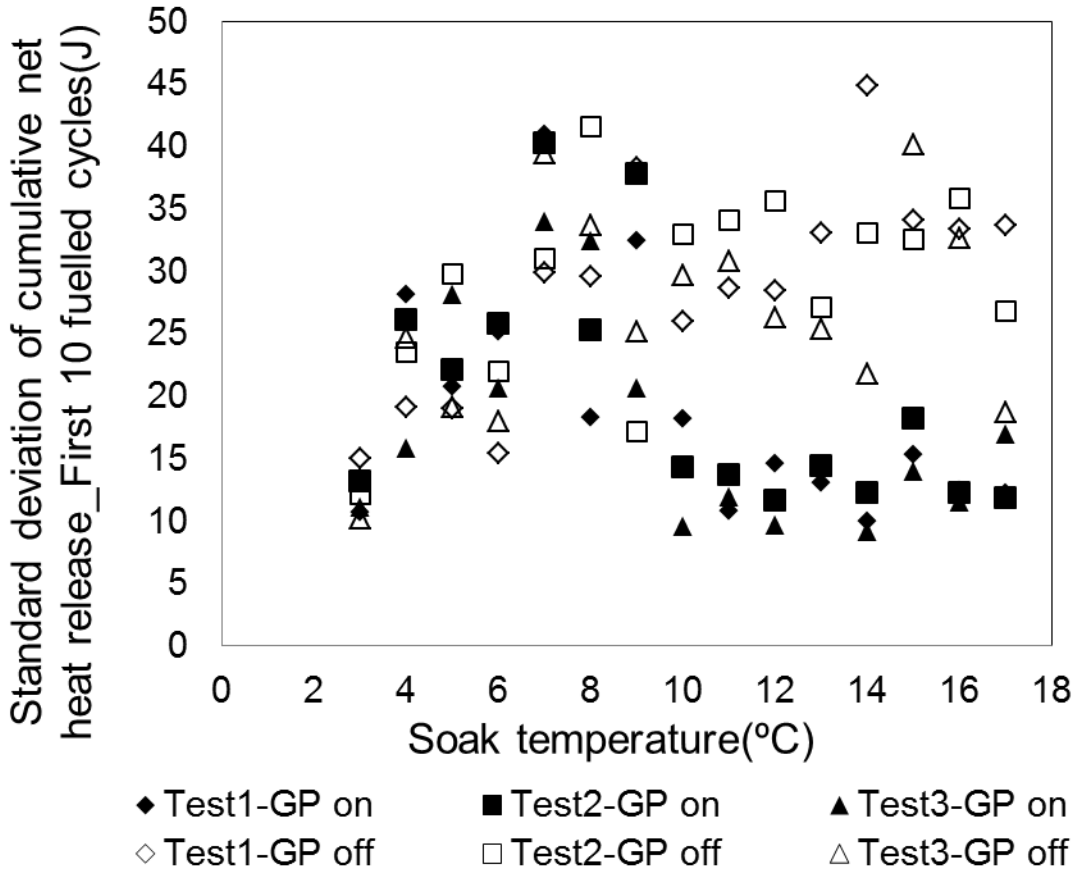

Figure 4-11: Standard deviation of cumulative net heat release over the first 10 fuelled cycles.Test parameters refer to Table 4-1

As the coefficient of variation of gross indicated mean effective pressure (CoV_{IMEPg}) with the glow plug on and off has been plotted against soak temperature in Figure 4-12, the engine is severely misfiring below 8ºC, above 8ºC, combustion initiation and reliable progression caused without the aid of the glow plug generates a positive work output. CoV_{IMEPg} was defined in Chapter 3 as the ratio of standard deviation of IMEPg to average IMEPg over the first 10 firing cycles. With the glow plug switched off, CoV_{IMEPg} decreases dramatically from 150% down to 40% as a result of increasing soak temperature from 8°C to 10°C, and gradually decreases with soak temperature increasing to around 15% at 17°C soak temperature. With the glow plug switched on, $CoV_{IMEPg}$is generally below 20% at soak temperature lower than 10°C, CoV_{IMEPg} is around 10% at 10°C

soak temperature, at higher soak temperature, CoV_{IMEPg} is always smaller than 10%. Similar to the influence of the glow plug on work output and cumulative heat release, extrapolation implies the glow plug improves cycle-by-cycle combustion stability up to soak temperature of 20°C.

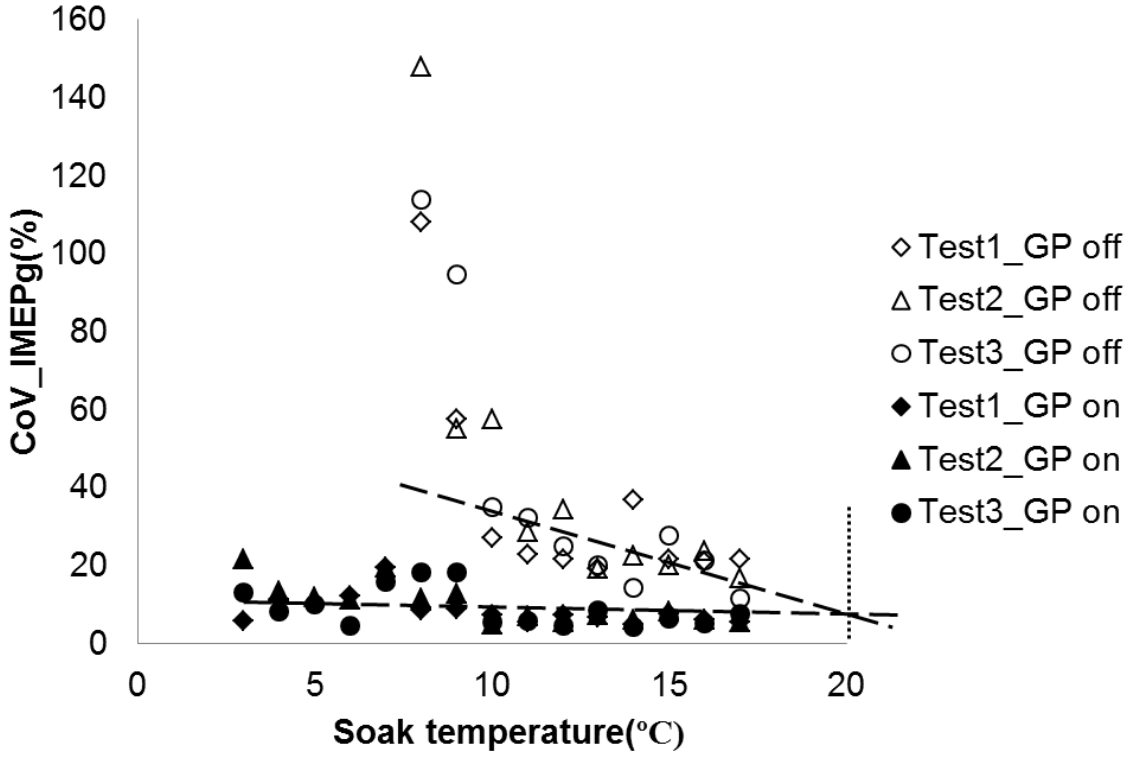

Figure 4-12: Coefficient of variation of IMEPg over the first 10 cycles. Test parameters refer to Table 4-1

4.3. Threshold In-Cylinder Temperatures

It has been demonstrated in previous sections that the glow plug is required to initiate self-sustaining reactions at soak temperature lower than 8°C, combustion development is improved until soak temperature of 20°C. However, compression gas temperature in cylinder corresponding to these soak temperatures is not acquired.

The compression process can be modelled using polytropic gas law which accounts for heat transfer to walls and blowby gas:

$$P_1 {V_1}^n = P_2 {V_2}^n = C$$

Equation 4-1

Where P is pressure, V is volume, n is polytropic index, and subscribes 1 and 2 refer to condition before and after compression respectively

Apply perfect gas law

$$P = \frac{mRT}{V}$$

Equation 4-2

Combine Equation 4-1, Equation 4-2

$$T_2 = T_1 \times (\frac{V_1}{V_2})^{n-1}$$

Equation 4-3

In this study, effective compression ratio was used to represent ratio of V_1 to V_2. Equation 4-3 becomes Equation 4-4

$$T_2 = T_1 \times (CR_{effective})^{n-1}$$

Equation 4-4

The effective start of compression was taken to be the point at which cylinder pressure begins to follow the polytropic compression line on logarithmic plots of cylinder pressure versus cylinder volume at 25º CA after BDC. The charge temperature is assumed to be equal to the intake air temperature at this point. The effective compression ratio was taken to be the ratio of the volume at this point to the volume at the start of main injection. The effective compression ratio determined in this study was 13.8:1, which is lower than the geometric compression ratio of 15.5:1, and higher than the compression ratio value of 13.3:1 that calculated using the volume at the point of inlet valve closing, which occurs at 37º CA after BDC.

n is polytropic index, which has been taken as magnitude of the gradient from log(P) vs log(V) diagram. Polytropic index (n) has been experimentally measured at a motored engine speed of 1000rpm across a wide range of temperatures. The variation of the index value with test temperature is shown in Figure 4-13.

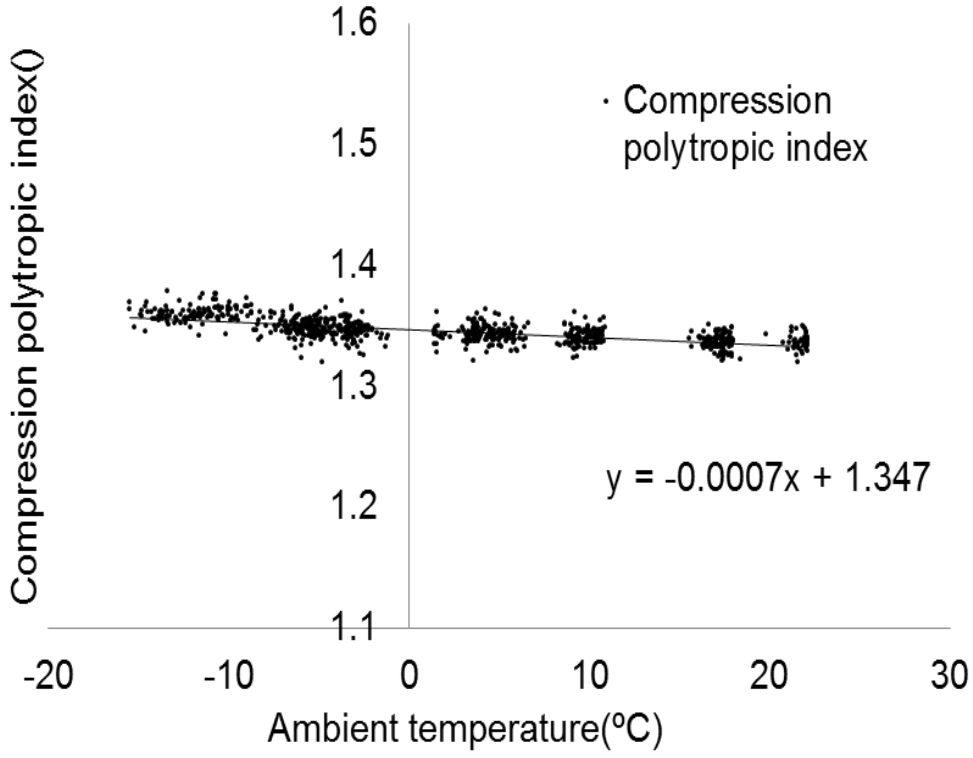

Figure 4-13: Compression polytropic index measured over a temperature range of -15ºC to 20ºC

In-cylinder bulk gas temperature at start of the main injection can be estimated provided that effective compression ratio, ambient temperature and polytropic index (n) are known. As has been illustrated in Figure 4-14, temperature range of 4ºC to 8ºC is the critical temperature range tested to be threshold temperature range for combustion initiation. In this study the critical temperature for self-sustaining combustion is between 410ºC

and 416ºC. The critical temperature of benefit using the glow plug is 430ºC.

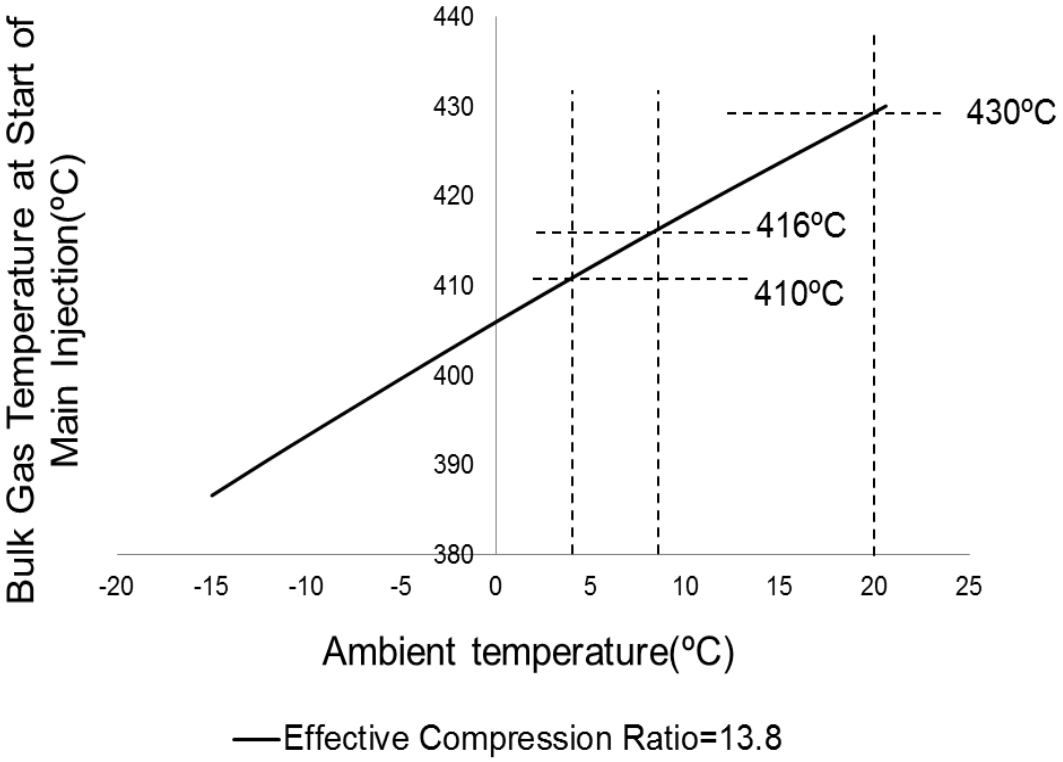

Figure 4-14: Bulk gas temperature at start of main injection versus ambient temperature calculated using Equation 4-4

As illustrated in Figure 4-15, the critical temperature for self-sustaining combustion is between 410°C and 416°C. Assuming this temperature band is independent of compression ratios and ambient temperatures, the band separating success and failure of self-sustaining combustion is shown in Figure 4-15 for a range of effective ratios and ambient temperatures.

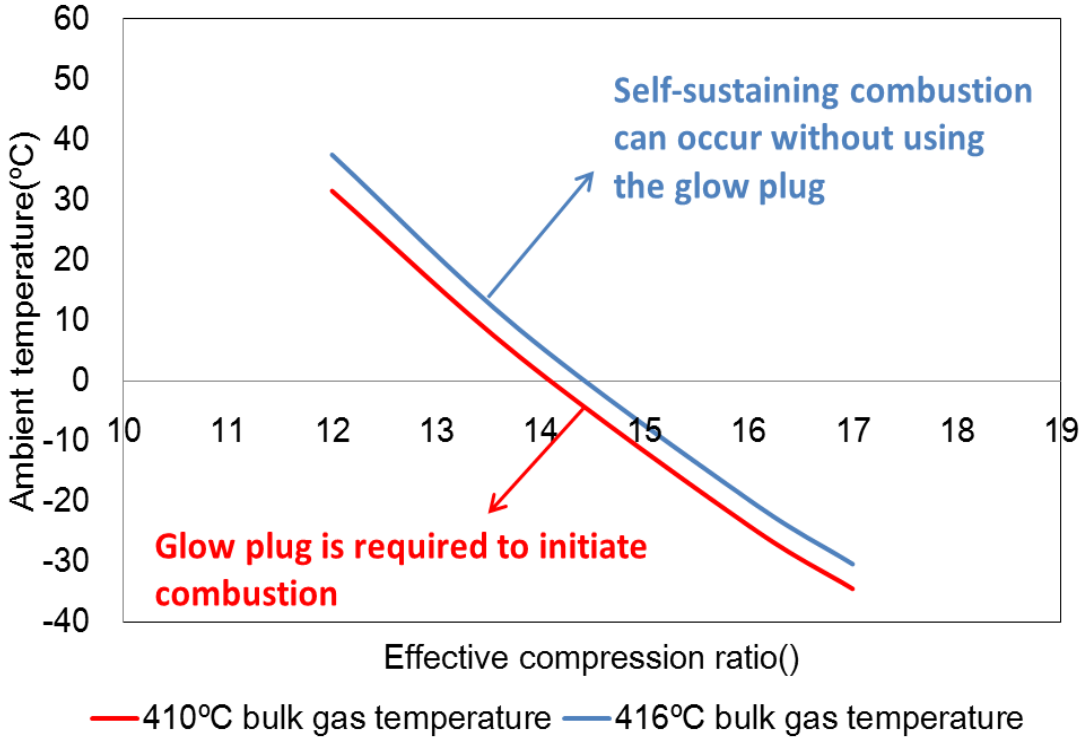

Figure 4-15: Threshold ambient temperatures for successful combustion initiation over various compression ratios

The temperature band here has been 410°C and 416°Cand taken to be the average, 413°C. The influence of the glow plug on combustion initiation and development has been illustrated in Figure 4-16. When the in-cylinder gas temperature at the start of the main injection is below 413°C the glow plug is required to assist the engine to start by eliminating misfire, and achieve satisfactory combustion characteristics. In this study where a twin-pilot-plus-main strategy is used, at the in-cylinder gas temperature range at the start of the main injection is between 413° C and 430° C, even though self-sustaining combustion can be achieved without using the glow plug, glow plug is still required to improve combustion development. When the in-cylinder gas temperature at the start of the main injection is above 430° C, the glow plug becomes redundant.

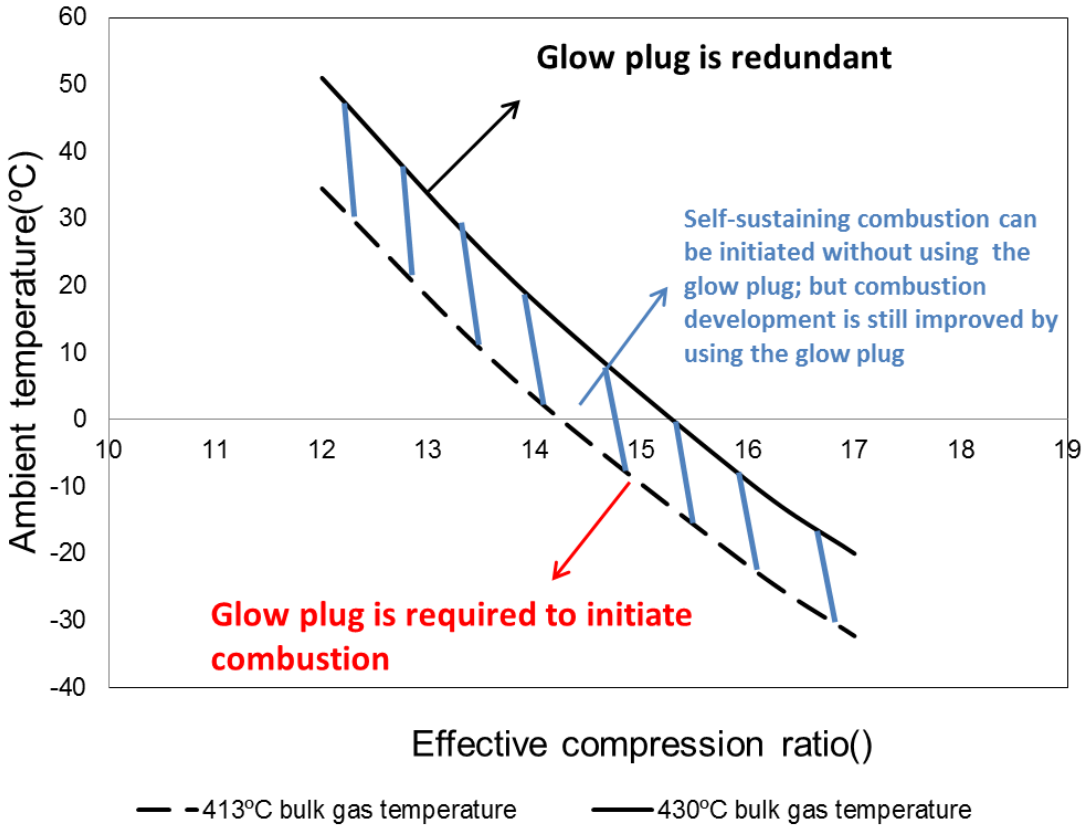

Figure 4-16: Threshold ambient temperatures for the influence of the glow plug on combustion initiation and development the over various effective compression ratios, twin-pilot-plus-main strategy is used, a fixed rail pressure of 400 bar is used

4.4. Influence of Injection Strategies on Glow Plug performance

The influences of injection strategies on combustion behavior aided by the glow plug have been reported in this section. Baseline test condition has been provided in Table 4-2. Tests have been conducted at soak temperature of 10°C with fixed fuel quantity. Pilot quantity was fixed at 4 mg/cycle with number of pilot injections varying from one to four. Engine speed, rail pressure is 1000rpm and 400bar, metallic glow plug used in the work demonstrated in previous sections with the surface temperature of 850 °C is still used in this investigation.

Table 4-2: Test parameters

Parameter	Base line	Sweep
Soak temperature(°C)	10	-
Glow plug tip surface temperature(°C)	850	-
Engine speed(rpm)	1000	-
Rail pressure(bar)	400	-
Total pilot quantity(mg)	4	-
Main quantity(mg)	5	-
Number of pilot injection()	1	1-4
SOI_main(°ATDC)	-8	-
Injection separation(°CA)	6	-

The influence of varying the number of pilot injections on IMEPg for the first 10 firing cycles has been illustrated in Figure 4-17. The magnitude of the IMEPg is around 0.5 bar by using a single-pilot-plus-main strategy. Increasing number of pilot injections from one to two, magnitude of the IMEPg increases to values close to 2 bar, substantially higher than IMEPg when using a single-pilot-plus-main strategy. A slight increase of IMEPg is observed when increasing number of pilot injections from two to three. Magnitude of the IMEPg decreases by increasing number of pilot injections from three to four, magnitude of IMEPg observed when using twin-pilot-plus-main strategy is similar to that using quad-pilot-plus-main strategy, the highest magnitude of IMEPg is achieved when a triple-pilot-plus-main strategy is used.

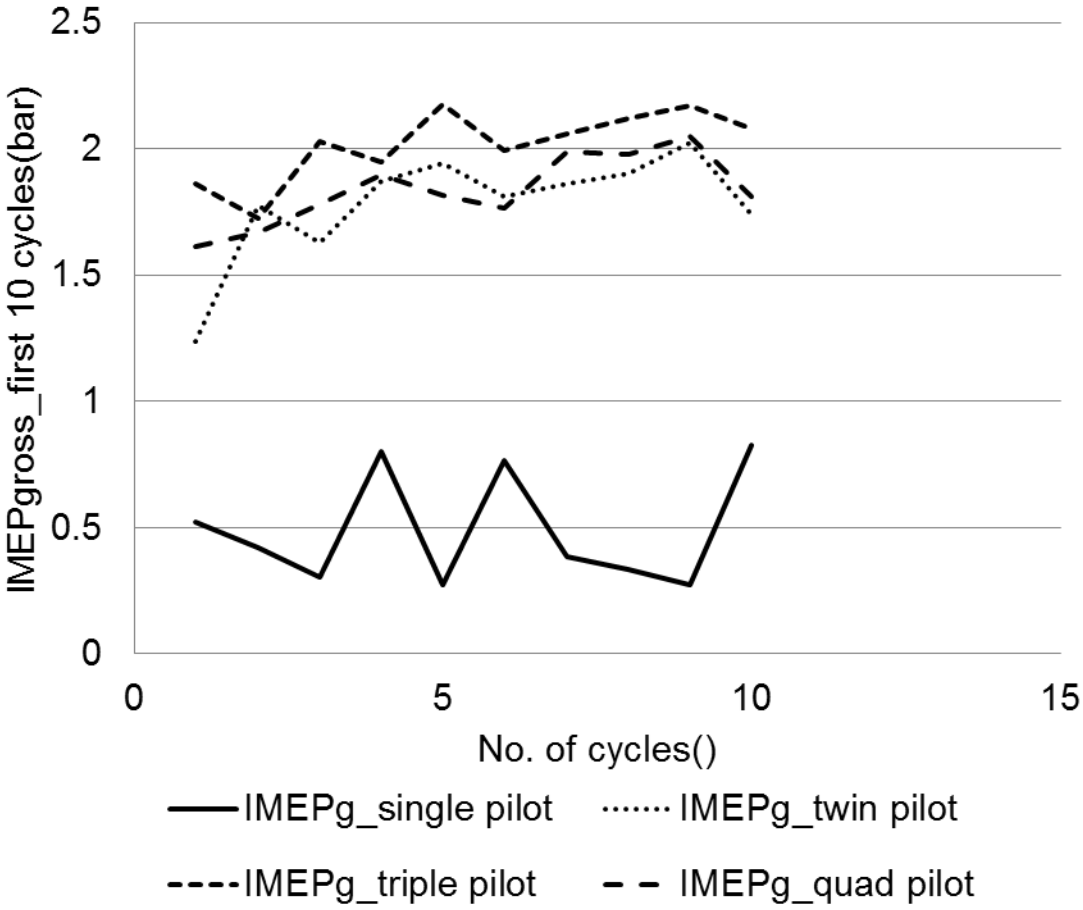

Figure 4-17: Gross IMEP for the first 10 firing cycles. Test parameters refer to Table 4-2

The influence of varying the number of pilot injections on CoV_{IMEPg} over the first 10 firing cycles has been illustrated in Figure 4-18. CoV_{IMEPg} is 46% when using a single-pilot-plus-main strategy, when increasing number of pilot injections from one to two, a considerable decrease of CoV_{IMEPg} is observed, CoV_{IMEPg} is 12% when using a twin-pilot-plus-main strategy. The smallest CoV_{IMEPg} of 7% is achieved when using a triple-pilot-plus-main strategy. However, CoV_{IMEPg} increases slightly to 7.7% by using a quad-pilot-plus-main strategy.

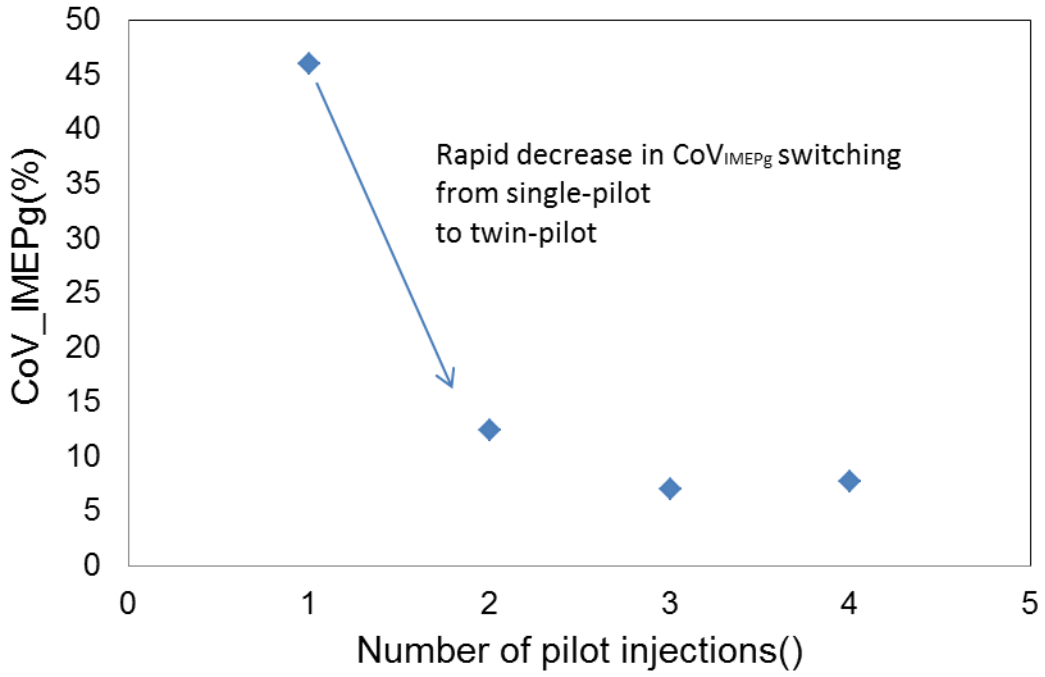

Figure 4-18: CoV_{IMEPg} of the first 10 firing cycles against number of pilot injections. Test parameters refer to Table 4-2

The influence of varying the number of pilot injections on heat release has been illustrated in Figure 4-19. Worse premixed combustion and mixing controlled combustion are shown using a single-pilot-plus-main strategy than using other strategies. The poor heat release rate using single-pilot-plus-main strategy reflects low cumulative heat release as has been shown in Figure 4-20, by using twin-pilot-plus-main strategy, large increase in cumulative heat release is observed from 82 J to 204 J, cumulative heat release achieves highest magnitude at 226 J by using a triple-pilot-plus-main strategy, the magnitude declines to 209 J by using a quad-pilot-plus-main strategy.

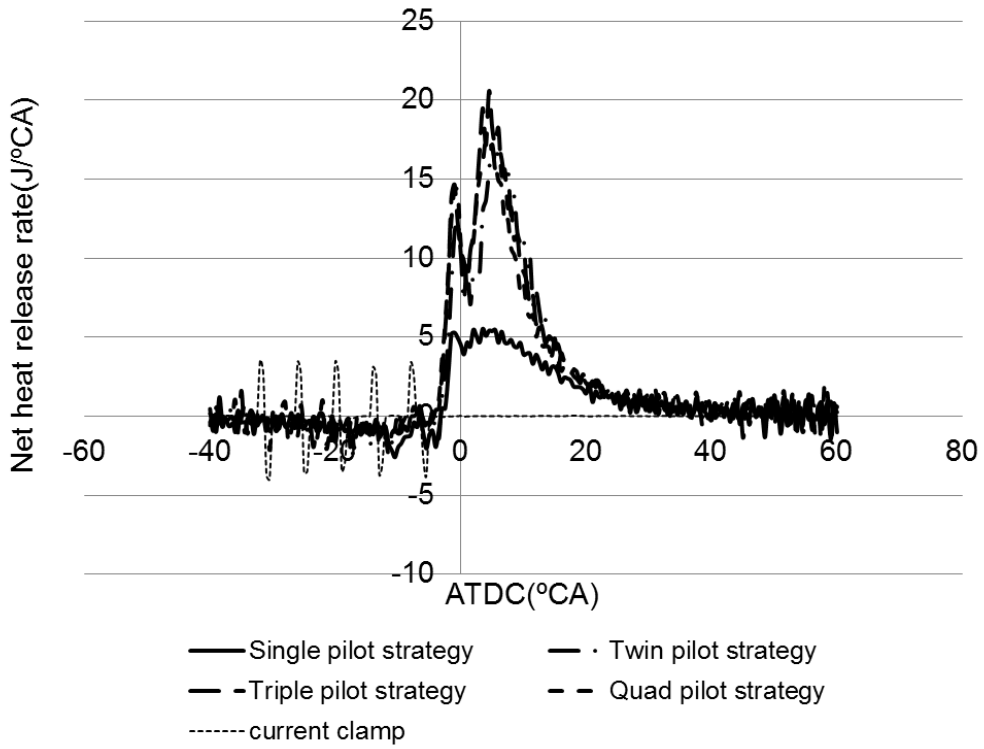

Figure 4-19: Ensemble averaged net heat release rate over the first 10 firing cycles.Test parameters refer to Table 4-2, injector current shown for quad-pilot case

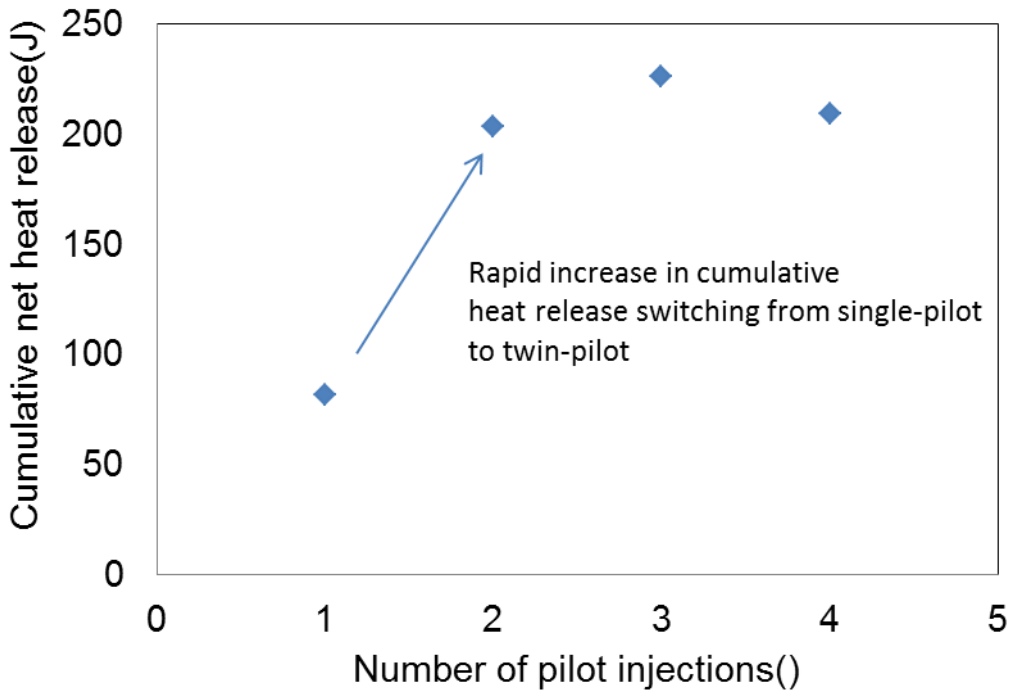

Figure 4-20: Ensemble averaged cumulative gross heat release over the first 10 firing cycles. Test parameters refer to Table 4-2

It is evidenced from the results illustrated in Figure 4-17 to Figure 4-20 that combustion behavior including work output, net heat release and cycle-by-cycle combustion stability is largely improved by using a twin-pilot-plus-main strategy than using a single-pilot-plus-main strategy.

4.5. Discussion and Conclusions

The influence of the glow plug on combustion initiation and development has been reported in this chapter. By using the glow plug, strong premixed combustion followed by vigorous mixing controlled combustion is generated as a result of flame propagation originated from the local combustion induced by the glow plug, in this way, efficient combustion associated with high work output, improved heat release and satisfactory cycle-by-cycle combustion stability is ensured.

The performance of the glow plug is certainly influenced by injection strategies. Work output and heat release is considerably improved by using a twin-pilot-plus-main strategy than using a single-pilot-plus-main strategy. The first pilot injection is in essence a small single-shot and produces a local vapour-air mixture with a low equivalence ratio but self-sustaining reactions only follow a second pilot injection or main injection. When using a twin-pilot-plus-main strategy, local combustion is initiated when the second pilot spray is introduced and much more vigorous main combustion is therefore aided by the local flame. Combustion is continuously improved by increasing the number of pilots to three but the benefit is relatively small.

When the in-cylinder gas temperature at the start of the main injection is below 413ºC, self-sustaining reactions are inhibited and the glow plug is required to support the successful initiation of combustion. In this investigation, combustion development including IMEPg, net heat release and combustion stability is continuously improved by using the glow plug until 430ºC. Above 430ºC, the glow plug becomes redundant. The

improvement of combustion development is associated with enhanced spray vaporization. The benefit of using a glow plug diminished up to ambient temperature of 20^{o}C or in-cylinder gas temperature of 430^{o}C, this conclusion was based on a fixed injection strategy (twin-pilot injection strategy) and glow plug temperature (850^{o}C) and will be uncertain by either varying glow plug temperature or number of injections, both glow plug temperature and injection strategies largely influence combustion characteristics.

Chapter 5 Optical Studies of Combustion Initiation

5.1. Introduction

In this chapter, key results of optical tests performed in this study are illustrated and described. In section 5.2, spray development and combustion initiation are studied. In section 5.3, success or failure of ignition is studied with regards to glow plug tip surface temperature, the glow plug tip surface to the visible spray edge distance and bulk gas temperature. In section 5.4, local equivalence ratio for success and failure of ignition is explored using ANSYS Fluent 14.0, which will be introduced with more details in Chapter 6. In section 5.5, an initiation delay model is developed. Finally, main conclusions are presented.

5.2. High Speed Video Records of Spray and Combustion Development

Evolution of the spray developments described in this section. In this setup, spray development was observed by using the high speed camera. Spray was injected from an injector nozzle under rail pressure of 400 bar into environment with pressure of 38 bar. Evolution of the spray penetration has been captured from the start until the end of injection as has been shown in Figure 5-1. The injection event was held for 1.6ms; images showing spray at 0.4ms ASOI, 0.8ms ASOI and EOI have been displayed in one picture. As illustrated in Figure 5-1, the head of the spray is relatively sharp at 0.4ms ASOI, because the drag force is strong after a small amount of time after leaving nozzle hole, at 0.8ms ASOI and later, the shape of spray head is more close to hemi-sphere as a result of reduced drag force attributed to smaller spray momentum. As has been shown in Figure 5-1, under a rail pressure of 400 bar, spray cone angle kept constant with two clear boundaries forming two straight spray edges,

this observations agrees with findings that have been reported in [72, 84, 85, 90] demonstrated the spray cone angle was a constant value provided that the rail pressure, gas density, fuel properties and injector characteristics were unchanged.

The spray motion is advection-dominated, which implies combustion initiation observed in optical tests by the glow plug in region near the glow plug is at the spray edge. If the spray does not directly impinge on the glow plug tip, ignition that occurred at the spray edge must be dictated by self-sustaining combustion of local fuel-air mixture. Hence, local temperature and local equivalence ratio near the spray edge close to the glow plug is of great interest in this study.

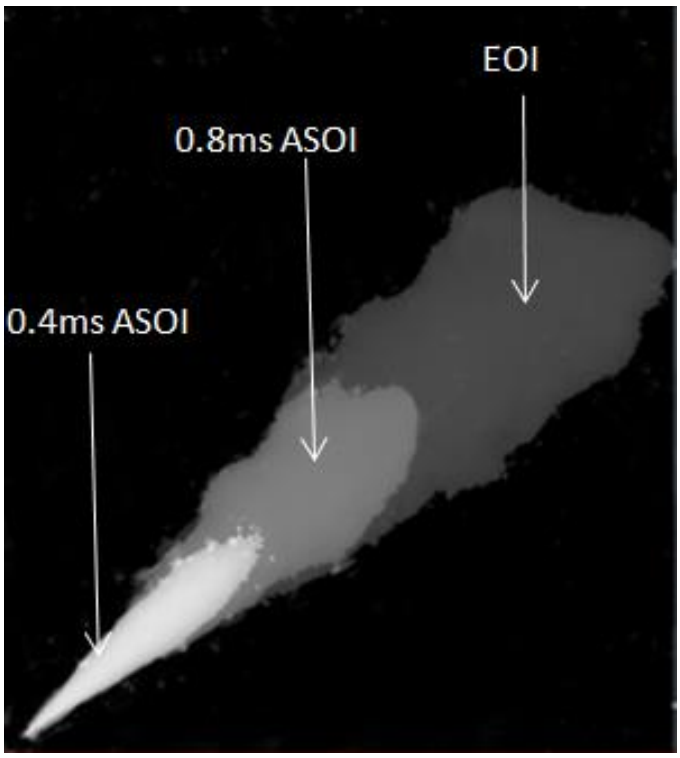

Figure 5-1: High speed image showing evolution of spray penetration after the spray passes the glow plug, rail pressure=400 bar, pressure=38 bar, bulk gas temperature=200°C, fuel temperature=15°C

The initiation and early development of combustion aided by the glow plug is described in this section. An example of a sequence of images illustrating the successful initiation of combustion is given in Figure 5-2 for

the baseline conditions summarized in Table 5-1. In this example where single pilot plus main strategy was used, pilot spray passed the glow plug but failed to be ignited. The first spots of luminous emissions appear close to the glow plug tip at the edge of the fuel spray after the start of the main injection and quickly formed clusters up to 0.8ms after start of the main injection. This local combustion stabilized between glow plug surface and spray edge until the end of the main injection. This local initiation triggers a rapid expansion of the enflamed volume after end of the main injection, principally in the downstream direction of spray penetration. There were no significant differences in the way a successful initiation and subsequent development took place when bulk air or glow plug temperature was increased, or distance from glow plug surface to spray edge decreased, from settings at which initiation failed. There is some evidence of pilot injection producing weak luminous soot emissions close to the glow plug tip, but disappear before the start of the main injection. Combustion was initiated during the main injection in majority of the tests conducted in this study where single pilot plus main strategy was used, the main role of the pilot injection was to raise equivalence ratio in the spray region. This statement is supported by La Rocca et al. [30] who have investigated the influence of injection strategies on in-cylinder fuel distribution. The work suggested that a pilot injection provides a more homogenously mixed environment in the vicinity of the glow plug.

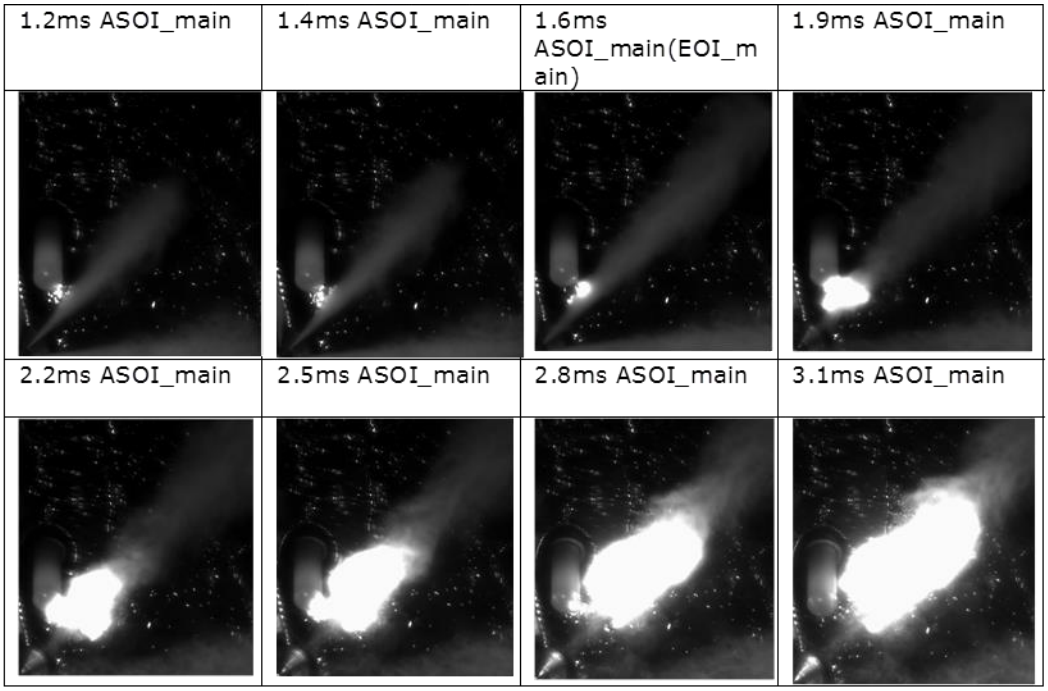

Figure 5-2: Initiation and development of combustion of a spray in a quiescent bomb using a glow plug. Test condition is referred to baseline condition expressed in Table 5-1

5.3. Factors Influencing Initiation Success and Failure

The successful initiation of self-sustaining combustion of local mixture is dependent on local temperature and equivalence ratio. Three factors have been investigated in this section. The influence of glow plug temperature on the success or failure of ignition depends on the distance between the glow plug tip surface and the visible boundary of the spray. The success and failure boundaries have been mapped for two bulk gas temperatures, 200°C and 160°C. The results are presented in Figure 5-3 and Figure 5-4 respectively. In all of these cases, the bulk pressure, fuel quantity and injection strategy were fixed at the baseline values given in Table 5-1. The distance between the glow plug tip surface and spray edge was varied in steps from zero to the point at which ignition always failed at the highest value of glow plug temperature. The distance was varied by rotating the injector. Fuel is stored in the tank and fuel temperature is equals to laboratory temperature, 15° C. A deflector plate was used to divert the

second adjacent spray away from the glow plug to prevent the ignition of this. For each position of the injector the glow plug tip surface temperature was swept from 300°C to 1100°C. Three tests were carried out at each setting. Triangles mark settings at which combustion initiation was always successful. Crosses mark settings at which initiation always failed. Triangle-cross overlapping points represent settings at which both successes and failures were recorded.

Table 5-1: Summary of test parameter settings

Parameter	Base line	Sweep range
Vessel pressure (bar)	38	—
Rail pressure(bar)	400	—
Pilot quantity(mg)	2	—
Pilot quantity(mg/spray)	0.25	—
Main quantity(mg)	18	—
Main quantity(mg/spray)	2.25	—
Pilot to main separation(ms) -SOI(pilot)-SOI(main)	1.7	—
Bulk air temperature(ºC)	200	20-200
Glow plug surface temperature(ºC)	900	300-1100
Glow plug to spray edge distance(mm)	1.3	0-2.6

As shown in Figure 5-3 and Figure 5-4, the surface temperature of the glow plug required for successful ignition rises with increasing separation between the glow plug and the spray edge. The required temperature is lowest when the spray passes close to the surface, but is never less than a minimum value of 413°C.The threshold temperature for self-ignition. The threshold temperature was obtained from engine test data reported in Chapter 4, which indicated a temperature of about 413°C is required for self-sustaining combusting without the aid of the glow plug. In the combustion bomb experiments, the bulk charge temperature could only be

pre-heated just above 200°C, and the surface temperature of the glow plug was the controlling minimum. The bulk gas temperature did influence the surface temperature required for success at greater separations between glow plug and spray. This can be seen in Figure 5-5; the required minimum temperature of the glow plug is higher at the lower bulk gas temperature at any given separation distance. This is indicative of the influence of bulk gas temperature on the temperature variation in the region near the glow plug and the need for a minimum temperature of 413°C at the site of ignition, which occurs further from the glow plug when glow plug to spray edge separation is greater.

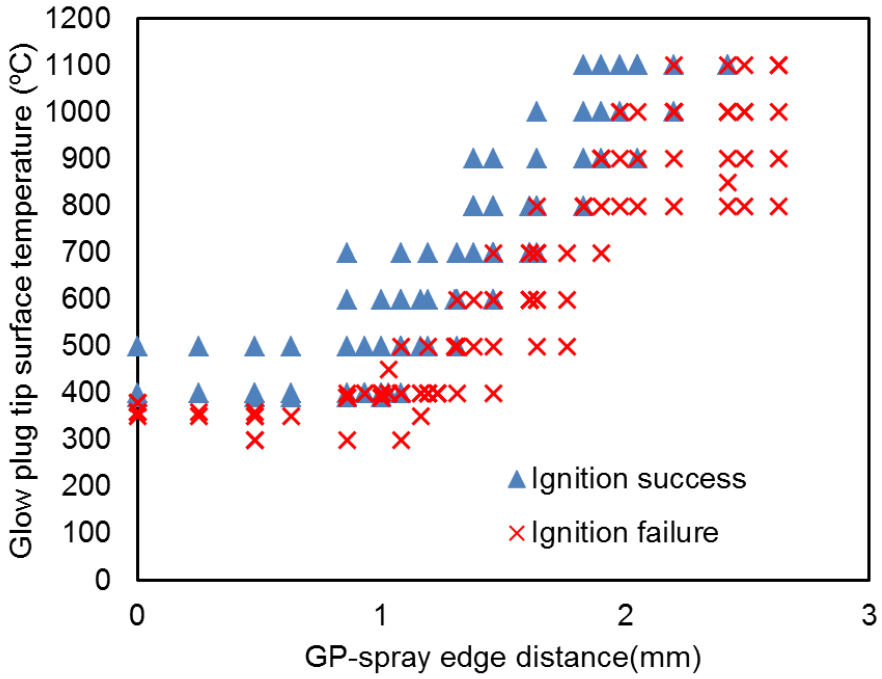

Figure 5-3: Combustion ignition success and failure tested at 200°C bulk gas temperature

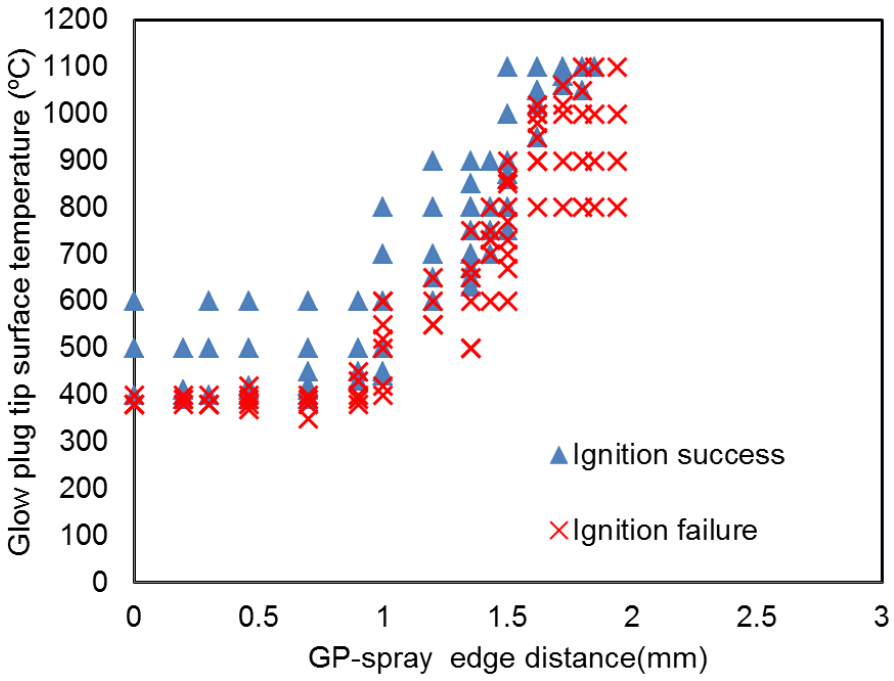

Figure 5-4: Combustion ignition success and failure tested at 160°C bulk gas temperature

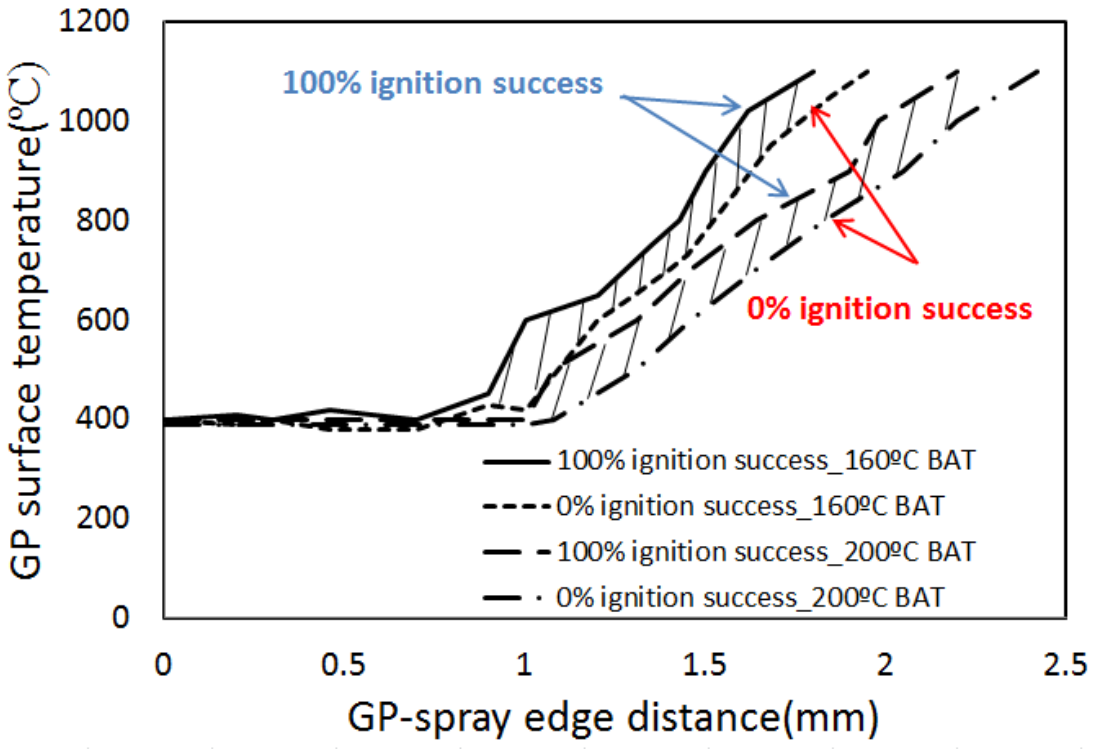

Figure 5-5: Success and failure boundaries

The influence of bulk gas temperature on the glow plug temperature required for ignition success is shown in Figure 5-6 for an extended range of gas temperatures, from 20°C to 200°C, and a fixed glow plug to spray

separation of 1.3mm. The results show a progressive reduction in the required glow plug temperature as the bulk gas temperature is raised. As before, three tests were performed per each data point and triangle, cross represents combustion success and combustion failure respectively. The band of glow plug temperatures spanning 100% failures to 100% successes is similar across the range of gas temperatures, at ~50°C. The influence of increasing bulk gas temperature is attributed to improved droplet vaporization.

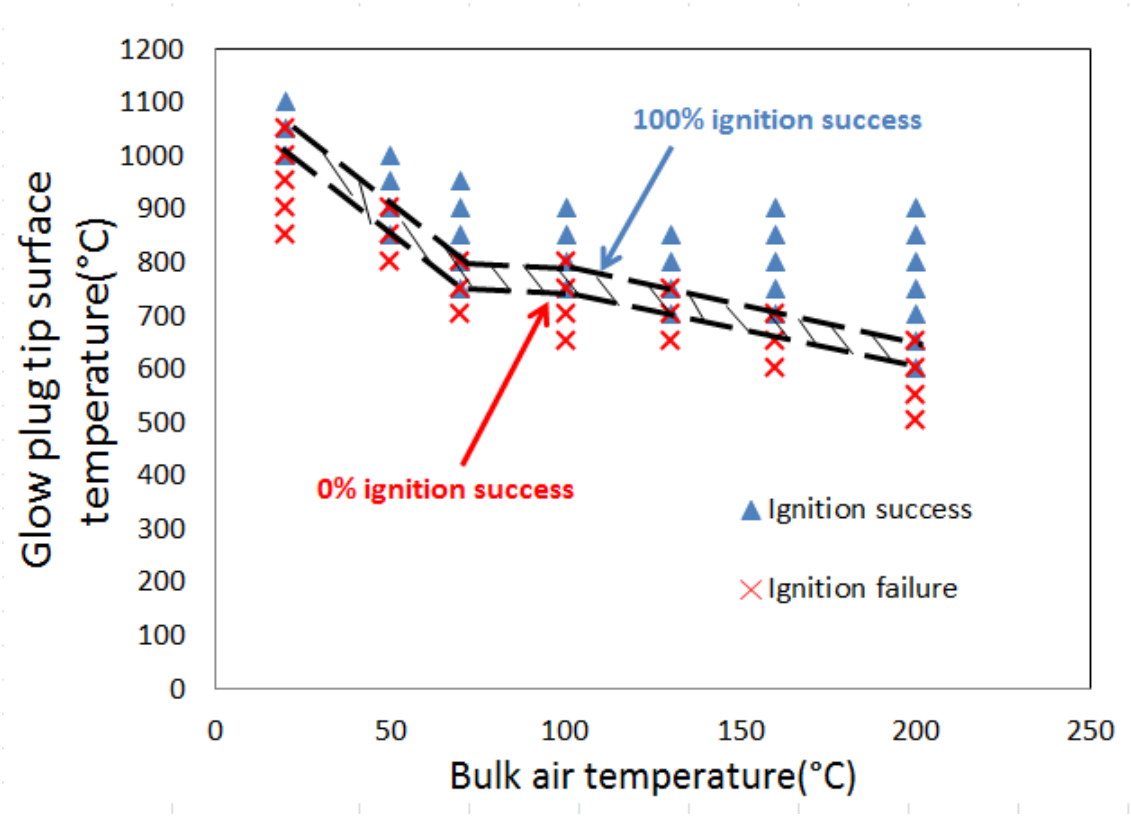

Figure 5-6: Influence of glow plug surface temperature and bulk gas temperature on ignition success and failure

The site of initiation has been explored by observing luminous soot emissions with extended separations between the glow plug tip surface and the spray edge. As illustrated in Figure 5-7, it can be observed that the site of initiation that represented by the first luminous soot emissions maintains its proximity to the edge of the spray as the distance between the glow plug and the spray is varied. This suggests that a local minimum

equivalence ratio as well as a minimum temperature is required for successful initiation.

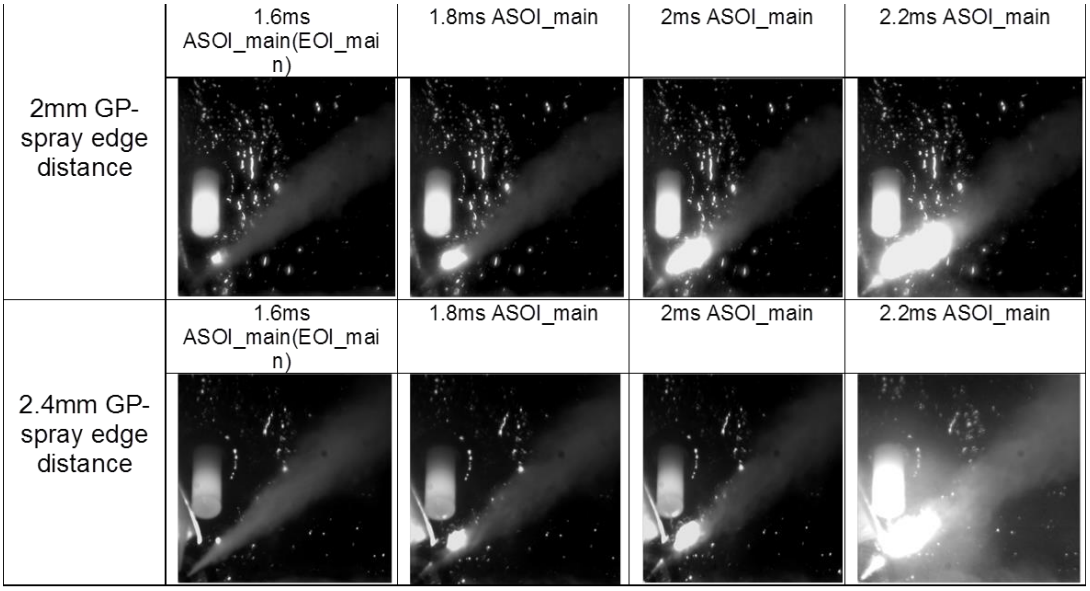

Figure 5-7 Images showing the site of initial luminous emissions occurs close to the edge of the fuel spray as separation between the spray and the glow plug is increased from 1.3mm in Figure 5-2 to 2.0mm (upper images) and 2.4mm (lower images), with a glow plug temperature setting of 1100°C

5.4. Effect of Varying Number of Pilot Injections on Combustion

Initiation and early development has been captured and shown in Figure 5-8 and Figure 5-9 for single and twin pilot strategy respectively, images from the combustion bomb experiments were shown and linked to the corresponding points in the heat release data. The information from these complementary sources aids understanding of the stages the initiation and development process goes through.

As illustrated in Figure 5-8, when a single-pilot-plus-main injection strategy is used, the pilot injection generates a region of premixed fuel vapour and air near the glow plug without producing any luminous emissions prior to the start of the main injection. Soot emissions first appear only after the main injection raises the local equivalence ratio above the required threshold. In the case illustrated, the glow plug is equally-distant from the two nearest fuel sprays and luminous emissions appear at the edges of both sprays.The momentum and mixing of the main spray can displace and distort the luminous area before inflammation expands downstream in both sprays adjacent to the glow plug. The heat release rate rises rapidly and achieves a premixed spike of 6 J/ºCA, after the premixed spike, the heat release rate flattens before increasing to a second peak of 8J/ºAssociated with mixing controlled combustion.

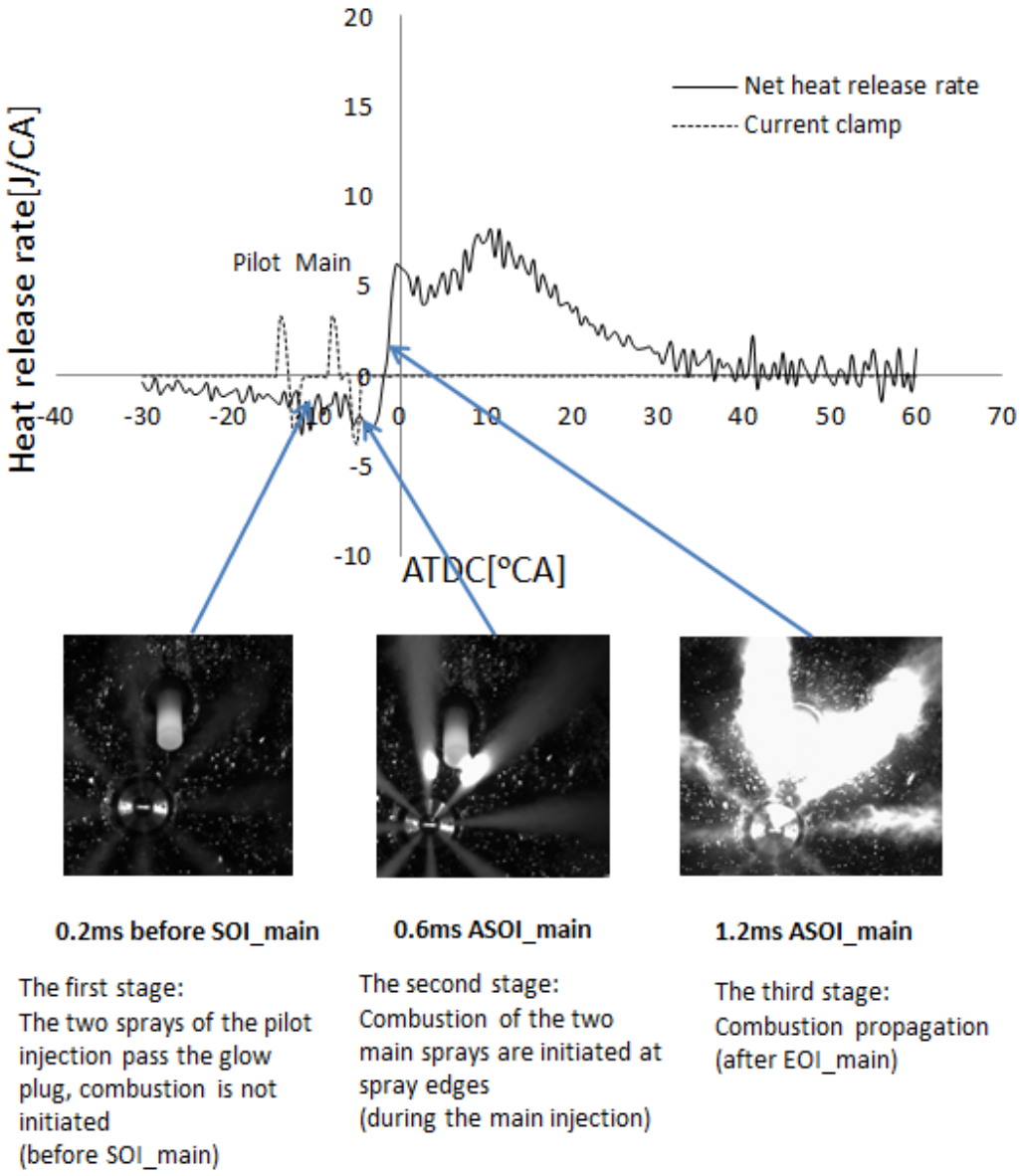

Figure 5-8: Net heat release rate, injection pulse as a function of crank angle after TDC, high speed images showing combustion events at corresponding time with engine operation. Conditions: 1000rpm engine speed, 10°C soak temperature, 400 bar rail pressure, Main injection started at -8°CA ATDC with 6° CA separation, fuel quantity is (2,7) mg for pilot and main

A similar compilation of images for an injection strategy comprised of two pilot injections and a main injection is shown in Figure 5-9, Again, the first pilot injection does not initiate combustion but generates a premixed region near to the glow plug. The first luminous emissions appear after the second pilot injection. The luminous area grows locally and aids the

development of combustion when the main injection takes place. Compared to the heat release rate from the single pilot strategy, a stronger premixed spike is observed followed by a more vigorous mixing controlled combustion. Even though total fuelling level is as same as when the single-pilot-plus-main strategy is used, improved heat release is observed compared with the one using single-pilot-plus-main strategy, premixed spike and mixing controlled spike is 11 J/° CA and 16J/° CA respectively, approximately twice of the magnitude of the heat release rate as shown in Figure 5-8.

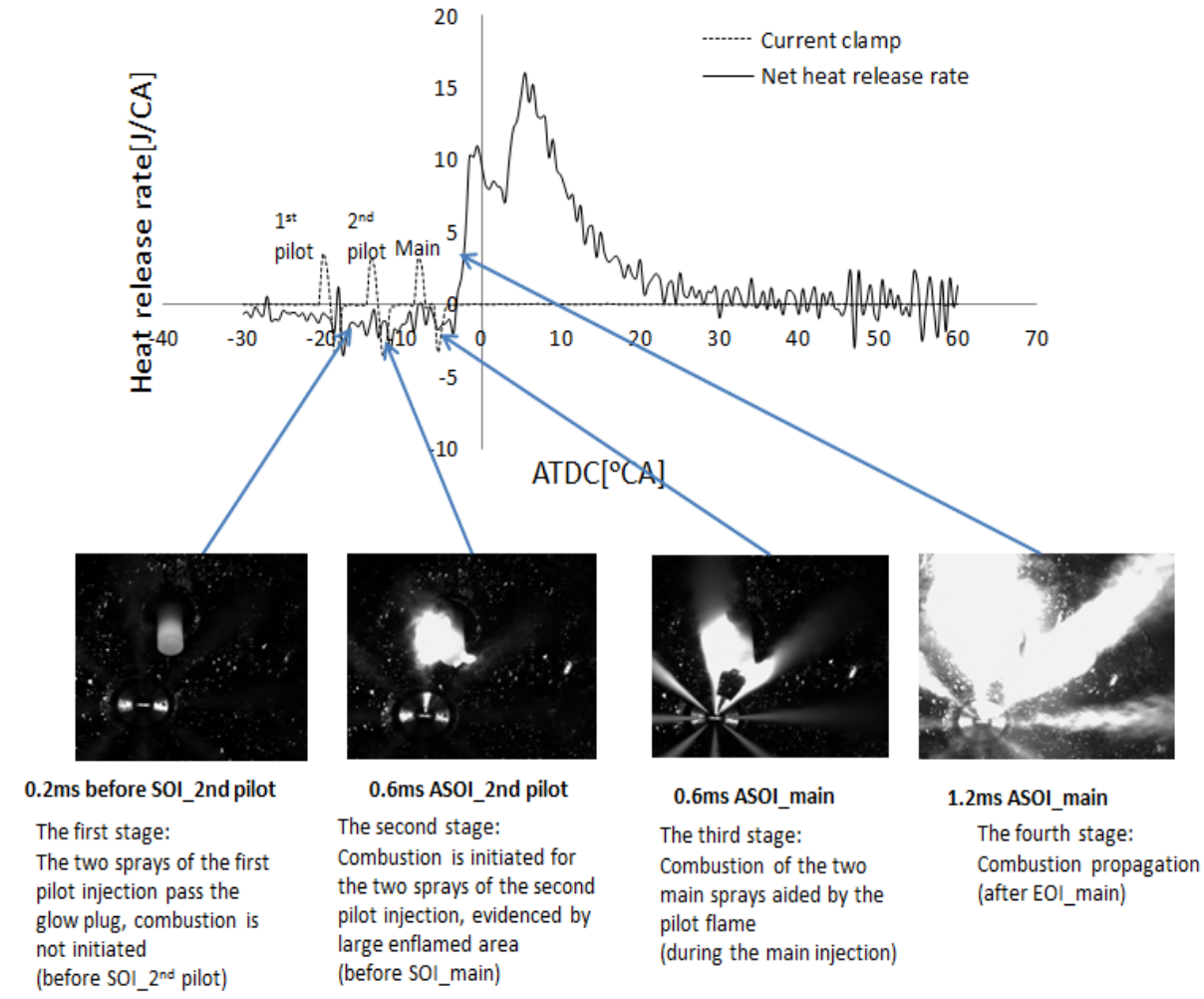

Figure 5-9: Net heat release rate, injection pulse as a function of crank angle after TDC, high speed images showing combustion events at corresponding time with engine operation. Conditions: 1000rpm engine speed, 10° C soak temperature, 400 bar rail pressure, Main injection started at -8° CA ATDC with 6° CA separation, fuel quantity is (2,2,5) mg for pilot and main

5.5. Local Equivalence Ratio

It has been observed in optical images that the combustion was initiated at spray edge and the local position was the shortest approach to the glow plug, both temperature and vapor/air equivalence ratio at this local position are key factors for a successful combustion initiation. This local position has been shown in Figure 5-10.

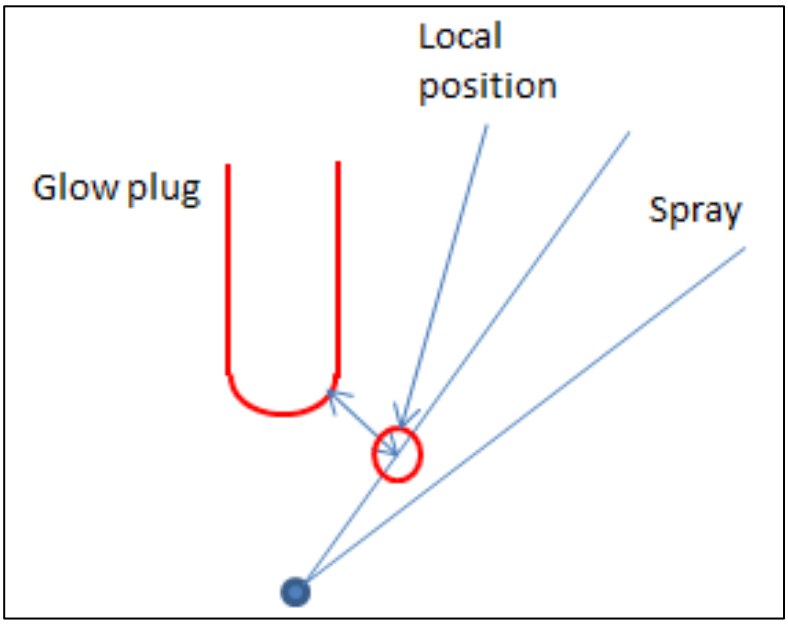

Figure 5-10: Illustration of local position at spray edge closest to the glow plug tip surface, where temperature and equivalence ratio are investigated

CFD code, ANSYS Fluent 14.0 was used in this study because neither the single cylinder engine nor the combustion bomb provided direct information on equivalence ratio in the vicinity of the glow plug. Details of spray modelling will be covered in Chapter 6. In short, the spray was simulated to penetrate into quiescent gaseous environment at a uniform temperature/pressure that equals to temperature/pressure that has been controlled in the optical tests. A cylindrical rod with the same diameter of the glow plug was used with surface temperature equals to glow plug surface temperature. Simulations were carried out for bulk air

temperatures of 200ºC and 160ºC, from the start of the pilot injection to the time when the first luminous emissions were observed in the experimental work, or later for cases when ignition failed. For each case, the spatial variation of vapour air equivalence ratio in the vicinity of the 413ºC isotherm surrounding the glow plug was predicted for the time when the first luminous soot emission appeared. Various combinations of glow plug temperature, bulk air temperature and separation between glow plug and spray edge were covered. The ignition success and failure boundaries mapped from the experimental results are shown in Figure 5-5. The corresponding predictions of fuel air equivalence ratio at the 413°C isotherm are given in Figure 5-11. Along the boundary between ignition always failing and sometimes succeeding, the computational results show that fuel air equivalence ratio at the 413°C isotherm is approximately 0.15. Along the boundary between ignition sometimes failing and always succeeding, the predicted fuel air equivalence ratio at the 413°C isotherm is approximately 0.35. The lower and upper values of equivalence ratio between which ignition could fail or succeed did not vary with glow plug temperature, bulk air temperature or separation between glow plug and spray edge.

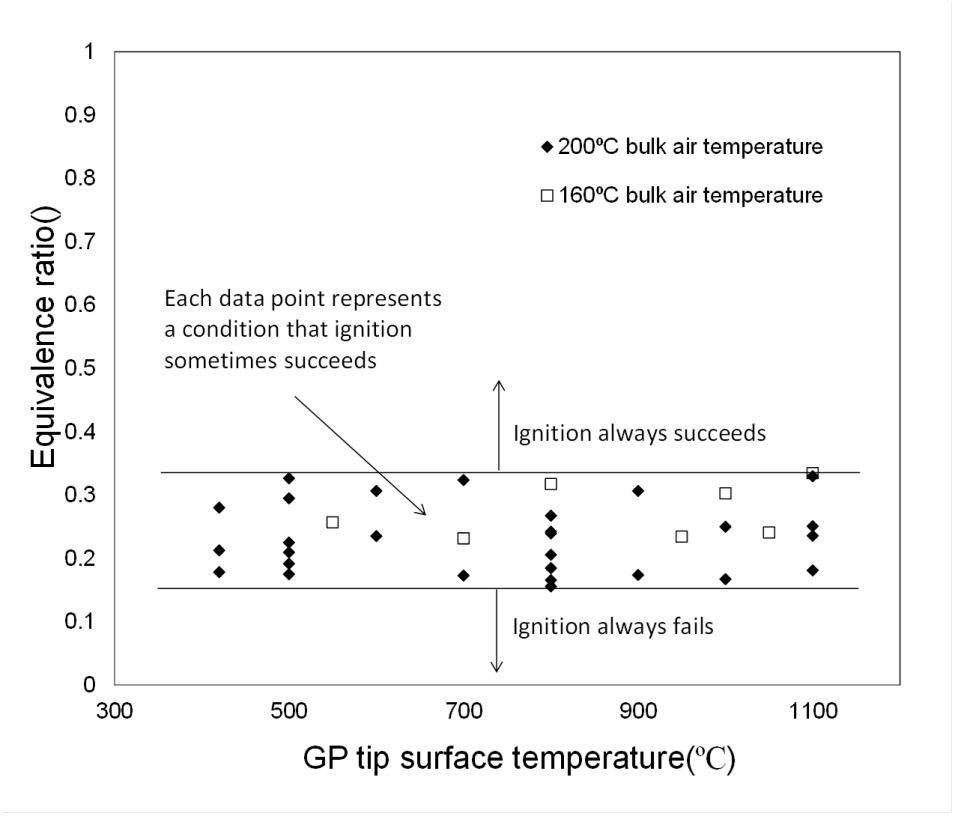

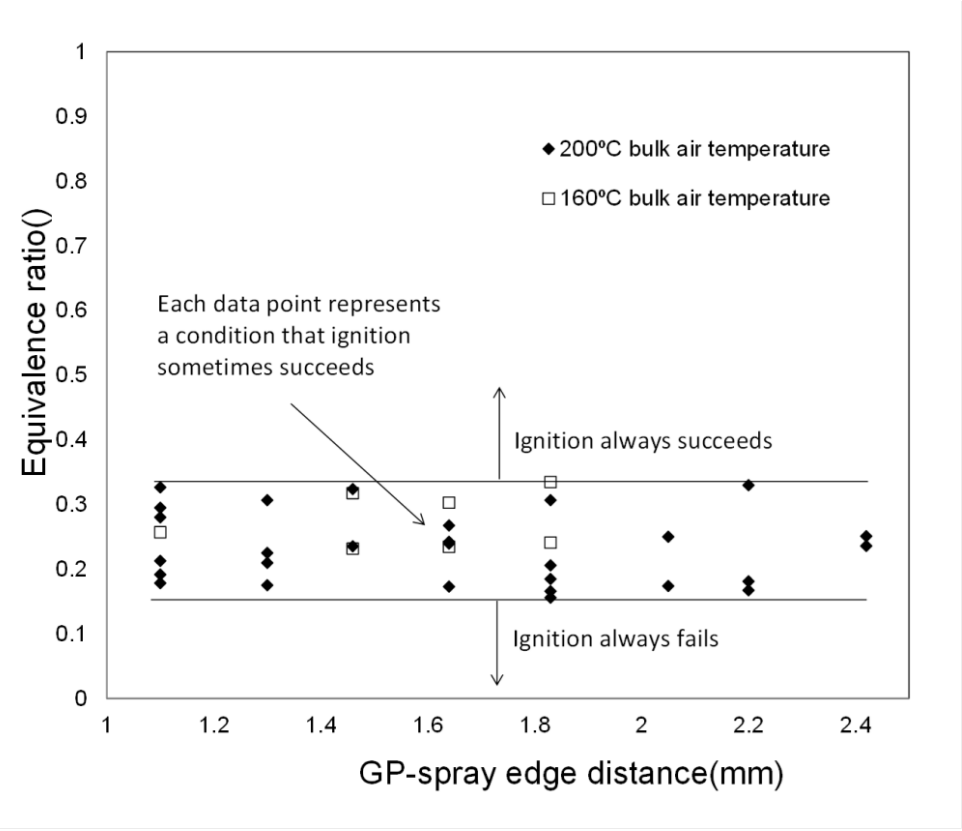

Figure 5-11: Equivalence ratio at 413oC isotherm at appearance time of the first luminous soot emission for points in shaded area shown in Figure 5-5, which means combustion success and failure co-exist

The tests performed in this study indicate self-sustaining reactions can be initiated at bulk gas temperature above 413°C to form a local exothermic site which grows to enflame the mixture produced by the main injection. At bulk gas temperature lower than 413°C, the assistance of the glow plug is required as illustrated in Figure 5-12, two requirements have to be satisfied for successful combustion initiation: a minimum local temperature of 413°C, and a minimum fuel-air equivalence ratio of 0.15-0.35.

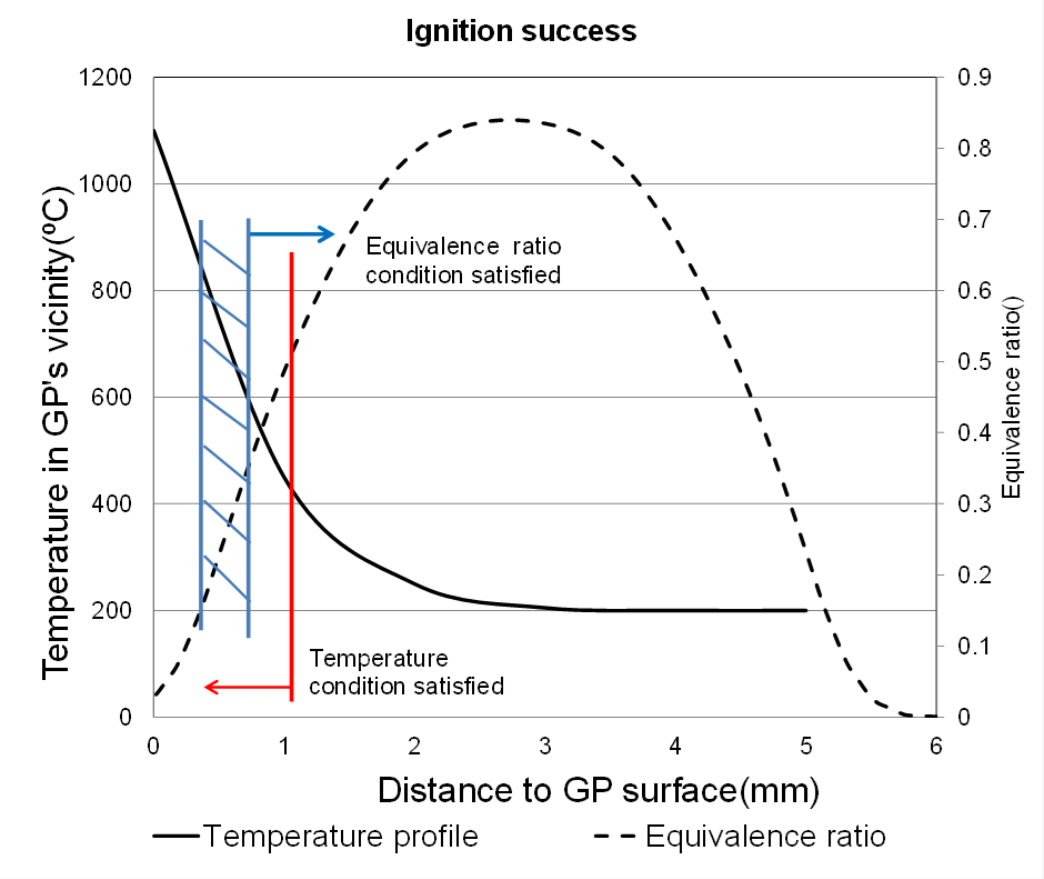

Figure 5-12: Illustration of combustion initiation mechanism

5.6. Modelling Initiation Delay

It has been shown in previous studies undertaken in the optical vessel [4], short initiation delay is associated with rapid increase of enflamed area and maximum enflamed area, indicating combustion characteristics is improved when the initiation delay is short. The initiation delay is defined

as the time from the start of the recent injection to when the combustion is successfully initiated. In this section, initiation delay is modelled and parameters influencing glow plug aided combustion are identified.

The combustion is initiated at the spray edge close to the glow plug, development of equivalence ratio in the vicinity of the glow plug is of interest and has been predicted using ANSYS Fluent 14.0, details regarding spray model setup will be covered in Chapter 6. Local equivalence ratio is monitored and plotted against time after the start of the main injection as illustrated in Figure 5-13. Local equivalence ratio versus time after the start of the main injection is shown, a pilot injection has been modelled prior to the main injection, and the motion of the pilot spray after the end of the injection is governed by the inertia. Equivalence ratio raises and declines as the spray cloud approaches and leaves the region in the vicinity of the glow plug.

The pilot injection is weak and unable to achieve successful ignition, which agreed with the test results shown in Chapter 4 that the pilot injection only generates premixed environment rather than promoting combustion when a single-pilot-plus-main strategy is used, combustion initiation occurs after the main spray is introduced. The main spray approaches the region near the glow plug at approximately 0.3ms after the start of the main injection, a step increase of equivalence ratio is observed as illustrated in Figure 5-13, the local equivalence ratio, local temperature and back pressure will remain relatively constant, this local equilibrium will last until the combustion is initiated or the end of the injection, whichever occurs first.

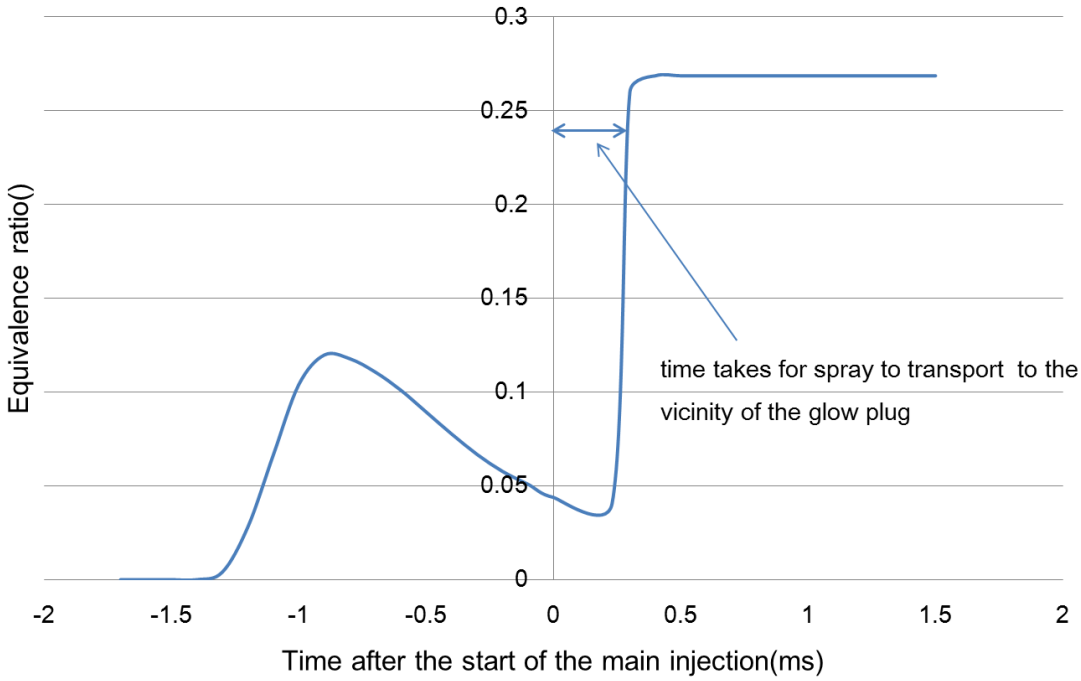

Figure 5-13: Local equivalence ratio development in the vicinity of the glow plug. Simulation was carried out to predict conditions refer to baseline in Table 5-1, the glow plug temperature which was 700°C, a single-pilot-plus-main injection strategy was used

The initiation delay could be spilt into two sequential parts separated by the moment when the spray approaches the glow plug. The first part prior to this timing is the period that the spray transports from the injector to the glow plug whilst atomization, droplet vaporization and fuel-air mixing take place; the second part is time required for the local mixture in the vicinity of the glow plug to go through cool flame reaction (OH oxidation process with flame temperature around 400°C). In general, these two sequential parts are named transport delay and chemical delay respectively. It is worth noting that the transport delay is only part of the physical delay, vaporization and mixing is included in the transport delay. In the current study where the rail pressure was fixed at 400 bar and the back pressure was fixed at 38 bar, the transport delay was deemed constant. The influence of gas temperature on spray tip penetration has been investigated in this optical study, local gas temperature of the region where the spray covered was influenced by switching on/off the glow plug

and modifying bulk gas temperature, it has been indicated in Figure 5-14, the influence of gas temperature on the early phase spray tip penetration was small. It is because the spray does not fully disintegrate into droplets, and at this early phase of spray development, the spray tip penetration is dictated by pressure difference between the rail pressure and the back pressure rather than gas temperature [72, 136, 137]. Given that gas temperature makes insignificant diffidence on the early phase spray tip penetration, the transport delay here is determined by pressure drop between the rail pressure and the back pressure as well as the injector hole diameter, based on studies carried out by Wakuri et al. [84], Dent et al.[85], Hiroyasu et al. [72] and Schihl et al. [138], spray tip penetration can be expressed as Equation 5-1.

$$S = A_{transport}(P_{Rail} - P)^{0.25} {d_0}^{0.5} t^{0.5}$$

Equation 5-1

If S is distance between the glow plug tip and the injector tip, time t refers to time for spray to transport to the vicinity of the glow plug, i.e. the transport delay ($\tau_{transport}$). $A_{transport}$ is the multiplying factor in this expression. In this study, rail pressure was 400 bar, back pressure was 38 bar, injector hole diameter was 0.12×10^{-3} m, distance between the glow plug tip and the injector tip was measured to be 0.01m, t was 0.3×10^{-3}s, multiplying factor $A_{physical}$ could be obtained using Equation 5-2.

$$A_{transport} = \frac{S}{(P_{Rail} - P)^{0.25} {d_0}^{0.5} t^{0.5}} = \frac{10}{(362)^{0.25} \times (120)^{0.5} \times (0.3 \times 10^{-3})^{0.5}} = 12.1$$

Equation 5-2

The transport delay can be expressed using Equation 5-3, note that in Equation 5-1, the unit of time is s, considering the consistency with the chemical delay expression, it is necessary to use ms, so the whole expression for the transport delay($\tau_{transport}$) should be multiplied by 1000, the expression of the transport delay($\tau_{transport}$) has been shown in Equation 5-3 by combining Equation 5-1 and Equation 5-2:

$$\tau_{transport} = \frac{1000S^2}{{A_{transport}}^2(P_{Rail} - P)^{0.5}d_0} = \frac{6.9S^2}{(P_{Rail} - P)^{0.5}d_0}$$

Equation 5-3

In Equation 5-3, S is the distance between the glow plug tip and the injector tip (mm), P_{Rail} is rail pressure (bar), P is back pressure (in bar) and d_0 is injector nozzle hole diameter (μm) and $\tau_{transport}$ is transport delay (ms).

	Spray development with glow plug switched off, bulk air temperature=100°C	Spray development with glow plug switched on(tip surface temperature=1000°C, bulk air temperature=200°C
0.3ms after the start of the injection	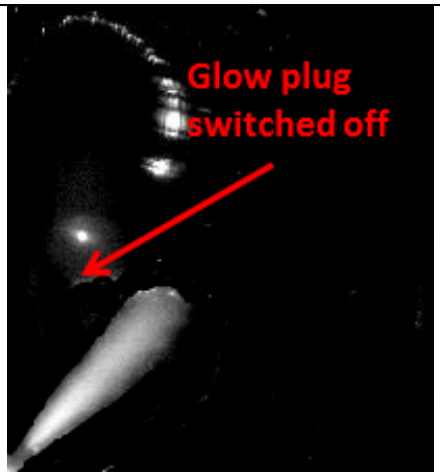	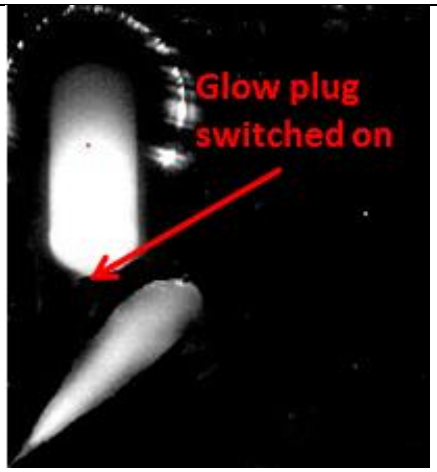

Figure 5-14: Optical observation of early development of spray. Sprays took 0.3ms to transport to the glow plug in both cases, indicating the influence of gas temperature on early phase of spray penetration is negligible

The chemical delay is governed by chemical kinetics that can be predicted using Arrhenius-type equation, which has been shown in Equation 5-4. In spite of its simple form it has been proved to be an accurate model to predict processes of exothermic reactions. The model does not account for individual collisions but it considers on a macroscopic perspective by using

term E_a the activation energy which is constant over a range of temperature conditions and is determined experimentally for a given fuel type.

$$\tau_{chemical} = A_{chemical} P^{-n} \exp(\frac{E_a}{RT})$$

Equation 5-4

Where P is the back pressure, T is temperature, E_a is activation energy, R is universal gas constant, and A, n are adjustable constants.

Based on the semi-empirical equation developed by Wolfer [65] back to 1938, Waston [66] experimentally studied engine ignition delay model, and integrated the activation energy term and universal gas constant into a fixed constant of 2100 (for diesel fuel), besides, the exponent of back pressure term has been assigned to -1.02, and the weak dependence of equivalence ratio has not been included. The model is shown in Equation 5-5.

$$\tau_{chemical} = A_{chemical} P^{-1.02} \exp(\frac{2100}{T})$$

Equation 5-5

The Arrhenius-type equation shown in Equation 5-5 will be used in this study to predict the chemical delay. As has been described earlier, transport delay is the time for spray to transport to the glow plug, so a sequential initiation delay consisting of physical part and chemical part is expressed in Equation 5-6.

$$\tau = \tau_{transport} + \tau_{chemical} = \frac{6.9 S^2}{(P_{Rail} - P)^{0.5} d_0} + A_{chemical} P^{-1.02} \exp(\frac{2100}{T_{local}})$$

Equation 5-6

Local temperature is the local temperature at the spray edge close to the glow plug, in Kelvin. For the Arrhenius-type equation, the temperature

refers to mean temperature during the chemical delay, which is difficult to obtain unless the chemical delay is already known. Kevric [139] suggested that when a sequential delay form is used, the mean temperature during the chemical delay can be replaced by the temperature at the end of the physical delay. Refers to the definition for the physical delay in this investigation, temperature distribution should not be disturbed by spray momentum by the time when the spray just gets the glow plug, so it is assumed local temperature in vicinity of the glow plug at the end of the physical delay is equal to the local temperature at the start of the main injection.

The local temperatures at location of spray edge close to the glow plug at the start of the main injection have been obtained either by experimental measurement or theoretical estimation. In this study, the temperature in the vicinity of the glow plug was measured experimentally by inserting a K-type thermocouple into the bomb where inside the bomb the bulk gas temperature is 200°C. The thermocouple tip was located horizontally to the glow plug tip at a variety of distances (0-2.5mm), the glow plug tip surface temperature (800°C-1100°C) was controlled by the voltage supplied, and the gas temperature was recorded once the glow plug temperature stabilized. Two major parameters control the local gas temperatures: the glow plug tip surface temperature and distance from the surface. A calibration was carried out to relate the local gas temperature to those two parameters as has been shown in Figure 5-15, the calibration equation was developed based on Figure 5-15 as shown in Equation 5-7 which gave a good fit to experimental results.

$$T_{local} = T_{GP}/(0.38x + 1)$$

Equation 5-7

Where T_{GP} is the temperature of glow plug tip surface, x is the distance to the glow plug tip surface. In this model, x refers to the distance between

the glow plug tip surface and the spray edge. The calibrated gas temperature is plotted against the measured gas temperature in Figure 5-15 with R^2 of 0.98.

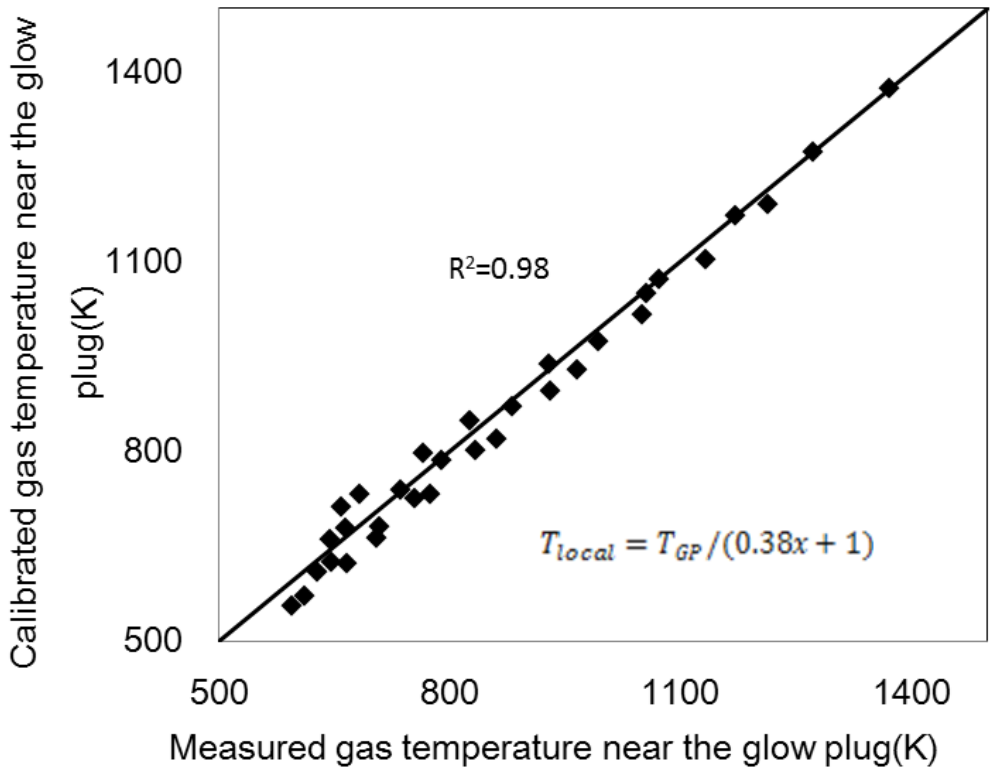

Figure 5-15: Calibrated gas temperature based on glow plug tip surface temperature and distance to the glow plug tip surface

In this optical study, the appearance of the luminous soot emissions is used as the indicator of the successful combustion initiation. Therefore initiation delay has been counted as time from the start of the main injection until the first appearance of luminous soot emissions. Multiplying factor $A_{chemical}$ in Equation 5-6 has been adjusted to 2.4 to fit the experimental data (for those successful combustion data points with glow plug tip surface temperature above 800ºC in Figure 5-3), The predicted transport delay ($\frac{6.9S^2}{(P_{Rail}-P)^{0.5}d_0}$) and the predicted chemical delay ($2.4P^{-1.02}\exp(\frac{2100}{T_{GP}/(0.38x+1)})$) has been plotted against local temperature (controlled by glow plug tip surface temperature and distance between the

glow plug and spray edge) at the location of the spray edge close to the glow plug in Figure 5-16. As discussed above, the gas temperature makes insignificant effect on spray penetration at early phase, the transport delay is fixed at 0.3ms, the chemical delay is dependent on gas temperature, and the chemical delay is shorter when the local gas temperature increases.

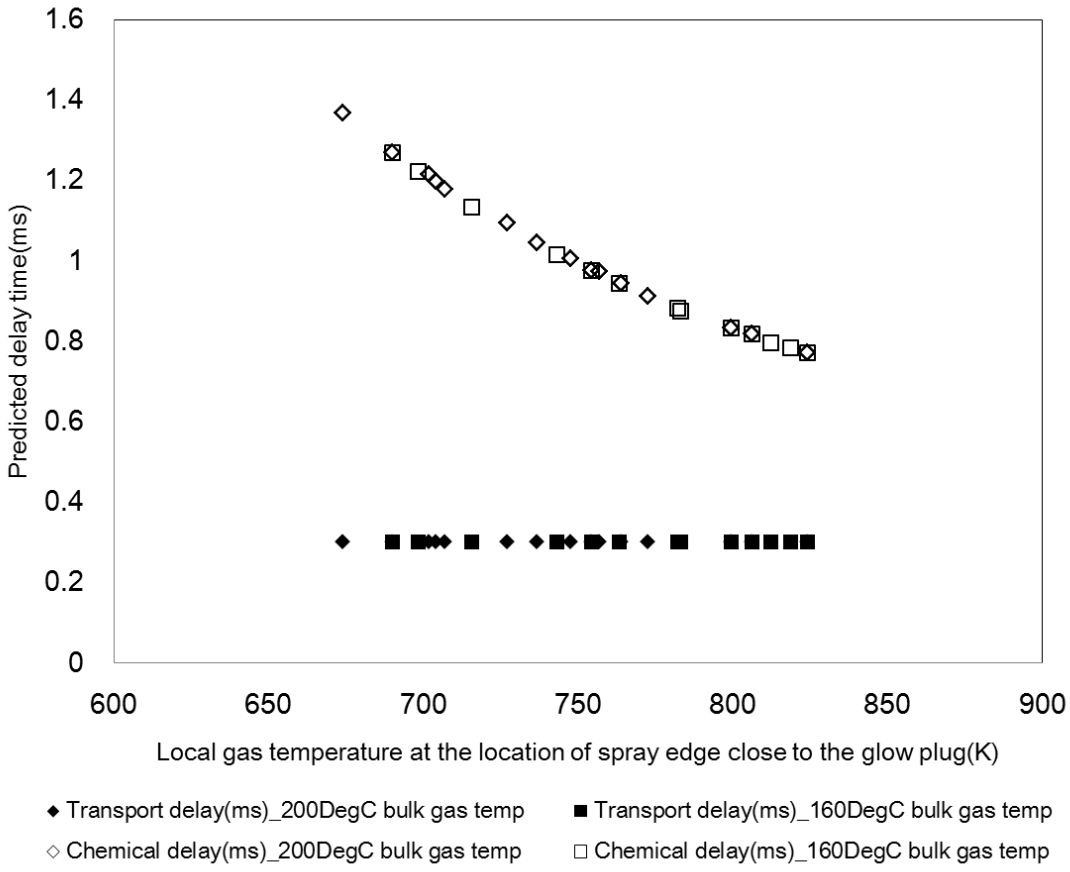

Figure 5-16: Predicted transport/chemical delay. S=10mm, P_{Rail}=400bar, P=38bar, d_0=120μm, local gas temperature determined by T_{GPs} and x

As shown in Figure 5-17, predicted initiation delay has been plotted against initiation delay observed in experiments with R^2 of 0.8. Finally, the developed semi-empirical initiation delay model has been expressed in Equation 5-8.

$$\tau = \tau_{transport} + \tau_{chemical} = \frac{6.9S^2}{(P_{Rail} - P)^{0.5} d_0} + 2.4P^{-1.02}\exp(\frac{2100}{T_{GP}/(0.38x + 1)})$$

Equation 5-8

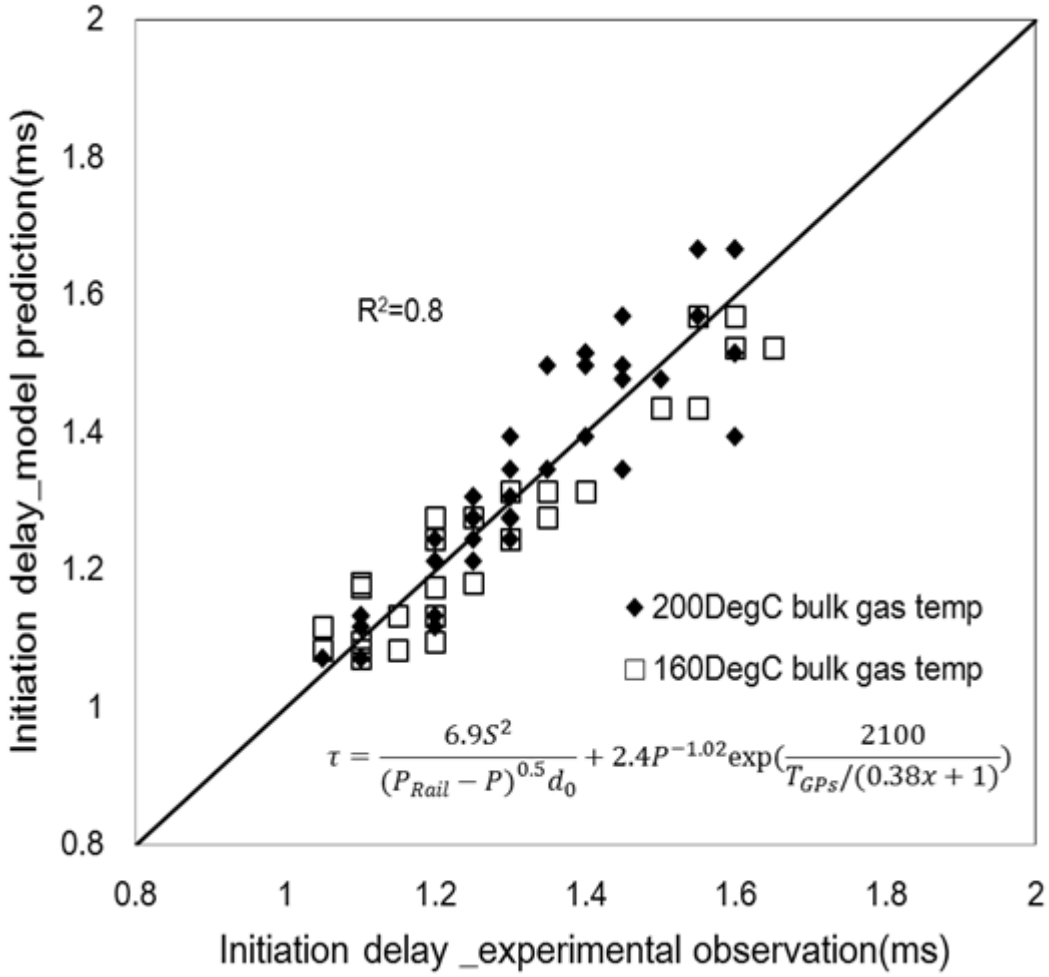

Figure 5-17: Predicted initiation delay against initiation delay observed in optical tests

The transport delay depends on spray penetration rate and distance from injector nozzle to the vicinity of the glow plug, the transport delay deemed constant provided that rail pressure and glow plug-injector configuration are fixed. The initiation delay is dictated by local temperature at spray edge which is controlled by glow plug tip surface temperature and distance between the glow plug tip surface and the spray edge. As illustrated in Figure 5-17, in general, the model accurately predict the initiation delay,

however, at 160ºC bulk gas temperature, underestimates the initiation delay when the distance between the spray edge and the glow plug tip surface is large, this is attributed to the effect of bulk gas temperature: gas temperature near the glow plug was calibrated based on measurements at 200ºC, the bulk gas temperature will have limited influence on the local gas temperature close to the glow plug since the glow plug dominates gas temperature in its vicinity, when the distance between glow plug and spray edge increases, the effect becomes sensible but still relatively small.

5.7. Discussion and Conclusions

The process of combustion initiation and early development has been examined in this chapter using a quiescent combustion bomb with optical access. Luminous soot emissions have been identified the indicator of combustion that was captured by the high speed camera.

The motion of the spray is dictated by flow advection, at a fixed rail pressure of 400 bar, the spray has a constant spray cone angle, subsequently forms two straight spray boundaries. The site of combustion initiation is at the spray edge close to the glow plug. The local flame triggers a rapid expansion of the enflamed volume after the end of the main injection, principally in the downstream direction of spray penetration.

Three important factors including glow plug tip surface temperature, glow plug to spray edge distance and bulk gas temperature have been investigated in terms of ignition success or failure. Two requirements must be met to achieve successful combustion initiated by the glow plug: minimum local temperature of 413^{o}C and a minimum vapour/air equivalence ratio of 0.15-0.35.

The initiation of combustion is strongly influenced by the injection strategy and the rail pressure. In this study where a single-pilot-plus-main strategy

was used under a fixed rail pressure of 400 bar, the pilot injection primarily raises equivalence ratio rather than promoting local combustion, the combustion is only initiated after the main injection is introduced, The initiation delay of combustion aided by the glow plug is defined as the time from the start of the main injection to when the combustion is successfully initiated. An initiation delay model consisting physical part ($\frac{6.9S^2}{(P_{Rail}-P)^{0.5}d_0}$ in ms) and chemical part ($2.4P^{-1.02}\exp(\frac{2100}{T_{GP}/(0.38x+1)}$ in ms)has been proposed, physical delay is time needed for the spray to transport to the vicinity of the glow plug and chemical delay is time for local mixture to go through cool flame reactions.

$$\tau = \tau_{transport} + \tau_{chemical} = \frac{6.9S^2}{(P_{Rail}-P)^{0.5}d_0} + 2.4P^{-1.02}\exp(\frac{2100}{T_{GP}/(0.38x+1)})$$

Chapter 6 Influence of the Glow Plug on Spray Vaporization

6.1. Introduction

Combustion characteristics including cumulative heat release are improved by using the glow plug at the temperature higher than those required for initiation of combustion, this indicates the glow plug aids vapour generation to meet the minimum equivalence ratio and to promote subsequent combustion development. The spray formation has been modelled using CFD code ANSYS Fluent 14.0 in this study. This provides direct information on equivalence ratio at the site and time of combustion initiation and shows the influence of the glow plug on improving vapour generation in early mixture preparation stage. In section 6.2, spray model has been validated through comparing spray pattern and tip penetration with experimental observations. In section 6.3, three important factors, the distance between the glow plug and the spray edge, glow plug tip surface temperature and bulk gas temperature are studied and their influences on spray vaporization are demonstrated. Finally, main conclusions are presented.

6.2. Model Settings and Validation

The fuel jet is simulated to penetrate from an injection point into quiescent air at a uniform temperature. A cylindrical rod with the same diameter and length as the ceramic glow plug is created in this setup. The mesh is displayed in Figure 6-1. The injection point can be moved in Z direction to simulate cases with varying glow plug surface to spray edge distance. The mesh structure is rectangular containing 178944 cells. The minimum orthogonal quality is 0.47, orthogonal quality larger than 0.2 is considered to be good mesh quality [140].

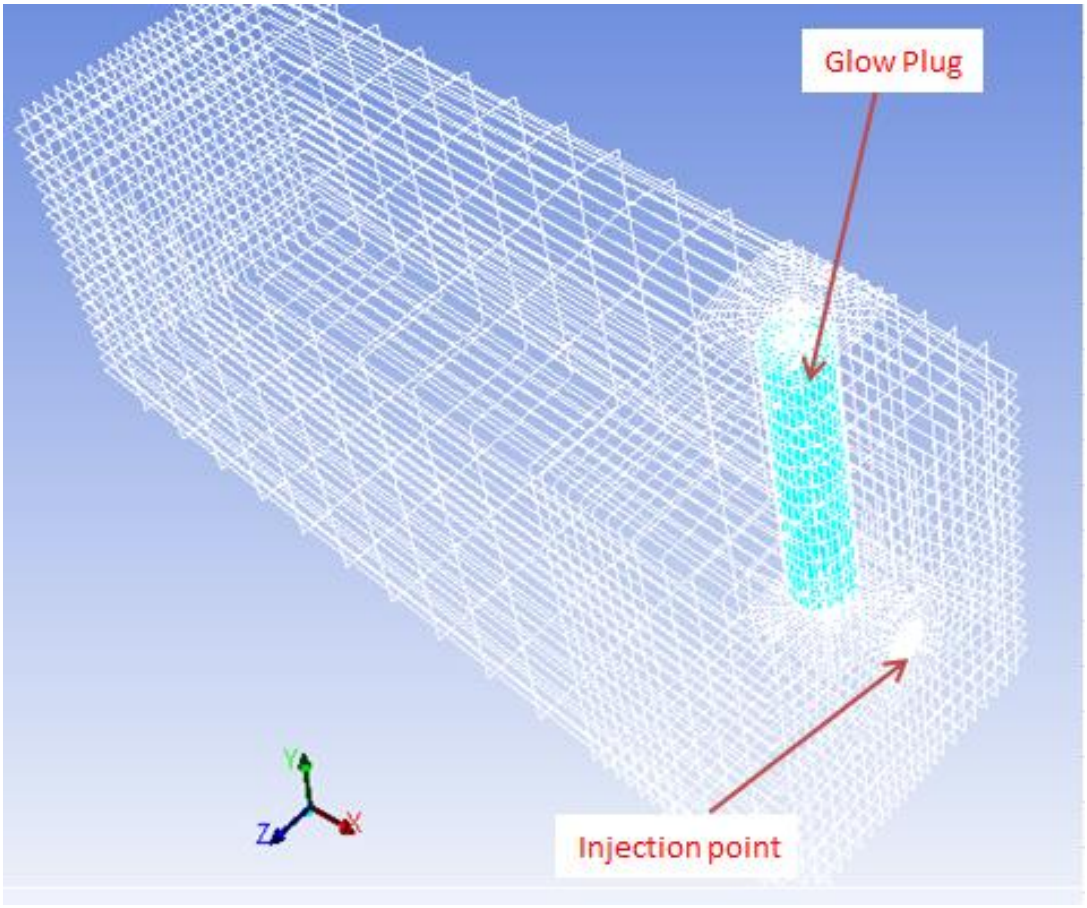

Figure 6-1: Mesh display

Mesh size dependence has been evaluated by comparing computational results predicted using a mesh with 178944 cells and a mesh with 271529 cells. Temperature and equivalence ratio at the spray edge near the glow plug predicted using these two mesh structures have been compared at the end of each time step, results indicated the mesh with 178944 cells is fine enough to be used in prediction, further refinement makes negligible changes in results. The time step of the transient solver has been evaluated in this investigation as well, no obvious changes can be observed in results when decreasing the time step to 5e-7s. The mesh containing 178944 cells and the time step of 5e-7s have been used throughout this study.

The spray angle remains constant because it is an input to the injection model, validation on the basis of spray cone angle is meaningless in this study. Validation of this spray formation model has been carried out by

comparing the spray tip penetration between experimental observations and CFD predictions. The liquid length of the spray is defined as the position at which all fuel is just evaporated. Liquid length of the spray can be measured experimentally using the scattering of light caused by small droplet, but unfortunately this technique is not the common practice at the moment for the current experimental setup. However, recording spray tip penetration is still feasible given that approximate droplet movement can be visually detected and the liquid length with time going on is able to be measured from screen. As illustrated in Figure 6-2, the spray tip penetration is measured from the screen refers to the glow plug diameter which is known as 3.3mm. To take into account the angle illustrated, the actual liquid length of spray penetration is converted from the one measured on the screen.

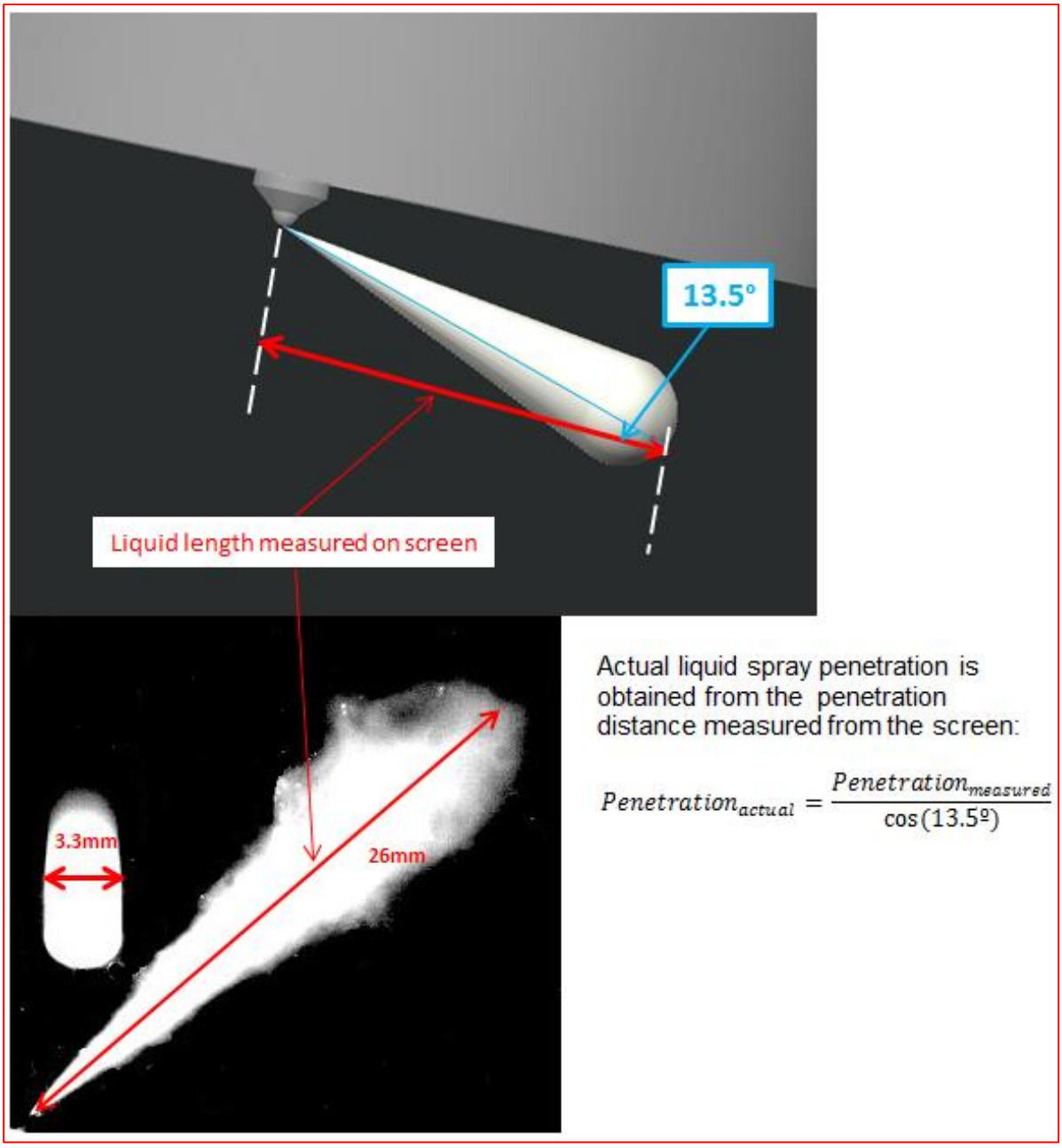

Figure 6-2: Actual spray tip penetration converted from measured spray tip penetration on screen

The spray tip penetration obtained experimentally has been compared with the one obtained from the CFD prediction. In ANSYS Fluent 14.0, the spray tip penetration is determined by the position of the droplet that is the most distant from the hole where the injection initiates. The validation test was based on main injection, rail pressure, injection quantity and bulk gas temperature/pressure is given in Table 6-1. Mean mass flow rate

according to calibration figure that has been shown in Figure 5-3 was used in CFD predictions.

The spray tip penetration obtained experimentally and numerically has been compared and has been shown in Figure 6-3. In the first 0.5ms, the predicted penetration is longer than the one observed in experiment. This is because a constant mass flow rate was assumed throughout the injection event in predictions. However, it is not true in real practice where injector nozzle hole requires small amount of time to fully open and hence the mass flow of spray takes time to develop. Penetration rate decreases as time goes by, at the end of the injection, predicted penetration is 7% shorter than experimental observations.

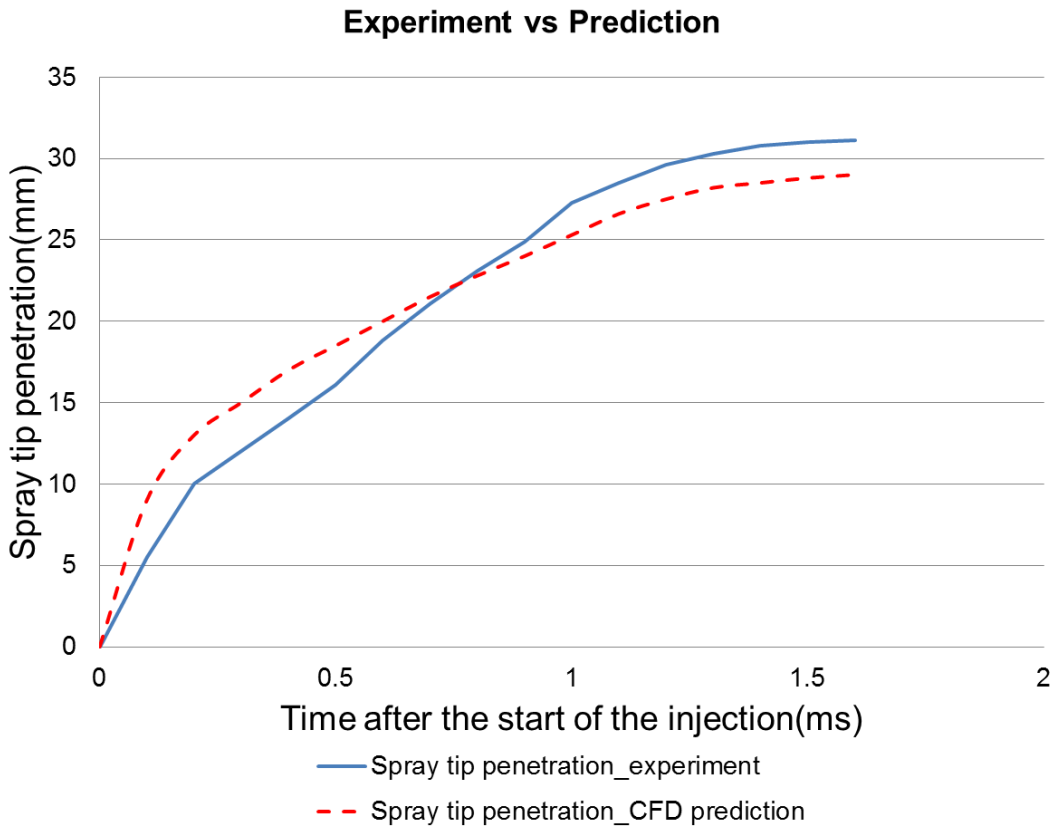

Figure 6-3: Comparison of spray tip penetration between experiment and CFD prediction

Apart from the spray tip penetration, the appearance of the spray was compared to validate the spray model made in this study. The appearance of the spray has been compared between experimental observations and CFD prediction as illustrated in Figure 6-4. In the CFD spray model, a constant spray cone angle has been prescribed and this assumption is supported by the experimental results. The spray is with two straight edges and a hemispherical head, these two features shown in experimental results also reflected in the CFD prediction, the shape of the spray is time dependent, at early time of the injection, the head of the spray is relatively sharp attributed to high droplet velocity.

Time	Spray appearance_experiment	Spray appearance_CFD prediction
0.4 ms after the start of the injection		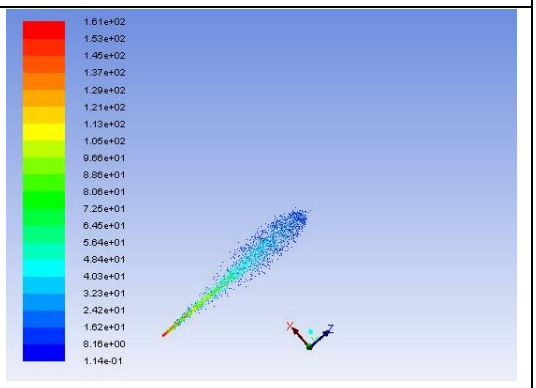
0.8 ms after the start of the injection		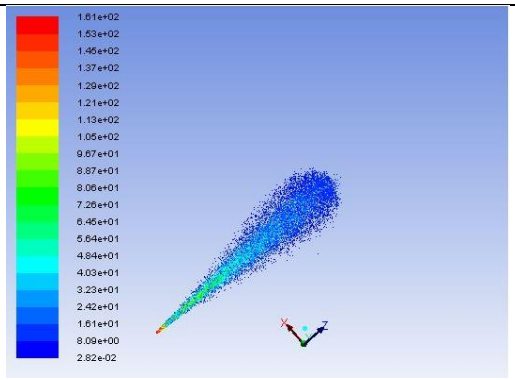
1.3 ms after the start of the injection	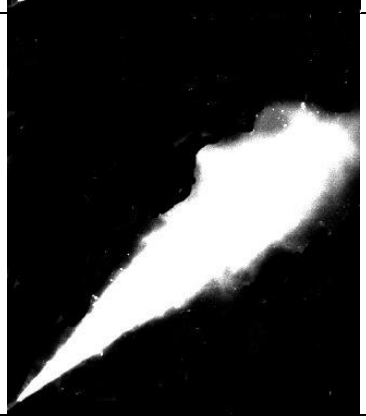	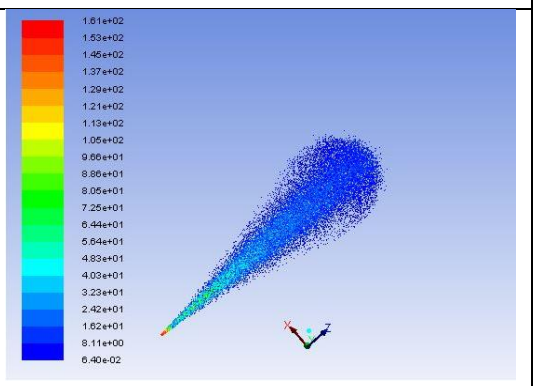

Figure 6-4: Spray appearance comparison between experimental observations and CFD prediction (particles coloured by the velocity), test conditions refer to Table 6-1

6.3. Parameters Influencing Spray Vaporization

6.3.1. Simulation parameters and baseline results

CFD tool ANSYS Fluent 14.0 was used to calculate spray vaporization in this study. Simulation parameters have been given in Table 6-1.

Table 6-1: Simulation parameters

Parameter	Base line	Sweep range
Operating pressure (bar)	38	—
Pilot mass flow rate(kg/s/spray)	0.000625	—
Main mass flow rate(kg/s/spray)	0.0015	—
Pilot to main separation(ms) -SOI(pilot)- SOI(main)	1.7	—
Bulk air temperature(ºC/K)	200/473	200/473-300/573
Glow plug tip surface temperature(ºC/K)	900/1173	700/973-900/1173
Glow plug to spray edge distance(mm)	1.3	1.3-1.8

Gas temperature and fuel vapour concentration at the end of the main injection at baseline condition has been illustrated in Figure 6-5. It has been shown in the contour of gas temperature that the glow plug created a high temperature field. The spray penetrates into this high temperature field, turbulence induced by spray momentum distorts the temperature distribution, local gas temperature in vicinity of the glow plug has been plotted and gas temperature reduces as it is away from the glow plug surface, gas temperature in the region where the spray occupies is particularly low attributed to the heat consumed for droplet vaporization. The influence of the gas temperature on droplet vaporization is indicated by vapour concentration that has been shown in Figure 6-5, vapour concentration is higher on the spray side close to the glow plug than vapour concentration on the spray side away from the glow plug,

indicating droplet vaporization is dictated by the gas temperature, gas temperature is higher close to the glow plug, so is vapour concentration.

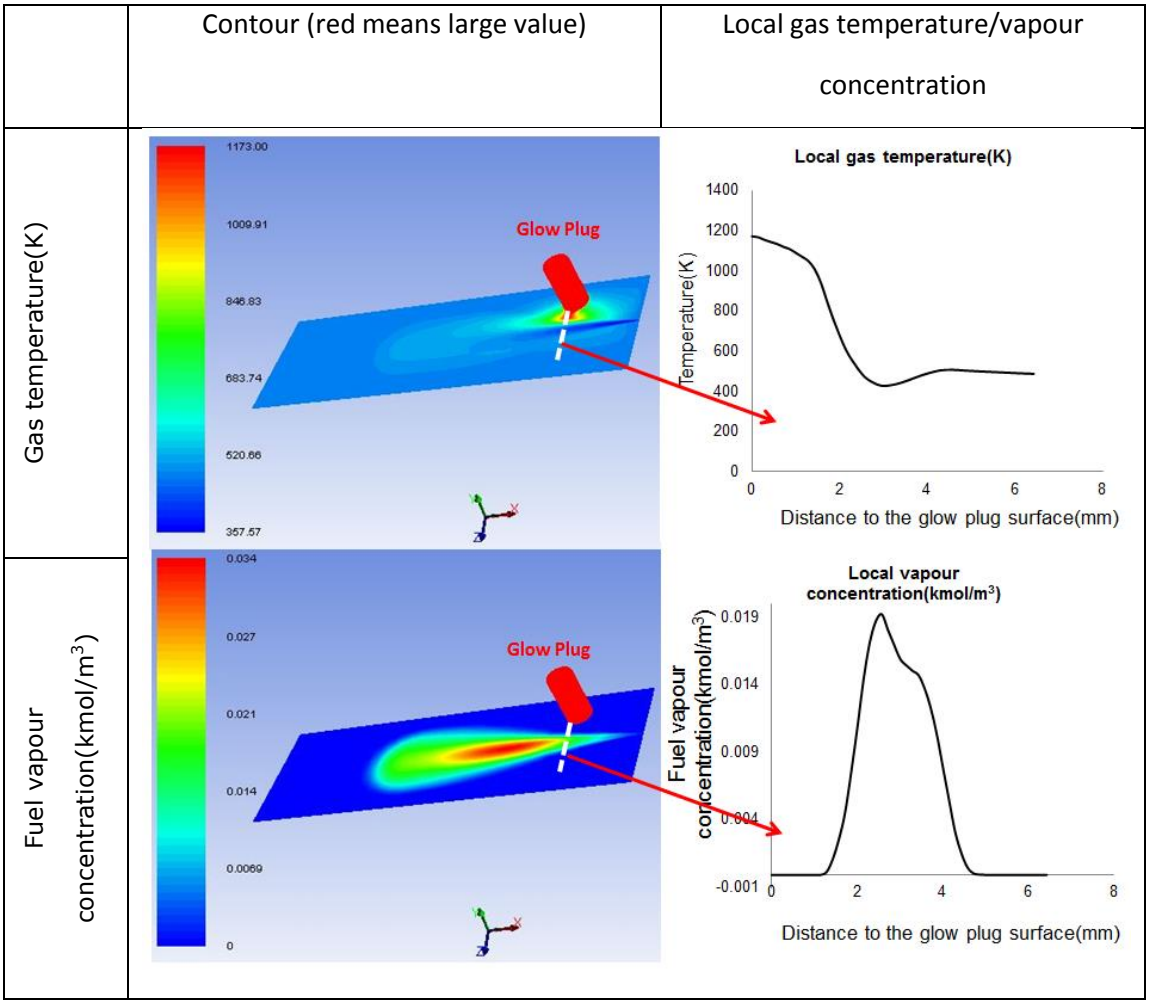

Figure 6-5: Gas temperature and fuel vapour concentration at the end of the main injection at baseline condition refers to Table 6-1

6.3.2. Influence of Glow Plug Temperature and Glow Plug-Spray Proximity

As illustrated in Figure 6-6, local gas temperature in the vicinity of the glow plug is low when the glow plug tip surface temperature decreases from 1173K(900ºC) to 973K(700ºC). It has been shown in Figure 6-6, that bulk gas temperature is not changed markedly by varying glow plug tip surface temperature; however, local gas temperature in the vicinity of the glow plug apparently reduces as a result of reducing glow plug tip surface temperature. In both cases, the local gas temperature reduces to a similar low level in the region where spray passes regardless of the glow plug tip surface temperature, whereas local temperature at the start of the injection is higher with higher glow plug tip surface temperature, indicating larger temperature drop or more heat is consumed for droplet vaporization. It has been shown in Figure 6-6, spray vaporization is deteriorated by passing the region with low gas temperature, suggesting the influence of the glow plug temperature is not restricted only on local vapour generation; the bulk vapour generation is also influenced.

The influence of the glow plug on the spray vaporization is achieved by raising the gas temperature of the region where the spray passes. This could be achieved by varying distance between the glow plug tip surfaces and spray edge alternative to varying glow plug temperatures. As illustrated in Figure 6-7, spray vaporization is worse by varying glow plug tip surface to spray edge distance from 1.3mm to 1.8mm.

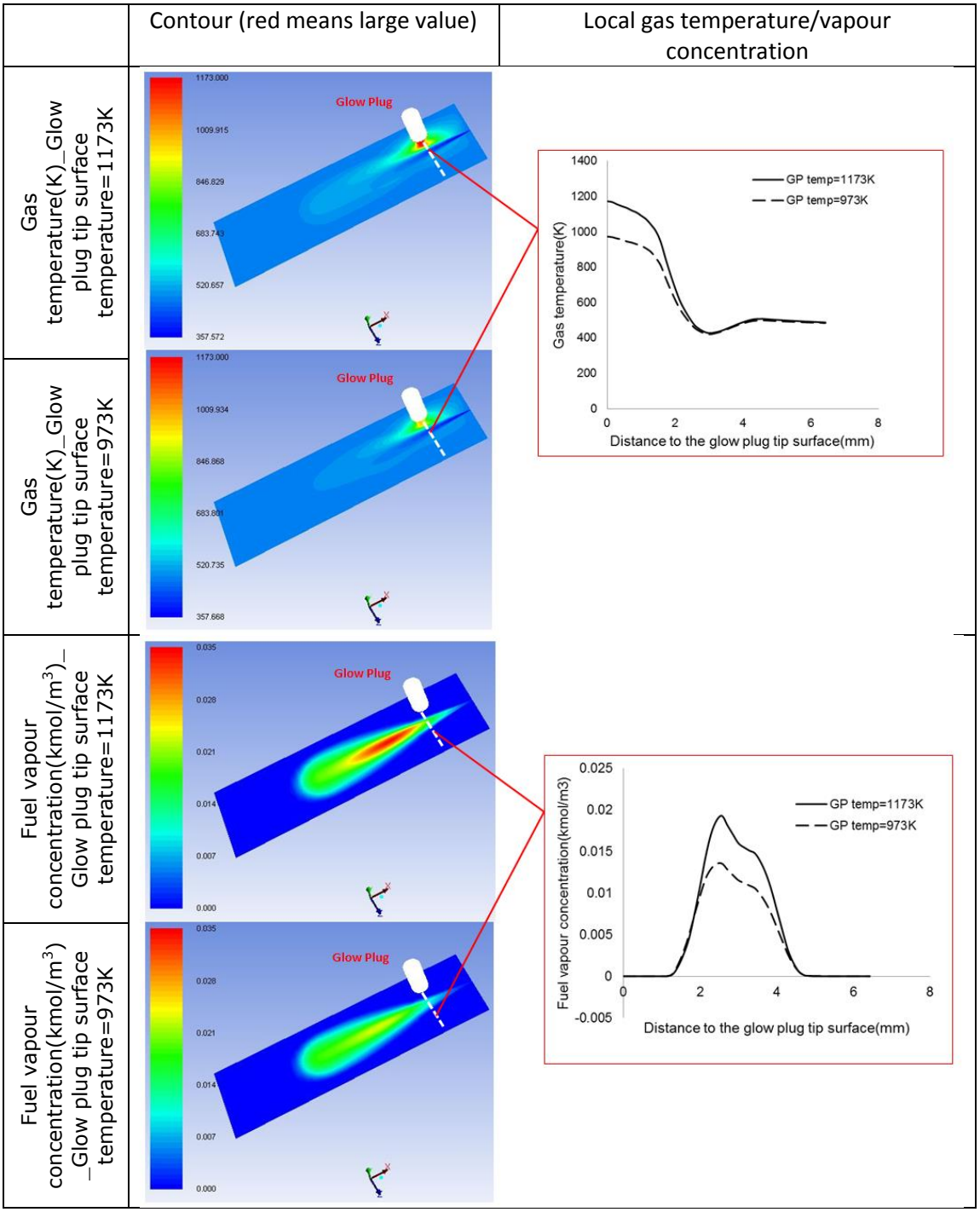

Figure 6-6: Comparison of gas temperature and fuel vapour concentration with glow plug tip surface temperature of 973K(700 °C) to 1173K(900°C), data was recorded at the end of the main injection, other conditions refer to baseline conditions specified in Table 6-1

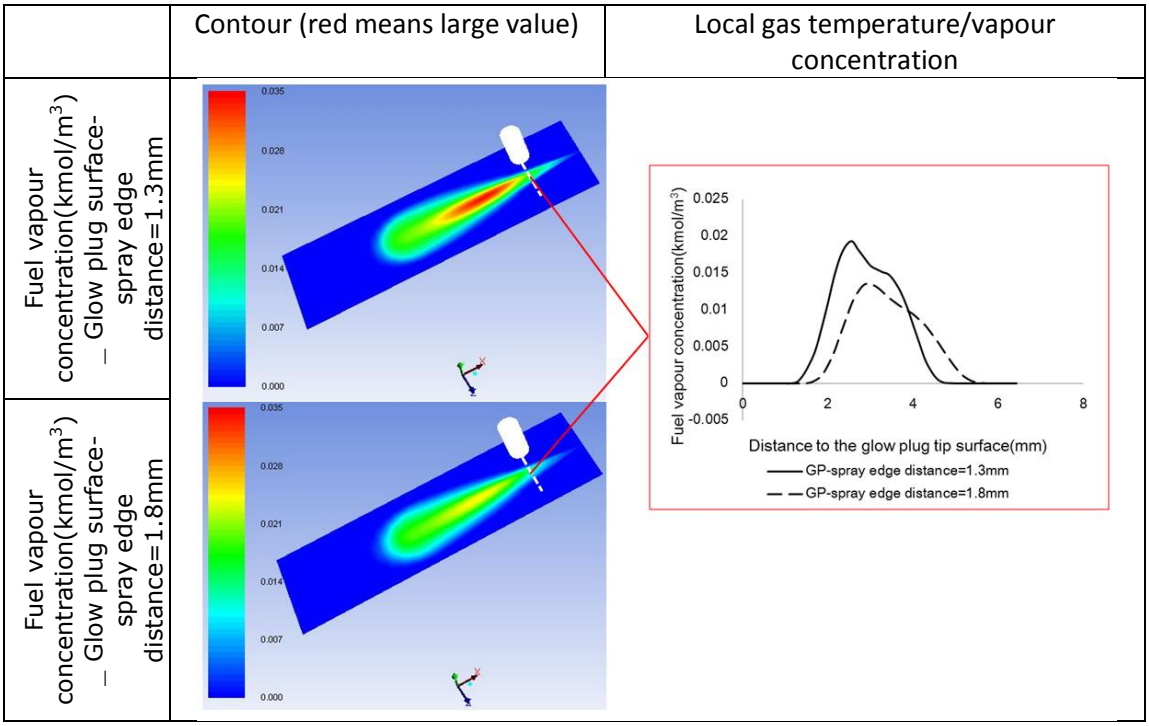

Figure 6-7: Comparison of fuel vapour concentration with glow plug tip surface-spray edge separation of 1.3mm to 1.8mm, data was recorded at the end of the main injection, other conditions refer to baseline conditions specified in Table 6-1

6.3.3. Influence of Bulk Gas Temperature

The influence of bulk gas temperature on spray vaporization has been investigated. As illustrated in Figure 6-8, local gas temperature in the region where spray passes is influenced by varying bulk gas temperature, the influence is obvious when the distance is far from the glow plug, and the influence is small in the vicinity of the glow plug where local gas temperature is dictated by the glow plug temperature. Hence the influence of raising bulk gas temperature from 473K (200ºC) to 573K (300ºC) on spray vaporization is relatively small as can be seen in Figure 6-8. The influence of bulk gas temperature on spray vaporization is more obvious when the spray is away from the glow plug or the glow plug is switched off. As illustrated in Figure 6-9.

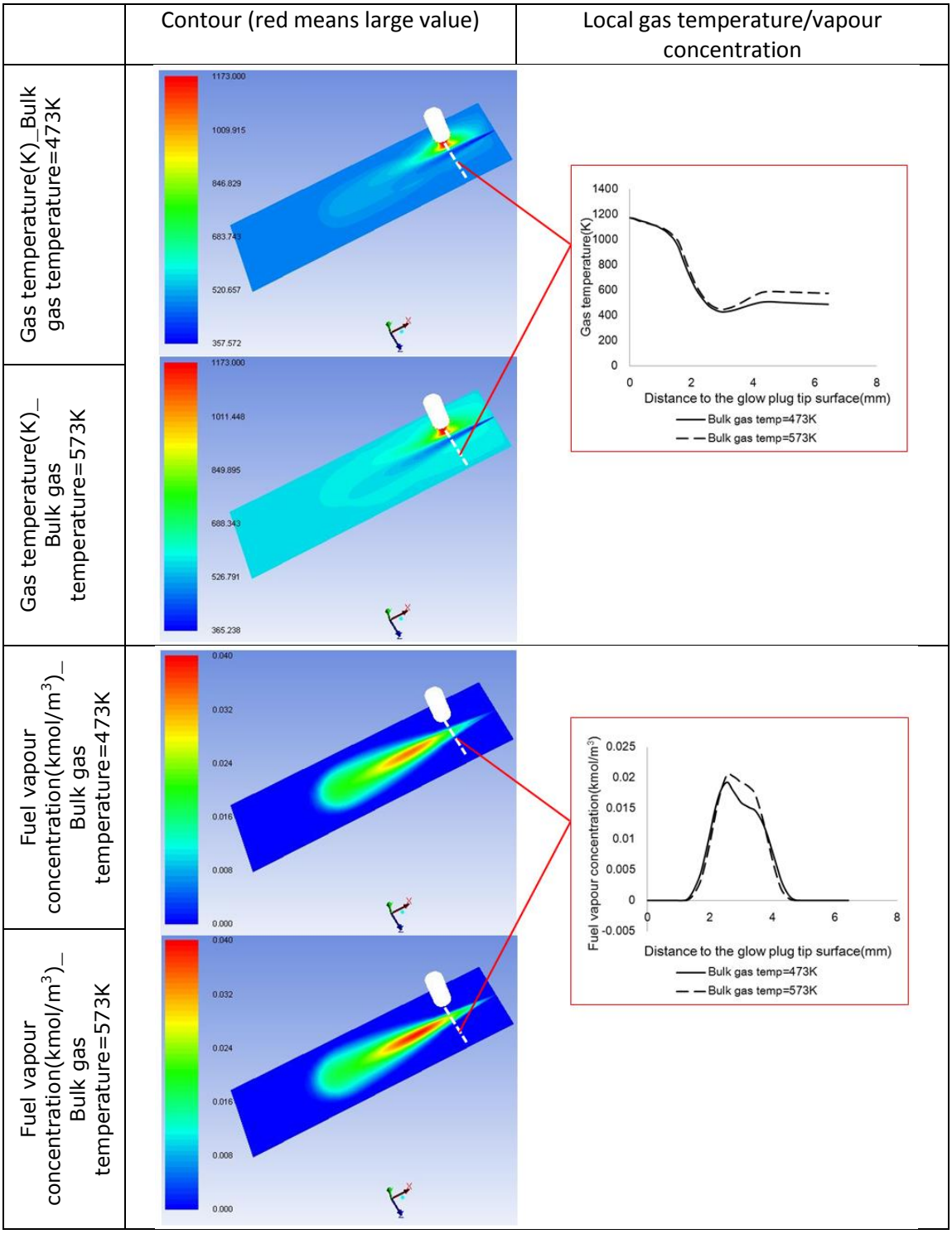

Figure 6-8: Comparison of fuel vapour concentration with glow bulk gas temperature of 473K (200°C) to 573K (300°C), data was recorded at the end of the main injection, other conditions refer to baseline conditions specified in Table 6-1

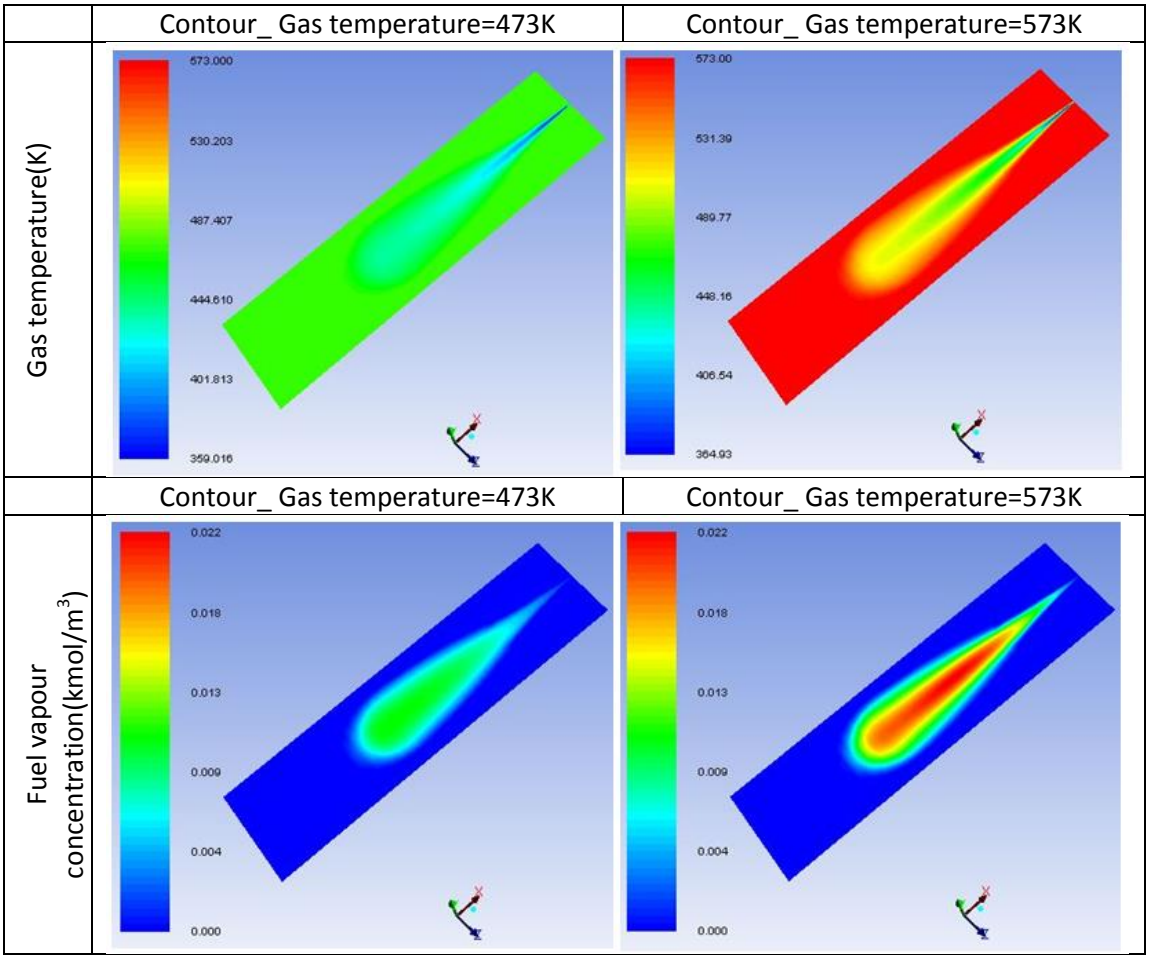

Figure 6-9: Comparison of gas temperature and fuel vapour concentration with bulk gas temperature of 473K(200°C) to 573K(300°C), data was recorded at the end of the main injection, glow plug is switched off, other conditions refer to baseline conditions specified in Table 6-1

6.4. Discussion and Conclusions

Influence of glow plug on spray vaporization has been studied computationally by using ANSYS Fluent 14.0. The droplets entering the static gaseous environment (which was treated by an Eulerian approach) were tracked in a Lagrangian frame. The initial droplet size distribution due to primary breakup was modelled by Rosin-Rammler distribution and handed over to the secondary breakup modelled by WAVE breakup model. Standard k- ε model was used to treat turbulence induced by spray momentum.

Fuel spray vaporization was driven by convective heat transfer; the contribution of direct radiative heating by the glow plug was small. Droplet vaporization was modelled based on convection controlled model which takes into account the influence of convective flow. Droplet vaporization is coupled with gas temperature and the glow plug improves droplet vaporization by raising local gas temperature in the region close to the glow plug where spray will pass.

For the two sprays adjacent to the glow plug, spray vaporization will markedly change by varying either glow plug tip surface temperature or the distance between the glow plug and spray edge, influence of bulk gas temperature is small. However, for those sprays away from the glow plug, spray vaporization is dictated by bulk gas temperature.

Chapter 7 Discussion, Future Work and Conclusions

7.1. Discussion

Advancing knowledge of diesel combustion characteristics and the role of the glow plug under post-cold start conditions has been the driving force for the investigations reported in this thesis. The work addresses the need for a deeper understanding of how the glow plug influences the initiation of combustion. A single cylinder engine unit and a quiescent optical vessel (combustion bomb) were used for the investigations. The quiescent optical vessel was used only to evaluate the initiation and the early development of combustion which effectively takes place at constant pressure. Air in the optical vessel is static prior to injection, this generally does not reproduce in-cylinder conditions, however, at the low engine speeds associated with engine start and post-start idling, turbulence levels are low and motion in the vicinity of the glow plug just prior to the start of combustion is dictated by the momentum of the fuel sprays entrainment and mixing. The outcomes of the work carried out using the optical vessel is therefore applicable to both cold start and cold idling conditions.

The engine which has been used in this investigation has a geometric compression ratio of 15.5:1, and the glow plug must be switched on for successful initiation and development of combustion when the ambient temperature is below around 8ºC. As has been examined in section 4.3, self-sustaining reaction of fuel-air mixture is inhibited and engine work output is hardly positive when the in-cylinder gas temperature at the start of the main injection is below 413ºC. Using the glow plug raises local gas temperature above 413^{o}C, as a consequence, the self-sustaining reaction are enabled, it has been shown in Figure 5-2, this local flame appears at the edge of the two sprays closest to the glow plug, enflamed volume

expands to downstream in spray direction, other sprays away from the glow plug will be ignited when the flame is transferred to them by the convective flow. In this way, a strong premixed combustion is enabled which later aids the development of vigorous mixing controlled combustion. The fuel used in the single cylinder engine was the same fuel that was used in the combustion bomb, the combustion bomb tests showed a similar but slightly lower threshold temperature of approximately 400ºC for successful combustion initiation, it is important to remember the quiescent combustion bomb was used as a supplement in order to better understand initiation process that was difficult to be detected in engine tests and it is the engine result that gives guiding conclusions. Pacaud [5]carried out a computational study of the auto-ignition mechanism using n-heptane to represent diesel. They concluded that the lowest temperature required to achieve auto-ignition of diesel under cold start conditions without the aid of a glow plug was 660K (387°C). This is low compared to the value of 413^{o}C determined in the current work, which is close to the value of 415^{o}C determined by Broatch et al. [141] following a similar experimental approach. It is also closer to the temperature of 700K (427°C) reported in [126] to be required for hydrocarbons to undergo β-scission to form olefins and stabilized alkyl radicals like CH_3 that can be oxygenated by OH radicals.

The glow plug contributes to more than improving combustion initiation. Combustion development is continuously enhanced by using the glow plug up to warm starting temperatures. In this study, a fixed twin-pilot injection strategy and a fixed glow plug temperature of 850 ºC were used, the benefit of using the glow plug diminished up to 430ºC in-cylinder temperature at the start of the injection, 17 ºC higher than that needed for a self-sustaining reaction. It is worth noting that this 430ºC is measured under this specific test condition, will vary with glow plug temperature and injection strategies since combustion behavior including

work output heat release and cycle-by-cycle stability are highly dependent on glow plug temperature and number of pilot injections. The continuing advantage of using the glow plug on combustion development is associated with improved droplet vaporization of the spray, strengthening the early development of combustion before heat release rates are achieved.

The radiation directly from the glow plug to the droplet is small and the droplet vaporization is dictated by convective heat transfer which is coupled with the local gas temperature. Glow plug heats the gas in the region close to it where the two adjacent sprays (one on each side of the glow plug) will pass, droplet vaporization is improved when travelling through this high temperature region. The local gas temperature is dominated by two parameters, glow plug tip surface temperature and distance between the spray edge and the glow plug.

CO and HC emissions are expected to be reduced when the initiation and development of combustion is improved by using the glow plug. Using the glow plug will be potentially advantageous in meeting future emission standards, if emission limits are introduced for diesel engines under test temperature of -7ºC, as they have been introduced since 2002 for gasoline engines[3, 4].

At a given glow plug temperature, the maximum spacing between the glow plug surface and the spray edge is determined for successful combustion initiation. As has been studied in Chapter 5, to achieve successful combustion initiation, at the site of initiation the temperature must above 413^{o}C and the vapour/air equivalence ratio must be at least 0.15-0.35. The minimum equivalence ratio requirement for a self-sustaining reaction was determined based on the fixed fuel rail pressure and injection strategy that were used, changing either rail pressure or injection strategy will influence mixture preparation and the evolution of

equivalence ratio near the glow plug. In turn this will influence ignition delay and the development of combustion [9, 142]. The effect on the minimum equivalence ratio requirement is more uncertain, but does not change the need for a minimum local heat release per unit volume to establish a self-sustaining reaction. If the separation between the glow plug and spray edge is properly controlled, successful combustion is able to be initiated by using cost-effective metallic glow plug capable of reaching sufficient but lower maximum temperature (1000^{o}C). The ceramic glow plug is capable of reaching higher temperature (1250^{o}C), however, is more expensive and less durable to tip breakage[4]. Metallic glow plug with relatively low maximum temperature is advantageous in fuel economy, as reported in[143, 144], 40-50% higher glow plug power is consumed to raise glow plug temperature from 1000^{o}C to 1250^{o}C, as a result, fuel consumption as well as CO_2 emission increase. The distance between the glow plug surface and the spray edge could also be reduced by producing sprays with wider spray cone angle, which can be achieved using injectors with proper designs. The influence of the nozzle aspect ratio or nozzle hole length to diameter ratio was examined by Arai et al.[90], who found a nozzle aspect ratio of 4 or 5 gave the maximum cone angle.

Increasing number of pilots and raising glow plug temperature are proved to be effective approaches to avoid misfire and improve engine work output as well as cycle-by-cycle stability. These two approaches are essentially aimed to get heat release per unit volume or local energy density at least of 20J/cm^3 in the vicinity of the glow plug. The energy density is associated with fuel vapor density that can be derived from fuel vapor/air equivalence ratio. Local fuel vapor/air equivalence ratio in the vicinity of the glow plug can be expressed using Equation 7-1.

$$\emptyset = \frac{(\frac{m_f}{m_a})}{(\frac{m_f}{m_a})_{stoich}}$$

Equation 7-1

Where $(\frac{m_f}{m_a})$ refers to mass ratio of fuel vapor to air, and $(\frac{m_f}{m_a})_{stoich}$ is the ratio when the mixture is stoichiometric.

For diesel fuel,

$$(\frac{m_f}{m_a})_{stoich} = \frac{1}{14.5}$$

Equation 7-2

Focus on a control volume near the glow plug, the volume is at local position refers to Figure 5-10, assume the fuel vapor and air is well mixed, the mass ratio is then equivalent to the density ratio, as expressed using Equation 7-3.

$$\frac{m_f}{m_a} = \frac{\rho_f}{\rho_a}$$

Equation 7-3

Combine Equation 7-1, Equation 7-2 and Equation 7-3 to have Equation 7-4.

$$\rho_f = \frac{\emptyset}{14.5}\rho_a$$

Equation 7-4

Air density can be obtained by applying perfect gas law assuming partial pressure of air in the control volume is equivalent to the total system pressure given that vapour pressure is too small to be considered negligible (Validation calculation for the pressure assumption is shown in Appendix), and fuel density is expressed in Equation 7-5.

$$\rho_f = \frac{\emptyset}{14.5} \times \frac{P}{RT}$$

Equation 7-5

The pressure here is 38 bar, which is the typical gas pressure near engine TDC for a modern light duty diesel engine with relatively low compression ratio, heat release per unit volume or energy density can be calculated by multiplying lower heating value (LHV) and fuel vapor density given those vapor is fully consumed, as shown in Equation 7-6.

$$\rho_{energy} = LHV \times \rho_f = 4 \times 10^4 (\frac{\emptyset}{T})$$

Equation 7-6

Energy density (ρ_{energy}) (J/cm^3) is proportional with ($\frac{\emptyset}{T}$), ($\frac{\emptyset}{T}$) is the ratio of local equivalence ratio to local gas temperature near the glow plug, it has been demonstrated that two requirements must be met to achieve successful combustion, a minimum gas temperature of 688K (413ºC) and a minimum equivalence ratio of 0.15-0.35, these requirements determines the required heat release per unit volume for stable cyclic combustion, as shown in Figure 7-1.

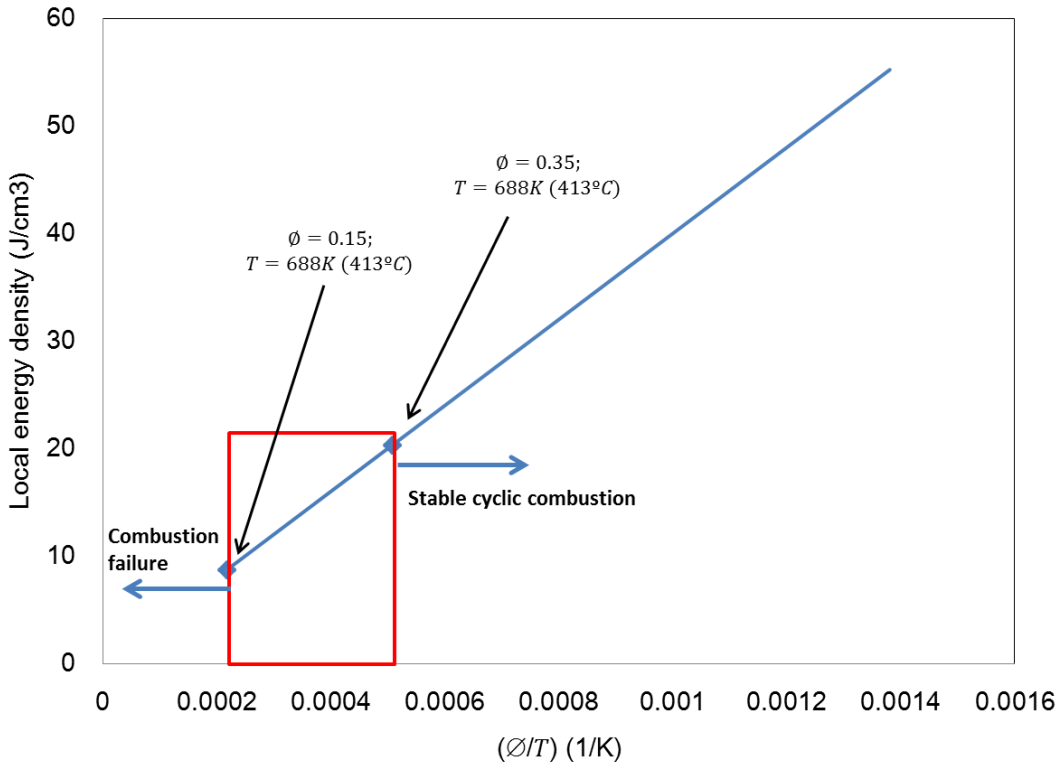

Figure 7-1: Relationship between local energy density and local fuel vapor/air equivalence ratio, local gas temperature in the vicinity of the glow plug, gas pressure=38 bar

If heat release per unit volume is higher than 20J/cm^3, combustion is always successful and the combustion is expected to be successful and stable over cycles. The local energy density needs to be maximized in order to improve engine combustion characteristics including work output, heat release and cycle-by-cycle stability. Energy density can be controlled by varying local equivalence ratio and local gas temperature. The temperature term in $(\frac{\emptyset}{T})$ is denominator, however, as droplet vaporization is improved as a result of raising gas temperature, increase in gas temperature will cause a higher value of equivalence ratio, the overall value of $(\frac{\emptyset}{T})$ is increased (imaging the temperature is very low, the value of $(\frac{\emptyset}{T})$ will not be a large value, but in turn, a very small value close to zero, because the droplet vaporization is poor at such low temperature). As has been investigated in [4, 11], stable cyclic combustion associated with a

higher premixed contribution and a following strong development of main combustion is achieved by using a multiple pilot strategy or increasing the glow plug temperature. The former directly raises local equivalence ratio near the glow plug, producing a higher energy density; the latter leads to an increase of local gas temperature in the vicinity of the glow plug, which improves droplet vaporization and hence raises the energy density.

The influence of bulk gas temperature on the performance of the glow plug is relatively small compared to the influence of glow plug temperature and distance between the spray edge and the glow plug. The glow plug improves spray vaporization to both meet the minimum equivalence ratio and aids combustion development. As has been shown in section 5.4, the effect of varying bulk gas temperature on combustion initiation diminishes as bulk gas temperature rises. Influence of bulk gas temperature higher than 200°C has not been examined in the optical work attributed to the rig restrictions. Alternatively, the influence of varying bulk gas temperature when the bulk gas temperature is high has been investigated computationally using ANSYS Fluent 14.0, as has been described in section 6.3, spray vaporization is not improved markedly by raising bulk gas temperature form 200°C to 300°C. This is because in the vicinity of the glow plug, the local gas temperature in the region where spray passes is governed by glow plug temperature and glow plug to spray edge distance. Influence of bulk gas temperature has been studied using the single cylinder engine in this investigation. As has been shown in section 4.2, when the glow plug is switched on, increasing the ambient temperature from 3° C to 17° C (translated to in-cylinder gas temperature is around 409 ° C to 425° C) makes insignificant changes to engine work output, heat release and cycle-by-cycle stability.

The combustion initiated by the glow plug could be understood through the influence of the initiation delay model. Initiation delay is defined as the

time between the start of the main injection and the successful initiation of combustion. A semi-empirical initiation delay model has been developed in the current work as has been shown in section 5.6; the model has been expressed in Equation 5-8 and is reproduced here:

$$\tau = \frac{6.9S^2}{(P_{Rail}-P)^{0.5}d_0} + 2.4P^{-1.02}\exp(\frac{2100}{T_{GP}/(0.38x+1)})$$

This sequential delay model was spilt into transport delay portion ($\frac{6.9S^2}{(P_{Rail}-P)^{0.5}d_0}$) and chemical delay portion ($2.4P^{-1.02}\exp(\frac{2100}{T_{GP}/(0.38x+1)})$). Transport delay is time for spray to transport to the vicinity of the glow plug, and chemical delay is time that takes for local mixture to go through cool flame reactions before hot combustion starts. Behaviour of combustion aided by the glow plug is directly linked to premixed combustion, work output and cycle-by-cycle stability are improved when the magnitude of premixed combustion peak is high [4, 11, 23], McGhee [4] has investigated the influence of initiation delay on early development of the combustion, as has been reported that rapid development of the main combustion is always associated with short initiation delay.

It is worth noting that the transport delay is only part of the physical delay, the droplet vaporization and process of fuel air mixing is included in the transport delay. The transport delay is associated with the distance between the glow plug tip and the injector tip (S), pressure difference between rail pressure and in-cylinder pressure ($P_{Rail}-P$), and injector nozzle hole diameter(d_0). P_{Rail} can be controlled by the ECU, and S and d_0 are determined by engine geometry and design.

The chemical delay is strongly connected to gas temperature, as collision frequency of reactants is greater and reactants have more thermal energy at higher temperatures. The local gas temperature in the vicinity of the glow plug can be controlled by varying glow plug temperature (T_{GP}) or the distance between the glow plug tip surface and the spray edge (x). The

influence of gas temperature on the transport delay is small. The injected liquid does not disintegrate into droplets instantly after the start of the injection, some unbroken portion like ligaments exist and the time required for the liquid to fully breakup into droplets is referred as the breakup time[72, 145]. Impact of gas temperature on spray penetration is small in the early phase of spray formation. As has been shown in Figure 5-14, local gas temperature was varied by switching on glow plug and increasing bulk temperature, the rate of spray penetration was not influenced and sprays performed in both tests took 0.3ms to get the glow plug.

The influence of the gas pressure on initiation delay has not been investigated in the current work, but it is worth demonstrating its relevance. Varying the pressure could influence both the transport delay and the chemical delay. Reducing pressure will lead to a longer chemical delay. This is because reducing the pressure in a gaseous reaction will reduce the number of collisions between reactants, which decreases the rate of chemical reactions (The dependence also has been expressed in the chemical portion displayed in the model). However, the reduction in pressure in turn will result in a shorter transport delay. Spray tip penetration rate is higher when the pressure difference between the rail pressure and the pressure is larger [72, 84, 85] (as has been reviewed in section 2.5.2), so the penetration rate is expected to increase with reduced pressure given that the rail pressure is not varied. McGhee [4] has investigated the influence of the pressure on the early development of combustion aided by the glow plug in an optical vessel, shorter initiation delay associated with more rapid combustion development was found when the pressure was reduced from 35 bar to 20 bar, this does not agree with the findings in this investigations, McGhee [4] observed interactions between the glow plug and the spray, and concluded that the splashing effect of the spray under lower pressure made spray impingement to occur

on the glow plug surface and generated more enflamed area which was indicated by luminous soot emission.

This initiation delay model was developed based on experiments conducted in a quiescent combustion bomb so the impact of convective flow due to the turbulence motion at initiation phase has not been taken into account. However, it is worth demonstrating the influences on both the transport delay and the chemical delay. The in-cylinder charge motion will disturb the temperature distribution near the glow plug, as shown in Figure 7-2, the effect of natural convection combined with air flow will cause inequality of temperature distribution on each side of the glow plug, gas temperature in flow upstream/downstream is lower/ higher and consequently, the chemical delay will become longer/ shorter. The transport delay is governed by spray penetration behavior and will be hardly influenced by the in-cylinder convective flow. Both Pastor et al. [9] and La Rocca et al. [30] investigated the influences of in-cylinder charge on spray pattern by means of CFD simulation, they found the impact of convective flow was small and spray motion in the vicinity of the glow plug is dictated by the momentum of the spray, the impact became more obvious after the end of the injection.

This initiation delay model may not directly apply on cases where multi-pilot injection strategy is used. As has been illustrated in section 4.4, ignition mechanism was different when using a twin-pilot injection strategy compared with that using a single-pilot injection strategy. Increasing number of pilot injections will improve combustion characteristics aided by the glow plug. When a twin-pilot-plus-main strategy is used, combustion is initiated when the second pilot is introduced. The local flame then triggers the rapid development of the following main combustion. In the current work, it has been shown that engine work output, heat release and cycle-by-cycle stability is improved

when increasing number of pilots from one to two, further increase to three shows continuous but small benefits. MacMillan [3] concluded that using a twin-pilot-plus-main strategy increased work output and achieved improved cycle-by-cycle stability due to reduced ignition delay and increased premixed heat release rate. Cold idling performance has been studied by McGhee [4] on a single cylinder engine with a compression ratio of 15.5:1, results indicated that a combination of high temperature glow plug and multiple-pilot-plus-main strategy was key to achieve satisfactory cycle-by-cycle stability at very cold ambient temperature of -20^{o}C. However, more pilots means a reduction of the total fuel delivered in the main injection, which can make idle speed control through fueling control more difficult.

Further to the earlier description, influences of in-cylinder flow on temperature distribution near the glow plug will be discussed with more details. It is concerned that temperature distribution in the vicinity of the glow plug may be distorted by the convective flow even it is relatively weak under cold start and idling conditions. Temperature distribution in the vicinity of the glow plug is influenced by natural convection. Natural or free convection is observed as a result of the motion of the fluid due to density changes arising from the heating process. The movement of the fluid in natural convection, results from the buoyancy forces imposed on the fluid when its density in the proximity of the heat transfer surface is decreased as a result of the heating process[146]. As illustrated in Figure 7-2, gas temperature upon the glow plug is high due to buoyancy force when the environment is static and will be affected by the convective flow in the combustion chamber, which causes gas temperature downstream of the flow direction is higher than upstream. This uncertainty principally will not affect the key findings although this will lead to asymmetric spray vaporization on each side of the glow plug attributed to the difference of local gas temperature.

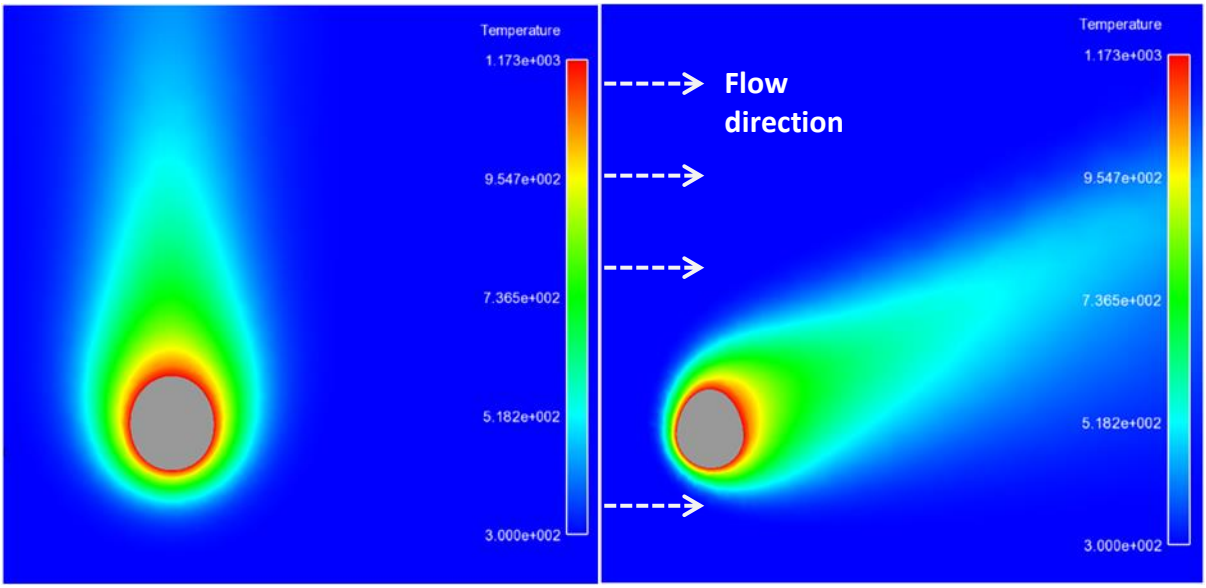

Figure 7-2: Illustration of influence of convective flow(to mimic swirl motion caused by piston movement) on temperature field change (due to natural convection) in the vicinity of the glow plug, temperature predicted by using CFD simulation, glow plug surface temperature=1173K(900°C), bulk gas temperature=300K(23°C), flow velocity at boundary=10m/s

7.2. Future Work

The current investigation has clarified the role of the glow plug and has explored the criteria of successful combustion initiation. An initiation model has been developed to study parameters influencing the process. However, there remain some questions worth investigating in future:

- The optical study provided valuable information regarding the process of combustion initiation and early development, but the transient period between the initial stage and further development has not been captured attributed to weak flow pattern in the quiescent combustion bomb. An alternative approach is to use a rapid compression machine with optical access [9], which will better replicate engine conditions and potentially reveals more information on the combustion development process but the cost will be higher.

- Distance between the glow plug tip surface and spray edge has been identified as one of the most important parameters influencing behaviour of combustion aided by the glow plug, as has been indicated in the optical studies. However, this has not been investigated on the engine rig. It will be useful to test on an engine based facility if the combination of close glow plug-spray proximity and relatively low glow plug temperature (with lower cost) can efficiently assist combustion. Maybe to use injectors with different number of holes to vary the distance between the glow plug tip surface and the spray edge.

- Exhaust emissions have not been investigated in the current work. Successful initiation and efficient development of combustion shows potential advantages of achieving more complete combustion with less CO, HC emissions. It is worth investigating the effects of using the glow plug on the emission reduction under cold starting temperatures, because it is very possible in the near future that emission tests are required for diesel engines at -7ºC as it was introduced for gasoline engines in 2002[3, 4].

- Combustion initiation and early development has been investigated from a 2D optical setup. 3D visualisation is potentially useful in capturing a detailed insight into the early stages of combustion. This can provide more precise position of initiation site and better describe the mechanism of glow plug assisted combustion, which is inherently 3D in nature.

7.3. Conclusions

7.3.1. Engine Study

- Glow plug was used to initiate combustion at ambient temperatures below 8ºC, work output, heat release and cycle-by-cycle stability was continuously improved up to ambient temperature of 20ºC.

- Threshold in-cylinder gas temperature for self-sustaining combustion of diesel fuel has been determined of around 413°C. Glow plug was required to be used to assist combustion initiation when in-cylinder gas temperature was below 413°C.

- Increasing number of pilot injections improved combustion aided by the glow plug without an expense of rising total fueling level. Triple-pilot strategy maximized the benefit, but idle speed control through main combustion was worse due to reduction in total fuel delivered in the main injection.

7.3.2. Optical Combustion Bomb Study

- Combustion was initiated at spray edge close to the glow plug, flame propagated after the end of the main injection in the downstream direction of spray penetration.

- Two necessary and sufficient conditions for the successful initiation and development have been identified. At the site of initiation the temperature must be above 413°C and the vapour/air equivalence ratio must be at least 0.15-0.35. The main role of the glow plug was to raise gas temperature in its vicinity above 413 °C.

- At a fixed rail pressure of 400 bar, combustion was initiated after the second shot, either the second pilot or the main injection was introduced to raise equivalence ratio above the threshold.

- A short initiation delay indicated more rapid combustion development. A semi-empirical initiation delay model was developed to understand the influence of parameters influencing combustion initiation and development:

$$\tau = \frac{6.9S^2}{(P_{Rail} - P)^{0.5} d_0} + 2.4P^{-1.02}\exp\left(\frac{2100}{T_{GP}/(0.38x + 1)}\right)$$

- The transport delay is more dependent on the rail if engine geometry is fixed. The chemical initiation delay was strongly dependent on gas temperature at spray edge close to the glow plug, this gas temperature was dictated by the glow plug tip surface temperature and distance between the glow plug tip surface and the spray edge.

7.3.3. Computational Study

- The secondary role of the glow plug was to improve droplet vaporization of the two sprays adjacent to the glow plug. This was helpful in meeting the minimum equivalence ratio for successful initiation and improving subsequent combustion development.

- Spray vaporization was dictated by convective heat transfer, which was related to gas temperature. Contribution of radiation from the glow plug to heat the droplet was small.

- Vaporization of the two sprays closest to the glow plug was dictated by both the glow plug tip surface temperature and distance between the glow plug tip surface and the spray edge.

Influence of bulk gas temperature on vaporization of these two sprays was small.

Reference

1. http://www.clm.co.uk/diesel-emissions-crackdown/. Accessed November 2015.

2. Crua, C., Combustion Processes in a Diesel Engine. PhD thesis, 2002, University of Brighton.

3. MacMillan, D., Influences on the Cold Start Behaviour of a Diesel Engine at Reduced Compression Ratio. PhD thesis, 2009: University of Nottingham.

4. McGhee, M., in Factors Influencing Cycle-by-Cycle Combustion Characteristics of a Diesel Engine under Cold Idling Conditions. PhD thesis, 2012, University of Nottingham.

5. Pacaud, P., Perrin, H., Laget, O, Cold start on diesel engine: Is low compression ratio compatible with cold start requirements? SAE Paper 2008-01-1310, 2008.

6. Walter, B., Perrin, H., Dumas, J.P, Laget, O, Cold Operation with Optical and Numerical Investigations on a Low Compression Ratio Diesel Engine. SAE Paper 2009-01-2714, 2009.

7. Chartier, C., Aronsson, U., Andersson, O, Effect of injection strategy on cold start performance in an optical light duty DI diesel engine. SAE paper 2009-24-0045, 2009.

8. Mueller, C., Musculus, M., Glow Plug Assisted Ignition and Combustion of Methanol in an Optical DI Diesel Engine. SAE Technical Paper 2001-01-2004, 2001.

9. Pastor, J.V., García-Oliver, J.M., Pastor, J. M., Ramírez-Hernández, J. G, Ignition and combustion development for high speed direct injection diesel engines under low temperature cold start conditions. Fuel, 2011. 90(4): p. 1556-1566.

10. Perrin, H.M., Dumas, J.P., Laget, O., Walter, B, Analysis of Combustion Process in Cold Operation with a Low Compression Ratio Diesel Engine. SAE Paper 2010-01-1267, 2010.

11. McGhee, M.J., Shayler, P. J., La Rocca, A., Murphy, M., Pegg, I, The Influence of Injection Strategy and Glow Plug Temperature on Cycle by Cycle Stability Under Cold Idling Conditions for a Low Compression Ratio, HPCR Diesel Engine. SAE International Journal of Engines, 2012. 5(3): p. 923-937.

12. Pastor, J.V., Bermúdez, V., García-Oliver, J.M., Ramírez-Hernández. J.G, Influence of Spray-Glow Plug Configuration on Cold Start Combustion for High-Speed Direct Injection Diesel Engines. Energy, 2011. 36(9): p. 5486-5496.

13. Tindle, C.R., An investigation of factors which influence the cold start performance of diesel engines. PhD Thesis, University of Nottingham, 2000.

14. Burrows , J.A., An investigation into the cold start performance of automotive diesel engines. PhD Thesis, University of Nottingham, 1998.

15. Austen, A.E.W., Lyn, W.T., Some investigations on the cold starting phenomena in diesel engines. Proceedings of Institute of Mechanical Engineers, 1959. 5: p. 1959-60.

16. Shayler, P.J., David, K. W. Leong., Contributions to Engine Friction During Cold, Low Speed Running and the Dependence on Oil Viscosity. SAE Technical Paper 2005-01-1654, 2005.

17. Caracciolo, F.a.M., M.L, Effect of engine oil viscosity on low-temperature cranking starting and fuel economy. SAE paper 790728, 1979.

18. Shayler, P.J., Baylis, W.S., Murphy, M., Main bearing friction and thermal interaction during the early seconds of cold engine operation. ASME 2002 internal combustion engine division fall technical conference, New Orleans, USA, 2002.

19. Shayler, P., Cheng, L., Li, Q., Wahab, E., A modified oil lubrication system with flow control to reduce crankshaft bearing friction in a 1.5 litre 4 cylinder diesel engine. SAE 2016-01-1045, 2016.

20. MacMillan, D., La Rocca, A., Shayler, P.J, Investigating the Effects of Multiple Pilot Injections on Stability at Cold Idle for a DI Diesel Engine. SAE Paper 2009-01-0612, 2009.

21. MacMillan, D., LaRocca, A., Shayler, P.J., The effect of reducing compression ratio on the work output and heat release characteristcs of a DI diesel engine under cold start conditions. SAE Paper 2008-01-1306, 2008.

22. Payri, F., Broatch, A., Salavert, J.M., Martin, J, Investigation of Diesel Combustion Using Multiple Injection Strategies for Idling After Cold Start of Passenger-Car Engines. Experimental Thermal and Fluid Science, 2010. 34.

23. McGhee, M.J., Shayler, P. J., La Rocca, A., Murphy, M., Pegg, I, Investigations of Injection Strategies for Stable Cold Idling of an HPCR Diesel Engine with a Compression Ratio of 15.5:1, in IMechE Conference C1342 Fuel Systems for IC Engines. 2012: London.

24. Cheng, K.Y., Processes Influencing the Indicated Work Output of Direct Injection Diesel Engines During Cold Starting. PhD Thesis, The University of Nottingham, 2002.

25. Bruno, L., Schmitz, H.G., Cold start equipment for diesel direct injection engines. SAE paper 1999-01-1244, 1999.

26. French, G., R., Scott, W .M., Giving the IDI diesel a fresh start. Sae paper 850452, 1985.

27. Kern, C., Dressler, W., Lindemann, G., Rothacker, V, An innovative glow system for modern diesel engines. SAE paper 1999-01-1240, 1999.

28. Payri, F., Broatch, A., Serrano, J.R., Rodríguez, L.F., Esmorís, A, Study of the potential of intake air heating in automotive DI diesel engines. SAE Paper 2006- 01-1233, 2006.

29. Imaoka, Y., Nishizawa, T., Lio, S., Hasegawa, M., Teraji, A., Kawamoto, K., Three-dimentional numerical analysis of diesel combustion under cold ambient conditions. International J of Engine Research, 2015. 16(1): p. 68-80.

30. La Rocca, A., MacMillan, D., Shayler, P., Murphy, M. et al., CFD Investigation on the Influence of In-Cylinder Mixture Distribution from Multiple Pilot Injections on Cold Idle Behaviour of a Light Duty Diesel Engine. SAE Technical Paper 2014-01-2708, 2014.

31. Ramírez-Hernández, J.G., Combustion studies for high speed direct injection diesel engines under low temperature cold start conditions. PhD thesis, 2012: Valencia.

32. Lindl, B., Schmitz, H.G, Cold Start Equipment for Diesel Direct Injection Engines. SAE Paper 1999-01-1244, 1999.

33. *http://www.ngk.de/en/technology-in-detail/glow-plugs/design-of-a-glow-plug/design-of-a-metal-glow-plug/*. Accessed March 2015.

34. http://beru.federalmogul.com/sites/default/files/ti_04_gb_2014_fm.pdf. Accessed March 2015.

35. Phatak, R., Nakamura, T., Cold startability of open-chamber direct injection diesel engines- Part II: Combustion design and fuel spray geometry and additional air and glow plug as a starting aid. SAE paper 831396, 1983.

36. Kobayashi, A., Suzuki, T., Nakajima, M., Combustion analysis of the vehicular diesel engine in cold starting condition via high speed photography. ASME 1980.

37. Heywood, J.B., Internal Combustion Engine Fundamentals. 1988, New York: McGraw-Hill.

38. Keeler, B., Constraints on the Operation of a DI Diesel Engine in Partially-premixed Combustion Mode. 2009, University of Nottingham.

39. Lippmann, M., Environmental Toxicants: Human Exposures and Their Health Effects. 2009, New Jersey: John Wiley & Sons.

40. Pugh, G.J., The Analysis of Heat Release in the Investigation of Split-Main Fuel Injection in a Diesel Engine. PhD Thesis, University of Nottingham, 2004.

41. Bosch, R., Diesel-Engine Management. 8th ed. 2011: GmbH: Professional Engineering Publishing Ltd.

42. *http://www.mazda.co.uk/aboutmazda/skyactiv-technology/*. Accessed October 2014.

43. *http://www.dieselnet.com/standards/eu/ld.php#stds*. Accessed November 2015.

44. Transportation, T.I.C.o.C., European Vehicle Market Statistics. Pocketbook 2014, 2014.

45. Ganesh, V., Deshpande, S., Sreedhara, S, Numerical investigation of late injection strategy to achieve premixed charge compression ignition mode of operation. International Journal of Energy Research, 2016. 17(4): p. 469-478.

46. SeungHwan, K., Pinaki, Pal., Hong, G. lm., Aristotelis, Babajimopoulos., Dennis, N. Assanis, Effects of fuel injection parameters on the performance of homogeneous charge compression ignition at low-load conditions. International Jouranal of Engine Research, 2016. 17(4): p. 413-420.

47. Ahmed, F.S., Laghrouche, S., Mehmood, A., and Bagdouri, M. E, Estimation of exhaust gas aerodynamic force on the variable geometry turbocharger actuator: 1d flow model approach. Energy Conversion and Management, 2014. 84: p. 436-447.

48. Pesiridis, A.R., S, Variable geometry turbocharger active control strategies for enhanced energy recovery. SAE Technical Paper 2013-01-0120, 2013.

49. Zhao, H., Advanced Direct Injection Combustion Engine Technologies and Development. 2010, USA: Woodhead Publishing Limited and CRC Press LLC.

50. Cursente, V., Pacaud, P., Gatellier, B, Reduction of the Compression Ratio on a HSDI Diesel Engine: Combustion Design Evolution for Compliance the Future Emission Standards. SAE Paper 2008-01-0839, 2008.

51. Beatrice, C., Avolio, G., Giacomo, N.D., Guido, C, Compression Ratio Influence on the Performance of an Advanced Single-Cylinder Diesel Engine Operating in Conventional and Low Temperature Combustion Mode. SAE Paper 2008-01-1678, 2008.

52. Payri, F., Lopez, J., Pla, B., and Graciano, Bustamante, D, Assessing the limits of downsizing in diesel engines. SAE Tecnical Paper 2014-32-0128, 2014.

53. Durnholz, M., Endres, H., Frisse, P, Preinjection: A Measure to Optimize Emission Behavior of DI Diesel Engines. SAE PAPER 940674, 1994.

54. Rinolfi, R., Imarisio, R., Buratti, R, The Potential of a New Common Rail Diesel Fuel Injection System for the Next Generation

of DI Diesel Engines. 16th International Vienna Motor Symposium, VDI- Verlag Reihe 1995. 12(239).

55. Pischinger, F., Verbrennungsmotoren. 1995: RWTH Aachen.

56. Tomoda, T., Ohki, H., Koyama, T., Fujiwara, K,, Study of Diesel Combustion Improvement for Ultra Low Compression Ratio. Aachener Kolloquium Fahrzeug-und Motorentechnik, 2010.

57. Ishida, M., Chen, Z-L., Luo, G-F., Ueki, H, The Effect of Pilot Injection on Combustion in a Turbocharged D.I. Diesel Engine. SAE Paper 941692, 1994.

58. Henein, N.A., Bolt, J.A., Ignition delay in diesel engines. SAE Paper 670007, 1967.

59. Kuniyoshi, H., Tanabe, H., Sato, G.T., Fujimoto, H., Investigation on the characteristics of diesel fuel spray. SAE Paper 800968, 1980.

60. Westbrook, C.K., Chemical kinetics of hydrocarbon ignition in practical combustion systems. Proc. Combust. Inst, 2000. 28: p. 1563-1577.

61. Assanis, D.N., Filipi, Z. S., FivelandS. B., Syrimis, M. , A Predictive Ignition Delay Correlation Under Steady-State and Transient Operation of a Direct Injection Diesel Engine. J. Eng. Gas Turbines Power 2003. 125(2): p. 450-457.

62. Finesso, R. and E. Spessa, Ignition delay prediction of multiple injections in diesel engines. Fuel, 2014. 119(0): p. 170-190.

63. Caton, P.A., Hamilton, L.J., Cowart, J.S., Understanding Ignition Delay Effects With Pure Component Fuels in a Single-Cylinder Diesel Engine. J. Eng. Gas Turbines Power 2010. 133(3).

64. Rosseel. E., S., R., The Physical and the Chemical Part of the Ignition Delay in Diesel Engines. SAE technical paper 961123, 1996.

65. Wolfer, H.H., Ignition lag in diesel engines. VDI-Forschungsheft, 1938. 392: p. 621-436.047.

66. Waston, E.W., Clarke, A.E., Clarke, J.S., A combustion correlation for diesel engine simulation SAE Paper 800029, 1980.

67. Zhao, H., Advanced direct injection combustion engine technologies and development: diesel engines. Elsevier, 2009. 2.

68. Kawano, D., et al., Fuel design concept for low emission in engine systems 3rd report: analysis of spray characteristics for mixed fuels. SAE Technical Paper 2002.

69. Arcoumanis, C., et al., Analysis of the flow in the nozzle of a vertical multi-hole diesel engine injector. SAE Technical Paper, 1998.

70. Afzal, H., Arcoumanis, C., Gavaiser, M., Kampanis, N., Internal flow in diesel injector nozzles-modelling and experiments. I.Mech.E, S492/S2/99, 1999.

71. Baumgarten, C., Mixture formation in internal combustion engines. 2006, Heidelberg: Springer.

72. Hiroyasu, H., Arai,M, Structures of Fuel Sprays in Diesel Engines. SAE Technical Paper 900475, 1990.

73. Reitz, R.D., Atomization and other breakup regimes of a liquid jet. PhD thesis, Princeton University, 1978.

74. Schneider, B., Experimentelle Untersuchungen zur Spraystruktur in transienten, verdampfenden und nicht verdampfenden Brennsto®strahlen unter Hochdruck. PhD thesis, Technische Wissenschaften, Eidgenossische Technische Hochschule Zurich, 2003.

75. Bekdemir, C., Numerical Modeling of Diesel Spray Formation and Combustion. Eindhoven University of Technology, Master thesis, 2008.

76. Dos Santos, F., Le Moyne, L., Spray atomization models in engine applications, from correlations to direct numerical simulations. Oil& Gas Science and Technology, 2011. 66(5): p. 801-822.

77. Elkotb, M., Fuel Atomization for Spray Modelling. Progr. Energ. Combust. Sci, 1982. 8: p. 61-90.

78. Varde, K.S., Popa, D.M., Varde, L.K., Spray angle and atomization in diesel sprays. SAE Paper 841055, 1984.

79. Merrington, A.C., Richardson, E.G. , The breakup of liquid jets. Proc. Phys. Soc, 1947. 59(1).

80. Lefebvre, G., Atomization and Sprays; Hemisphere Publishing Corporation. 1989, New York: Taylor&Francis.

81. Hiroyasu, H., Arai, M., Tabata, M., Empirical equations for the Sauter Mean Diameter of a diesel spray. SAE paper 890464, 1989.

82. R.D.Reitz, Modeling atomization processes in high pressure vaporizing sprays. Atomisation and Spray Technology, 1987. 3(4): p. 309-337.

83. ANSYS Fluent 14.0 Theory Guide.

84. Wakuri, Y., Fujii, M., Amitani, T., Tsuneya, R., Studies of the Penetration of a Fuel Spray in a Diesel Engine. JSME International Journal of Hazardous Materials, 1960. 3: p. 123-130.

85. Dent, J.C., Basis for the comparison of various experimental methods for studying penetration. SAE Paper 710571, 1971.

86. Hiroyasu, H., Kadota, T., Tasaka, S., Study of the penetration of diesel. JSME International Journal 1978. 44: p. 3208-3219.

87. Levich, V., Physicochemical Hydrodynamics. 1962: Prentice-Hall Inc. 639-650.

88. Mojtabi, M., Optical analysis of multi-stream GDI sprays under various engine operating conditions. PhD thesis, 2011, Loughborough University.

89. Mitroglou, N., et al., Spray characteristics of a multi-hole injector for direct injection gasoline engines. International Journal of Energy Research, 2006. 7(3): p. 255-270.

90. Arai, M., Tabata, M., Hiroyasu, H., Shimizu, M., Disintegrating process and spray characterization of fuel jet injected by a diesel nozzle. SAE paper 840275, 1984.

91. Wakuri, Y., Residual fuel sprays-evaporation, dispersion and combustion characteristics. Proc. International Sympo. COMODIA, 1990. 90: p. 539.

92. Spalding, D.B., Experiments on the burning and extinction of liquid fuel spheres. Fuel, 1953. 32: p. 169–185.

93. Zhou, Z., Wang, G., Chen, B., Guo, L., Wang., Y, Evaluation of Evaporation Models for Single Moving Droplet with a High Evaporation Rate. Powder Technology 2013. 240: p. 95-102.

94. Abramzon, B., Sirignano. W. A, Droplet Vaporization Model for Spray Combustion Calculations. International Journal of Hear Mass Transfer, 1989. 32(9): p. 1605-1618.

95. Yao, G.F., Abdel-Khalik, S.I., Ghiaasiaan, S.M., An investigation of simple evaporation models used in spray simulations. ASME J Heat Transfer, 2003. 125: p. 179-182.

96. Sazhin, S.S., Advanced Models of Fuel Droplet Heating and Evaporation. Progress in Energy and Combustion Science and Technology, 2006. 32: p. 162–214.

97. Sazhin, S.S., Abdelghaffar, W.A., Sazhina, E.M., Heikal, M.R Models for droplet transient heating: Effects on droplet evaporation, ignition, and break-up. International Jouranal of Thermal Sciences, 2005. 44: p. 610-622.

98. Sazhin, S.S., Kristyadi,T., Abdelghaffar, W.A., Heikal, M.R. , Models for Fuel Droplet Heating and Evaporation: Comparative Analysis. Fuel, 2006. 85: p. 1613-1630.

99. Kristyadi, T., Modelling of the Heating and Evaporation of Fuel Droplets. PhD thesis, 2007, University of Brighton.

100. Sirignano, W.A., Fluid Dynamics and Transport of Droplets and Sprays. Second Edition ed. 2010: Cambridge University Press.

101. Goldfarb, I., Gol'dshten, V., Kuzmenko, G., Greenberg, J.B., On thermal explosion of a cool spray in a hot gas. Proceedings of the 27th international symposium on combustion(Colorado, USA), 1998. 2: p. 2367-74.

102. McIntosh, A.C., Gol'dshtein, V., Goldfarb, I., Zinoviev, V., Thermal exposion in a combustible gas containing fuel droplets. Combust Theory Model, 1998. 2: p. 153-65.

103. Sazhin S.S., F.G., Heikal M.R., Goldfarb I., Goldshtein V. and Kuzmenko G, Thermal Ignition Analysis of a Monodisperse Spray with Radiation. Combustion and Flame 2001. 124(4): p. 684-701.

104. Abraham, M., Wichman, I. S., Mono-component fuel droplet evaporation in the presence of background fuel vapor. International Journal of Heat and Mass Transfer, 2011. 54: p. 4090-4098.

105. Bilger, R.W., A mixture fraction framework for the theory and modeling of droplets and sprays. Combustion and Flame, 2011. 158: p. 191-202.

106. De, S., Kim, S. H., Large eddy simulation of dilute reacting sprays: droplet evaporation and scalar mixing. Combustion and Flame, 2013. 160: p. 2048-2066.

107. Deepu, P., Basu, S., Kumar, R., Vaporization dynamic of functional droplets in a hot laminar air jet. International Journal of Heat and Mass Transfer, 2013. 56(69-79).

108. Honnery, D., Nguyen, D., Soria, J., Microdroplet evaporation under increasing temperature conditions: experiments and modelling. Fuel, 2013. 105: p. 247-257.

109. Protheroe, M.D., Al-Jumaily, A., Nates, R. j., Prediction of droplet evaporation characteristics of nebuliser based humidification and drug delivery devices. International Journal of Hear Mass Transfer, 2013. 60: p. 772-780.

110. Camm, J.D., Stone,R., Davy, M.H., Richardson, D, The Modelling of Single and Multi-Component Droplet Evaporation, in THIESEL 2014 Conference on Thermo- and Fluid Dynamic Processes in Direct Injection Engines. 2014.

111. Turns, S.R., An Introduction to Combustion: Concepts and Applications. 2012, New York: McGraw-Hill.

112. Bird R.B., S.W.E., Lightfoot E.N, Transport Phenomena. 2002, Chichester: Wiley.

113. Brown, N., Gupta, V., Rocca, A. LA, Shayler, P.J., Murphy, M., Pegg, I, Watts, M, Effects of Injection Strategies on the Cold Start up of DI Diesel Engines. Proc. IMechE, 221 (Part D): 1415-1423, 2007, 2007.

114. Chao, F., D., Brian, M, Scilzo., The e®ects of electrode design on mixture ignitability. SAE paper 960606, 1996.

115. Tomohiro, k., Takazo, H., Tatsuya, Uchimoto., Jyunichi, Hatano., Naoto, Kitayama., Hiroshi, Sono, PCCI operation with early injection of conventional diesel fuel. SAE Paper 2005-01-0378, 2005.

116. Fanhua, M., Yu, Wang., Haiquan, Liu., Yong, Li., Junjun, Wang., Shangfen, Ding, Effects ofhydrogen addition on cycle-by-cycle variations in a lean burn natural gas spark-ignition engine. International Journal of Hydrogen Energy, 2008. 33(2): p. 823-831.

117. Brunt, M.F., Rai, A., Emtage, A.L, The Calculation of Heat Release Energy from Engine Cylinder Pressure Data. SAE Paper 981052, 1998.

118. Brunt, M., Platts, K., Calculation of Heat Release in Direct Injection Diesel Engines. SAE Paper 1999-01-0187, 1999.

119. Gatowski, J.A., Balles, E.N., Nelson, F.E., Ekchian, J.A., Heywood, J.B, SAE Paper 841359. Heat Release Analysis of Engine Cylinder Pressure Data, 1984.

120. Dec, J.E., Espey, C, Chemiluminescence Imaging of Autoignition in a DI Diesel Engine. SAE Paper 982685, 1998.

121. Gaydon, A.G., The Spectroscopy of Flames. The Second ed. 1974, London: Chapman and Hall.

122. Dec, J.E.a.E., C, Ignition and Early Soot Formation in a D.I. Diesel Engine Using Multiple 2-D Imaging Diagnostics. SAE Transactions, 1995. 104(3): p. 853- 875.

123. Rothrock. A. M., W.C.D., Effect of Nozzle Design on Fuel Spray and Flame Formation in a High-Speed Compression-Ignited Engine. C.A.C.A. reported No. 561, 1936.

124. Ragucci, R., Cavaliere, A., D'Alessio, A., and Noviello, C, Auto-Ignition Characteristics of Diesel Sprays Under Different Injection Conditions, in Proceedings of the Third International Conference on Innovation and Reliability in Automotive Design and Testing. 1992, Obtained from the SAE, reference number 92A076: Firenze, Italy.

125. Baritaud, T.A., Heinze, T. A., and Le Coz J. F, Spray and Self-Ignition Visualization in a DI Diesel Engine. SAE Transactions, 1994. 103(3): p. 1129-1144.

126. Edwards, C.F., Siebers, D. L., and Hoskin, D. H, A Studyof the Autoignition Process of a Diesel Spray via High Speed Visualization. SAE Transactions 1992. 101(3): p. 187-204.

127. Fabian, P.K., Numerical modelling of diesel spray injection, turbulence interaction and combustion. PhD thesis, 2008, Chalmers University of Technology.

128. Guan Jhong, W., Chia Jui,C., Yu Hsuan. S., Yong Yuan, K., CFD Modelling of a Turbo-charged Common-rail Diesel Engine. SAE International, 2013.

129. Wei, J., Dracos, N., Energy Modeling of Large 2-Stroke Marine Diesel Engine using CFD. Low Carbon Shipping Conference, London, 2013.

130. Abbas, G., Kohei, Fukuda., Ram, Balachandar., Ronald, Barron., Numerical Investigation of Spray Characteristics of Diesel Alternative Fuels. SAE International Journal of Engines 2012-01-1265, 2012.

131. Kayhani, M.H., Zamani Aghaie, A., Modarres Razavi, M.R., Investigation of different numerical models in spray behavior simulation in order to predict the spray tip penetration. International Conference on Mechanical, Automobile and Robotics Engineering (ICMAR'2012) Penang. Malaysia, 2012.

132. Liu, A.B., Mather, D., Reitz, R. D., Modeling the Effects of Drop Drag and Breakup on Fuel Sprays. SAE technical Paper 930072, 1993.

133. Mohamed Ismail, H., H.K. Ng, and S. Gan, Evaluation of non-premixed combustion and fuel spray models for in-cylinder diesel engine simulation. Applied Energy, 2012. 90(1): p. 271-279.

134. Felske, J.D., Approximate Radiation Shape Factors between Two Spheres. J. Heat Transfer, 1978. 100(3): p. 547-8.

135. K.K.Y.Kuo, Principles of Combustion. 1986, New York: John Wiley and Sons.

136. Wang, Z., Experimental study on diesel spray with single and multiple injection under room temperature and low temperature. PhD thesis, 2015, University of Birmingham.

137. Wang, Z., Ding, H., Ma, X., Xu, H., Wyszynski, M. L, Ultra-high speed imaging study of the diesel spray close to the injector tip at the initial opening stage with single injection. Applied Energy, 2016. 165: p. 335-344.

138. Schihl, P., Bryzik, W., Altreya, A., Analysis of current spray penetration models and proposal of a phenomenological cone penetration model. SAE paper 960773, 1996.

139. Kevric, A., Combustion Characteristics of a Compression Ignition Engine Running on Biodiesel and Gasoline Blended Fuels. PhD thesis, 2013: University of Nottingham.

140. Introduction to ANSYS Meshing: Mesh Quality.

141. Broatch, A., Ruiz, S., Margot, X., Gil, A, Methodology to Estimate the Threshold In-Cylinder Temperature for Self-Ignition of Fuel During Cold Start of Diesel Engines. Energy, 2010. 35: p. 2251-2260.

142. Desantes, J.M., Garcia-Oliver, J.M., Pastor, J.M., Ramirez-Hernandez, J.G, Influence of Nozzle Geometry on Ignition and Combustion for High-Speed Direct Injection Diesel Engines under Cold Start Conditions. Fuel, 2011. 90: p. 3359-3368.

143. http://www.beru.com/download/produkte/whitepaper_iss_en.pdf. Accessed March 2015.

144. http://www.beru.com/download/produkte/fachvortrag_influence_en.pdf. Accessed April 2015.

145. Hiroyasu, H., Arai, M., Tabata, M, Empirical equations for the Sauter mean diameter of a diesel spray. SAE Technical Paper 890464, 1989.

146. Holman, J.P., Heat Transfer. 2010, Singapore: McGraw-Hill.

Appendix

According to Dalton's law, in mixture, ratio of partial pressure of fuel vapor to partial pressure of air is equal to mole fraction of fuel vapor to mole fraction of air, as expressed in equation (1):

$$\frac{p_f}{p_a} = \frac{n_f}{n_a} \quad (1)$$

Where p refers to pressure for each gas, n refers to amount of substance for each gas.

Ratio of substance can be expressed in equation (2)

$$\frac{n_f}{n_a} = \frac{(\frac{m_f}{M_f})}{(\frac{m_a}{M_a})} = \frac{m_f}{m_a} \times \frac{M_a}{M_f} \quad (2)$$

And the mass ratio can be expressed in equation (3)

$$\frac{m_f}{m_a} = (\frac{m_f}{m_a})_{stoich} \times \emptyset = \frac{\emptyset}{14.5} \quad (3)$$

Where m refers to mass and M refers to molar mass. Combine equation (1), (2) and (3) to have equation (4)

$$\frac{p_f}{p_a} = \frac{\emptyset}{14.5} \times \frac{M_a}{M_f} \quad (4)$$

Here using $C_{10}H_{22}$ to represent light diesel, the molar mass of fuel vapor is 142, and molar mass of air is 29.

$$\frac{p_f}{p_a} = \frac{\emptyset}{14.5} \times \frac{M_a}{M_f} = 0.014\emptyset \quad (5)$$

Portion of partial pressure of fuel vapor in total gas pressure can be expressed in equation (6)

$$\frac{p_f}{p_a + p_f} = \frac{0.014\emptyset}{1 + 0.014\emptyset} \quad (6)$$

The percentage of partial pressure of fuel vapor is plotted against equivalence ratio, as has been shown in figure 1, the partial pressure of fuel vapor increases with increasing equivalence ratio, it reaches a small fraction of 0.7% when equivalence ratio equals 1, partial pressure of fuel vapor is too small to be neglected here and the partial pressure of air is assumed equivalent to the total pressure of mixture or the system pressure.

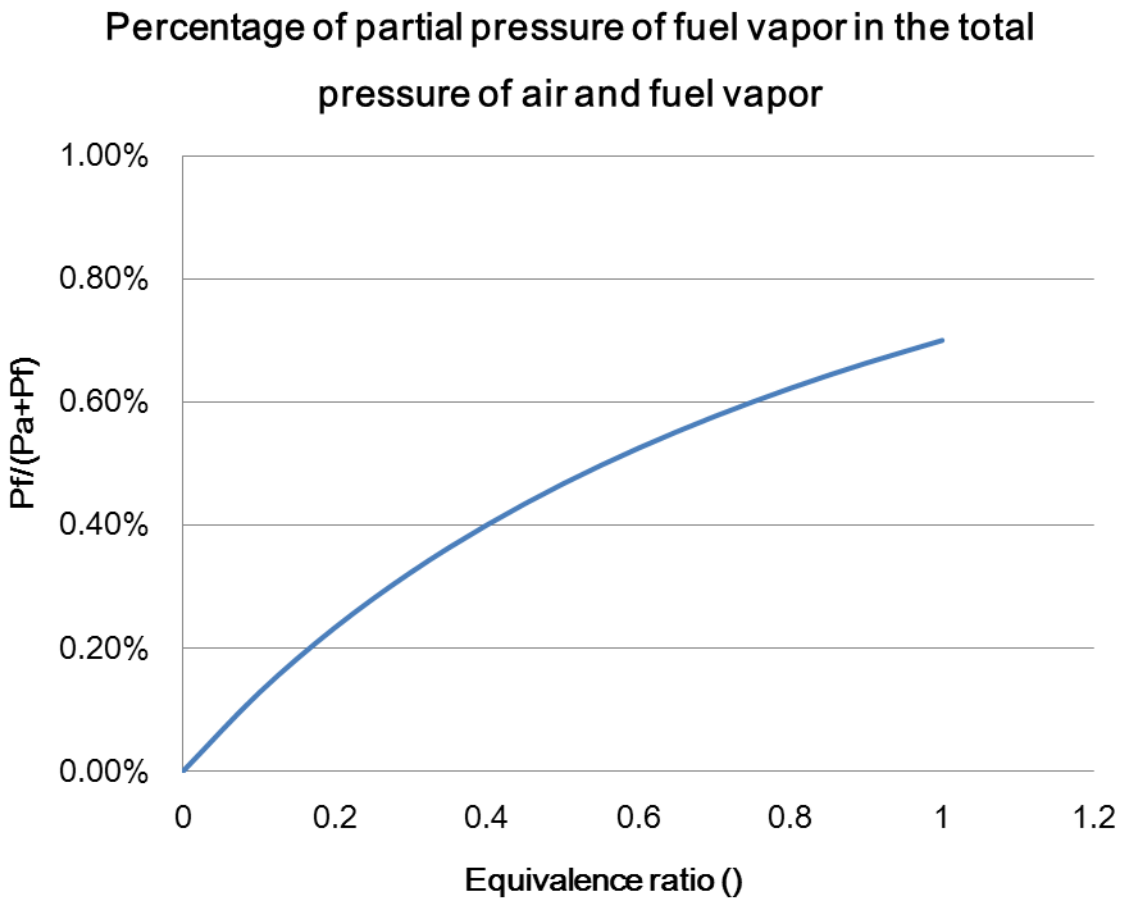

Figure 1: Percentage of partial pressure of fuel vapor in the total pressure of mixture against equivalence ratio, partial pressure of fuel vapor is too small and can be neglected